Lawrence Berkeley National Laboratory
Recent Work

Title

VAPORIZATION KINETICS OF ZINC OXIDE AND CADMIUM SULFIDE SINGLE CRYSTALS

Permalink

https://escholarship.org/uc/item/2dv5t8tx

Author

Leonard, Ralph Beaumont.

Publication Date

1970-05-01

VAPORIZATION KINETICS OF ZINC OXIDE AND
CADMIUM SULFIDE SINGLE CRYSTALS

Ralph Beaumont Leonard
(Ph.D. Thesis)

May 1970

LAWRENCE RADIATION LABORATORY
UNIVERSITY of CALIFORNIA BERKELEY

DISCLAIMER

TABLE OF CONTENTS

VAPORIZATION KINETICS OF ZINC OXIDE AND
CADMIUM SULFIDE SINGLE CRYSTALS

Ralph Beaumont Leonard

Inorganic Materials Research Division, Lawrence Radiation Laboratory
Department of Materials Science and Engineering, College of Engineering
University of California, Berkeley, California

ABSTRACT

The vacuum vaporization kinetics of cadmium sulfide and zinc oxide single crystals have been studied by use of a microbalance. These two compounds crystallize in the non-centrosymmetric wurtzite structure with the result that opposite basal faces are not crystallographically equivalent.

Zinc oxide was studied at $1107°C$. The $Zn(0001)$ face vaporizes at a rate that is higher than the $O(0001)$ face by a factor of approximately 2.8. The opposite basal faces also develop different steady state morphologies. The steady-state $Zn(0001)$ face resembles sharp mountain peaks separated by narrow valleys with no obvious crystallographic features while the steady-state $O(0001)$ face is an array of hexagonal pits with stepped sides.

Introduction of methane, carbon monoxide, and oxygen does not effect the vaporization rate of either face, but exposure of the crystal to water vapor at room temperature reduces the initial vaporization rate of the $Zn(0001)$ face by more than a factor of ten. Doping the crystals with excess zinc has no effect on its vaporization behavior; attempts at oxygen doping were unsuccessful, presumably because of surface contamination.

Cadmium sulfide was studied over the temperature range of $609°C$ to $676°C$. The Cd(0001) face vaporizes at a rate that is higher than the $S(000\bar{1})$ face by a factor of approximately 1.3. The observed pressure from the Cd(0001) face was an order of magnitude less than the equilibrium pressure.

The steady-state Cd(0001) face is an array of hexagonal pits while the steady-state S(0001) face resembles rounded mountain peaks separated by narrow valleys. The average apparent activation enthalpies of vaporization for the reaction

$$CdS_{(s)} \rightarrow Cd_{(g)} + 1/2 S_{2(g)}$$
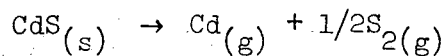
for the two faces was measured to be:

$$S(000\bar{1}) \qquad 96.66 \pm 3.39 \text{ kcal/mole CdS}$$
$$Cd(0001) \qquad 85.41 \pm 1.09 \text{ kcal/mole CdS}$$

The equilibrium enthalpy of vaporization for this reaction between $882°$ to $1107°K$ is 77 kcal/mole CdS.

I. INTRODUCTION

Vaporization studies may be divided into two catagories: (1) equilibrium studies yielding thermodynamic data and (2) non-equilibrium studies yielding kinetic data. While a very large number of equilibrium studies have been carried out for a wide variety of materials, very few kinetic studies have been undertaken.

In vaporization kinetic studies one must be concerned with the gas phase over the surface, the vaporizing surface itself and the solid phase. Let us look at these three aspects more closely. The gas phase includes atoms or molecules which have just vaporized from the surface in addition to foreign residual gases. One must always be cognizant of possible contamination of the surface by foreign gases, or of possible reactions of the solid with residual gases.

The vaporizing surface itself may almost be considered a separate phase. The vaporizing surface is not well understood but it may, for instance, include a highly mobile layer of adsorbed atoms and/or molecules which occasionally combine to form "activated complexes". The top few atomic layers of the lattice can be considered to be part of the surface phase and not part of the bulk since the defect structure and impurity concentration of these layers may be very different from the bulk. Also highly important is the crystallographic plane being vaporized since different planes have different atomic arrangements which in turn may influence the vaporization rate. In addition, such imperfections as dislocations may play an important role since they may themselves be favored vaporization sites or be sources for ledges that provide favored sites.

The vaporization kinetics of compounds may be strongly dependent on the exact bulk composition, even though the composition range is very small. Depending on the diffusion rate of impurities with respect to the velocity of surface recession, the impurities may diffuse to the surface faster than the surface recedes or they may essentially remain distributed throughout the bulk. Depending on the relative vaporization rates of the impurities with respect to the lattice constitutents, the impurities may congregate on the surface or immediately vaporize.

The purpose of a study of vaporization kinetics is to determine which of these chemical and physical factors influence the vaporization process, and ultimately to ascertain the exact steps through which the atoms or molecules go as they pass from the solid phase and enter the gas phase.

A concept which is useful in discussing vaporization kinetics is the vaporization coefficient α_v. If one has a solid in equilibrium with its vapor at temperature T, the flux of atoms or molecules from the surface is related to the equilibrium pressure over the surface by the equation:

$$J \frac{(moles)}{(cm^2-sec)} = \frac{P_{equil.}}{(2\pi MRT)^{1/2}}$$

where R is the gas constant and M is the mass of the atom or molecule. This equilibrium flux is the maximum flux possible from the surface. If, however, the surface is vaporized into a vacuum, the flux of species from the surface may be less than the equilibrium flux and the vaporization coefficient is defined as follows:

$$\alpha = \frac{J_{vacuum}}{J_{equil}} = \frac{P_{vacuum}}{P_{equil}}$$

The only quantitative model for vaporization is one developed by Hirth and Pound for metals.[1] This model is essentially the reverse of the model used for growth from the vapor of metal single crystals. The model considers the movement of atoms from kink sites to sites at ledges and the diffusion of atoms from the ledge sites to adsorption sites on the surface from which they desorb into the gas phase (Fig. 1).

The Hirth and Pound model predicts a value of 1/3 for the vaporization coefficient for low dislocation density, low index planes of metal single crystals. Although this model is conceptually satisfying for the vaporization of metals, a recent investigation by Mar[2] of the vaporization of the (0001) planes of zinc single crystals showed that the vaporization coefficient is actually very close to unity.

In any event, one cannot directly apply this model to the vaporization of a solid when two or more kinds of atoms are in the solid phase and a complicated gas phase is produced over the solid. Many solids dissociate upon vaporization. For example ZnO and CdS vaporize as follows:

$$ZnO_{(s)} \rightarrow Zn_{(g)} + 1/2\ O_{2(g)}$$

$$CdS_{(s)} \rightarrow Cd_{(g)} + 1/2\ S_{2(g)}$$
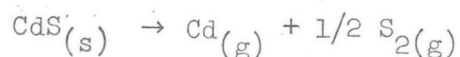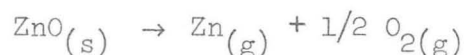
Attempts to develop quantitative models for dissociative sublimation reactions are hampered by the inadequacies of present experimental data. The present study of zinc oxide and cadminum sulfide vaporization was undertaken in an effort to improve our understanding of the effects of surface orientation and surface structure on vaporization rates.
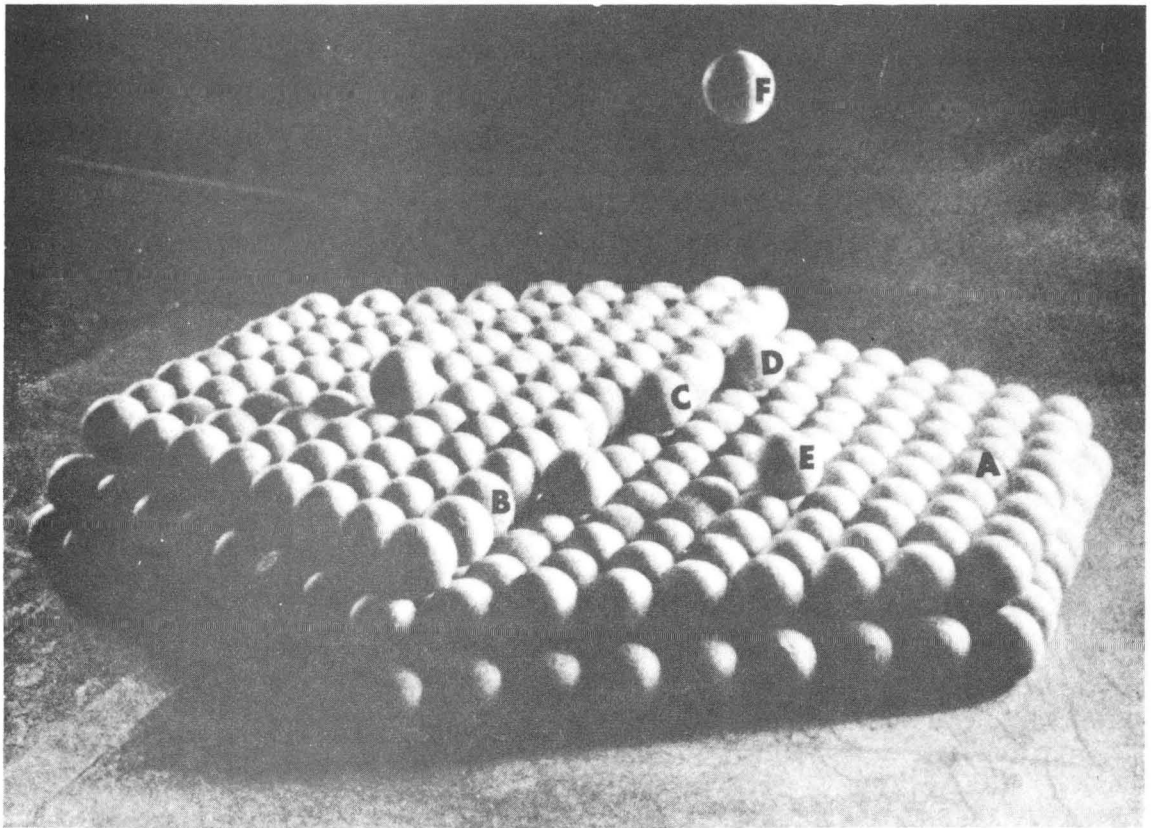
A — atom in surface

B — atom in ledge

C — atom in kink

D — atom at ledge

E — adsorbed atom

F — vapor atom

XBB687-4159

Fig. 1. Hirth and Pound Model for Vaporization of Metal Single Crystals.

II. PROPERTIES AND SOLID STATE CHEMISTRY OF ZINC OXIDE

Zinc oxide has been known since the days of the alchemists[3] who called it "cadmia". This was an impure zinc oxide contaminated with copper which they produced as a by product from copper smelting. They believed that they could increase the size of a piece of gold by smelting it with "cadmia", but actually their process produced brass from the "cadmia" which alloyed with the gold. It was a nice try, and must have pleased the alchemists no end.

Zinc oxide also occurs in nature as the mineral zincite. Scharowsky[4] describes how zinc oxide single crystals may be grown by passing a mixture of nitrogen and hydrogen over metallic zinc at $600°C$ and reacting this mixture with oxygen in an oven at some temperature between $1150°C$ and $1350°C$. The mechanism of the growth process is not known and the growth of large cyrstals by this method is difficult.[5] The Minnesota Mining and Manufacturing Company[6] has perfected a growth process which produces crystals 1 cm long and up to 8 mm in diameter. The process is a company secret, but presumably is similar to the method of Scharowsky. Park and Reynolds[7] have recently developed a method of growing large crystals in the form of needles and platelets by subliming zinc sulfide and zinc selenide and reacting the gas with oxygen.

Zinc oxide crystallizes only in the hexagonal wurtzite structure $(a = 3.24Å$ and $c = 5.19Å)$ in which the oxygen ions are hexagonally close packed. The zinc ions occupy one-half of the tetrahedral sites with the same relative arrangement as the oxygen ions (Fig. 2). This crystal packing leads to a layered structure with pairs of zinc-oxygen layers stacked normal to the c-axis (Fig. 3). Consequently, opposite faces of
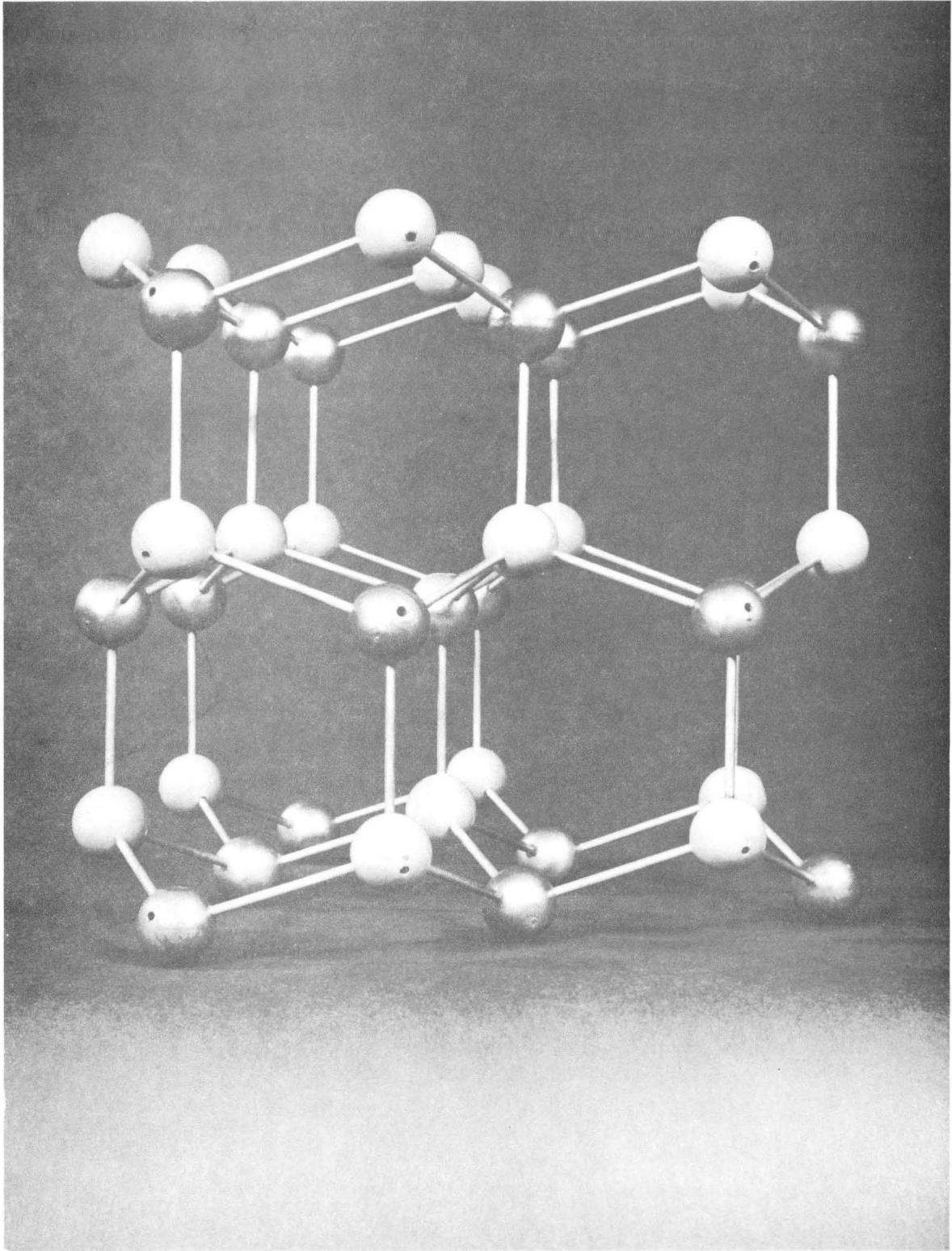
XBB692-1286

Fig. 2. Wurtzite Crystal Structure

Zinc face

c — axis

Oxygen face
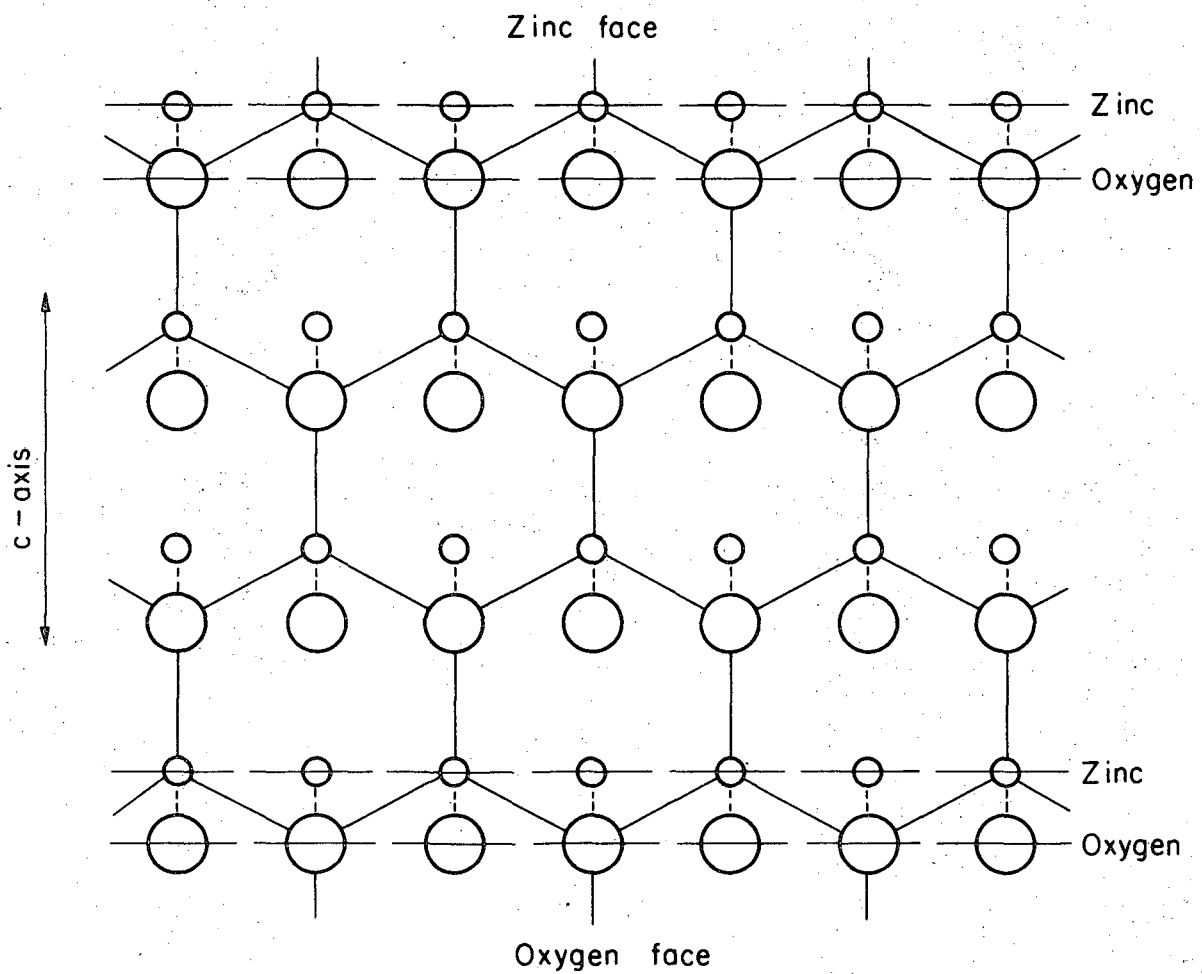
XBL693 – 2169

Fig. 3. Alternate Layers of Zn and O Atoms Perpendicular to the c-axis (Similar for Cd and S atoms in CdS)

a wafer cut perpendicular to the c-axis are not equivalent. Methods of identifying the Zn-face and O-face will be discussed in the experimental section.

Zinc oxide is used as a catalyst[8] in many reactions and hence its surface properties have been of interest to many investigators. The catalytic properties of the zinc oxide seem to be due to its ability to transfer electrons to the adsorbed species and hence; its catalytic activity is greatly dependent on its surface conductivity. The catalytic properties will not be discussed here, but a review and discussion of the details of the surface electronic properties has been given by Morrison[9] and a review of the bulk electronic properties and some catalytic reactions has been given by Heiland and Mollowo.[10] Most of the studies concerning zinc oxide were done in the 1950's because of the sudden large interest in new semiconducting materials which resulted from the invention of the transistor.

Several studies have been carried out on the surface conductivity of both powders and single crystals. Melnick[11] and Medved[12,13] have studied the effect of adsorbed oxygen on the surface conductivity of sintered samples and have produced evidence showing that the oxygen removes an electron from the conduction band near the surface and becomes chemically adsorbed as O^-. This ionic adsorption results in a lowering of the surface conductivity since the negatively charged adsorbed oxygen ions produce a surface barrier which inhibits diffusion of bulk electrons to the surface. Irradiation by ultraviolet light of band gap energy (3.3 eV or 3750Å) produces hole-electrons pairs, and the holes can discharge the negative oxygen ions, thus restoring the surface conductivity.

However, a different process has been described by Thomas and Lander[14] and Collins and Thomas[15] for the surface conductivity of single crystals of zinc oxide. These investigators argue that the surface conductivity is due to an excess of zinc on the surface which results from a loss of oxygen ions from surface layers and thus increases the conductivity by the formation of an electron - rich layer. This conductivity was produced by several methods, namely by using ultraviolet light to discharge surface lattice oxygen ions, by annealing a crystal in hydrogen, or by depositing a layer of zinc on the surface. This last method did not produce a conducting film, but rather apparently produced the same electron-rich layer as that produced when surface oxygen ions were removed.

It is not clear which of these mechanisms is responsible for the surface conductivity of zinc oxide. Sintered samples may behave differently from single crystals because of the much larger surface to volume ratio of powders, or the exact mechanism may be greatly influenced by impurity band conduction, as suggested by Thomas and Lander.[14]

Hutson[16] has measured a large number of the electronic properties for single crystals and gives data on the density of states, temperature dependence of the mobility, electron effective mass, thermoelectric power, magnetoresistance, Hall mobility, optical-mode scattering, and conductivity isotropy. Hahn[17] has studied the electrical properties of sintered zinc oxide. He points out that the conductivity of sintered samples may be largely controlled by the conductivity of the necks between grains. A discussion of the sintering process itself for zinc oxide is given by Gray[18] and by Lee and Parravano.[19]

Thomas and Lander[20] studied hydrogen in zinc oxide. They believe that the increase in conductivity which is observed is due to ionized hydrogen atoms and not due to the indiffusion of zinc atoms from the reduced zinc oxide at the surface. They surmise that a hydrogen atom forms an OH^- center that is easily ionized since the odd electron is spread over a large volume.

Lander[21] has shown that lithium can be both a donor and an acceptor in zinc oxide. If lithium is interstitial it becomes a donor due to the simple loss of the outer electron, and it acts as an acceptor if the Li^{+1} ion replaces the Zn^{+2} ion in the lattice.

Thomas[22] has studied the behavior of indium in zinc oxide. Indium doped crystals have a higher conductivity than the undoped material since the In^{+3} ion substitutes for the Zn^{+2} and the extra electron contributes to the conductivity.

An extensive discussion of the defect chemistry of zinc oxide is given by Garrett.[23] His article is essentially a review of the solid-state work done on zinc oxide in the 1960's. He points out that the main defects that can be expected in zinc oxide are interstitial zinc, zinc vacancies, and oxygen vacancies; interstitial oxygen can be ruled out because it is too large to be incorporated into the close packed lattice of oxygen ions.

The data concerning diffusion of zinc in zinc oxide is very confused. Secco and Moore[24] grew small single crystals containing radioactive Zn^{65} and studied the exchange reaction between the lattice Zn^{65} and an atmos- phere of ordinary zinc. They concluded that the reaction was controlled by the diffusion of zinc into the lattice and calculated the diffusion coefficient to be:

$$D = 4.8 \exp (-73 \text{ kcal/RT}) \text{ cm}^2\text{-sec}^1$$

$$900° -1025°; \text{ not stated if } °C \text{ or } °K$$

Moore and Williams[25] then diffused Zn^{65} into zinc oxide and found the diffusion coefficient to be:

$$D = 1.3 \ 10^5 \exp(-43.5 \text{ kcal/RT}) \text{ cm}^2\text{-sec}^{-1}$$

$$1080° - 1265°; \text{ not stated if } °C \text{ or } °K$$

Thomas[26] studied the diffusion of interstitial zinc in the zinc oxide single crystals from 180° to 350°C by following the conductivity. He found the solubility of interstitial zinc to be:

$$n(\text{atoms/cm}^3) = 3.4 \times 10^{20} \exp (14.9 \text{ kcal/RT})$$

and the diffusion coefficient to be

$$D = 2.65 \times 10^{-4} \exp (-12.6 \text{ kcal/RT}) \text{ cm}^2\text{-sec}^{-1}$$

This value of the activation enthalpy is more reasonable for the diffusion of small interstitial species than the one given by Moore et al. and Thomas' data leads to a reasonable value for the vibrational entropy of an interstitial atom.

Although no reason can readily be given for the discrepancies in these results, a possible explanation can be found in the work by Mohanty and Azaroff[27] on electron density distributions in zinc oxide single crystals. Their results indicate a density of interstitials 10^3 times greater than that calculated from conductivity measurements. Also they found different behavior for "virgin" crystals and crystals which had been previously doped with zinc. Virgin crystals took much longer to reach saturation than crystals previously zinc doped. Hence, newly grown crystals might be expected to show a different diffusion coefficient from aged crystals.

Heavily zinc doped zinc oxide is bright red-orange. The earliest work on red zinc oxide was done by Greenstone[28] who presented evidence that the red color was due to excess zinc. Hannay[5] also found zinc doped zinc oxide to have a red color. Naturally occurring crystals of zincite are sometimes red due to large concentrations of Mn and Fe. Larach and Turkevich[29] have presented electron spin resonance evidence that nitrogen impurities may also impart a red color to zinc oxide. Zinc doped zinc oxide was prepared in this study under conditions which excluded contamination by nitrogen, iron, or manganese and bright red-orange crystals were obtained. This result will be discussed later in the experimental section.

No valid data are available on the diffusion of oxygen in zinc oxide. Moore and Williams[25] studied this problems and their results are widely quoted, but their work has been shown to be incorrect.[30]

Anthrop and Searcy[31] studied the equilibrium vaporization of zinc oxide using a mass spectrometer. They confirmed the fact that zinc oxide vaporizes congruently to gaseous zinc atoms and oxygen molecules with no detectable ZnO molecules. They also report an interesting reaction between zinc oxide and silica. When zinc oxide was in close contact with silica, the zinc oxide surface apparently became coated with a reaction product that lowered the vaporization rate. They hypothesized that this occurred via surface diffusion because the vapor pressure of silica was too low at their temperatures to transport silica by the vapor phase. The use of aluminum oxide cells presented no such surface difficulties.

Anthrop and Searcy were able to explain the anomously high vapori-
zation rate observed by Moore and Williams[32] for the vaporization of zinc
oxide in the presence of zinc vapor. Residual water in the system was
decomposed by the zinc and the resulting hydrogen reduced the zinc oxide.

The only work on the vaporization kinetics of zinc oxide was done by
Hoenig[33] who found an enthalpy of activation of 140 kcal/mole for the
vaporization of prismatic planes into vacuum. This is 23% higher than
the equilibrium enthalpy. The second law Langmuir entropy was equal to
the equilibrium entropy, 52.5 cal/deg-mole.

III. EXPERIMENTAL SECTION

The zinc-oxide crystals were grown by the 3M Co.[6] by a vapor phase process similar to that of Scharowsky.[4] The resistivity of the crystals at 25°C, as reported by the 3M Co., ranged from 0.5 to 100 ohm-centimeters, with a nominal range of one to two ohm-cm. No attempt was made to measure the resistivity here because of many problems due to contaminants on the surface and surface roughness.

The 3M Co. grows the crystals as hexagonal needles up to 10 mm long with a maximum diameter of 8 mm, and routinely supplies basal slices (Fig. 4). In addition, prismatic slices were requested as shown. The basal slices were 1 mm thick and 8 mm in diameter, while the prismatic slices were 2 mm thick and had faces which were 5 mm by 6 mm.

Each order of wafers was identified by the 3M Co. according to the lot and batch number of the parent crystal. Accordingly, for this work each wafer was assigned a number refering to this 3M Co. number. For example, the wafers of Lot 40 Batch 51 were numbered L40B51 No. 1, L40B51 No. 2, L40B51 No. 3, etc. One order of wafers was identified by the 3 M Co. only as lot 307, hence these crystals were designated as L307 No. 1, L307, No. 2, L307, No. 3, etc. This numbering system allowed each crystal to be correlated with the emission spectrographs of the various lots and batches.

The 3M Co. cuts the crystal wafers with a diamond saw using an aqueous coolant containing a rust inhibitor. They then lightly polish the surfaces with 600 grit SiC abrasive paper. The as-recieved basal slices were examined with a Materials Analysis Company electron beam
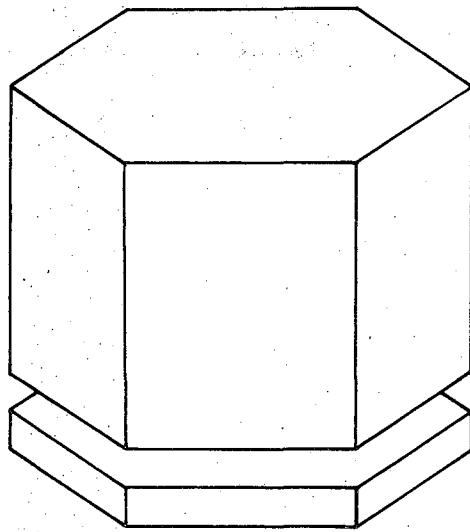
BASAL
SLICE
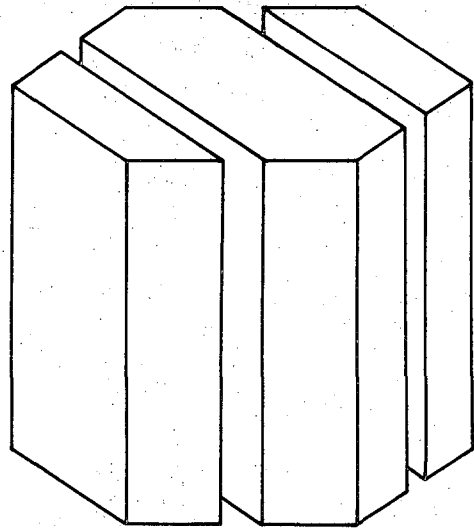
PRISMATIC
SLICES

XBL 698-1330

Fig. 4. Zinc Oxide Wafers

micro-probe, and large concentrations of Si (probably as SiC) and Al were found. The Al was probably Al_2O_3 and might have arisen from the SiC abrasive paper having been stored with alumina abrasive paper. The Si and Al were still present, although in lesser amounts, after extensive etching with nitric acid. A batch of basal slices was ordered that were not polished after being cut, and no Si or Al was detected on these surfaces. No difference in vaporization behavior was found for the crystals whether or not they initially had Si or Al on the surface.

Table I shows typical emission spectrographs of the impurities in two batches of crystals.

As mentioned in Section II, opposite faces of basal slices are not crystallographically equivalent (see Figs. 2 and 3). Warekois[34] et al. have investigated the crystallographic polarity of several II-VI compounds by x-ray analysis and by studies of chemical etching heavior. The crystallographic polarity of zinc oxide has been investigated by Mariano and Hanneman.[35] Because of the asymmetry of the crystal structure along the c-axis, opposite basal faces exhibit slightly different geometric scattering factors and Mariano and Hanneman correlated the intensities of the zinc K absorption edges on opposite sides of a basal cut wafer with the chemical etching behavior. They found that an etch with 20 Vol. % HNO_3 produced hexagonal pits on the zinc face but non-distinct hillocks on the oxygen face. The prismatic faces produced triangular pits with the apexes pointed toward the zinc face. Figures 5a and 5b show the etch morphology produced in this study on opposite sides of a basal slide after a 20 min. etch with 20 vol. % HNO_3. Figure 5c shows the etch morphology produced by a similar etch on the prismatic faces where the triangular pits point toward the basal face with hexagonal pits.

TABLE 1

Emission spectrographic data (units are ppm)

Element	Detection limit	Concentrations Batch L40B85	Batch L307
Sr	3	0	0
Co	3	0	0
Zr	3	0	0
Ag	< 1	< 1	0
Cu	< 1	5	5
Cd	3	0	0
Ti	< 1	0	0
V	< 1	0	0
Ca	10	1	1
Sn	< 1	5	9
Mo	< 1	0	0
Be	< 1	0	0
Al	3	6	3
Bi	< 1	0	0
In	3	0	0
Ge	< 1	0	0
Fe	< 1	1	0
Cr	< 1	0	0
Ni	< 1	0	0
Si	5	6	< 5
Sb	10	0	0
Mg	< 1	< 1	0
Pb	3	0	0
Mn	< 1	0	0
B	< 1	2	1
sample ground in a BC mortar			
Te	10	0	0
As	10	0	0
Ba	3	0	0
Li	< 1	0	0
Ga	< 1	0	0
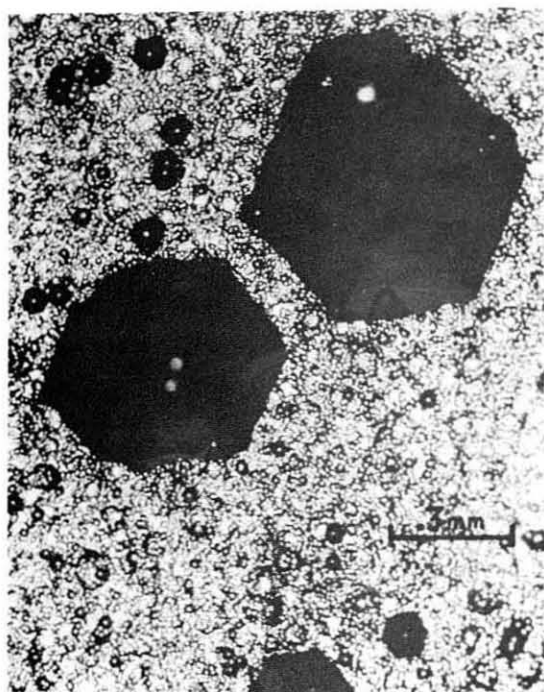
(a)

(b)
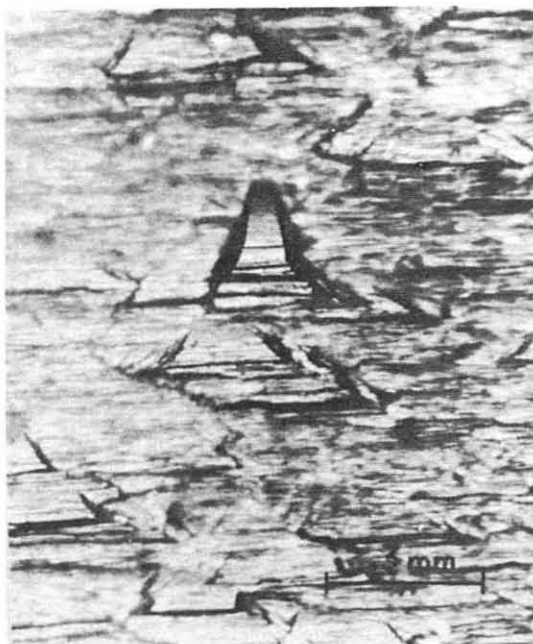
(c)

XBB 701-439

Fig. 5. Etch Patterns Developed By 20 Vol.% HNO_3

    (a) Zn(0001)
    (b) O(000$\bar{1}$)
    (c) Prismatic Face

In accord with the results of Mariano and Hanneman, Fig. 5a is identified as the zinc face and Fig. 5b as the opposite oxygen face. The etch pits on the zinc face of some crystals were not as distinct as those seen in Fig. 5a, but rather were "chunky". The oxygen faces however, always produced a morphology like that shown in Fig. 5b, and no difficulty was encountered in distinguishing between the two faces.

Some crystals were zinc doped in an evacuated and sealed quartz tube containing zinc metal. Each crystal was loosely wrapped with platinum foil so that it did not come into contact with the quartz tube, and the wrapped crystal was prevented from dropping into the molten zinc by a constriction in the tube. The crystals were annealed for two to three hours at $800°$ to $1000°C$. After all anneals, the crystals were a bright red-orange throughout the entire bulk. The nitric acid etch described previously gave identical etch patterns as those found for undoped crystals.

For vaporization rate measurements the crystal wafer was held in an aluminum oxide cell designed so that only the chosen face was exposed (Fig. 6). Essentially no vaporization was observed from the rear face which was masked by a tight fitting plug which fit against the crystal. The cell was fabricated from 99.5% aluminum oxide. Anthrop and Searcy[31] found no reaction between aluminum oxide and zinc oxide at $1150°C$, a result that is not surprising because the two oxides form a simple eutectic system with the solidus at $1700°C$. After 300 hours of use, no physical change was observed in the cell.
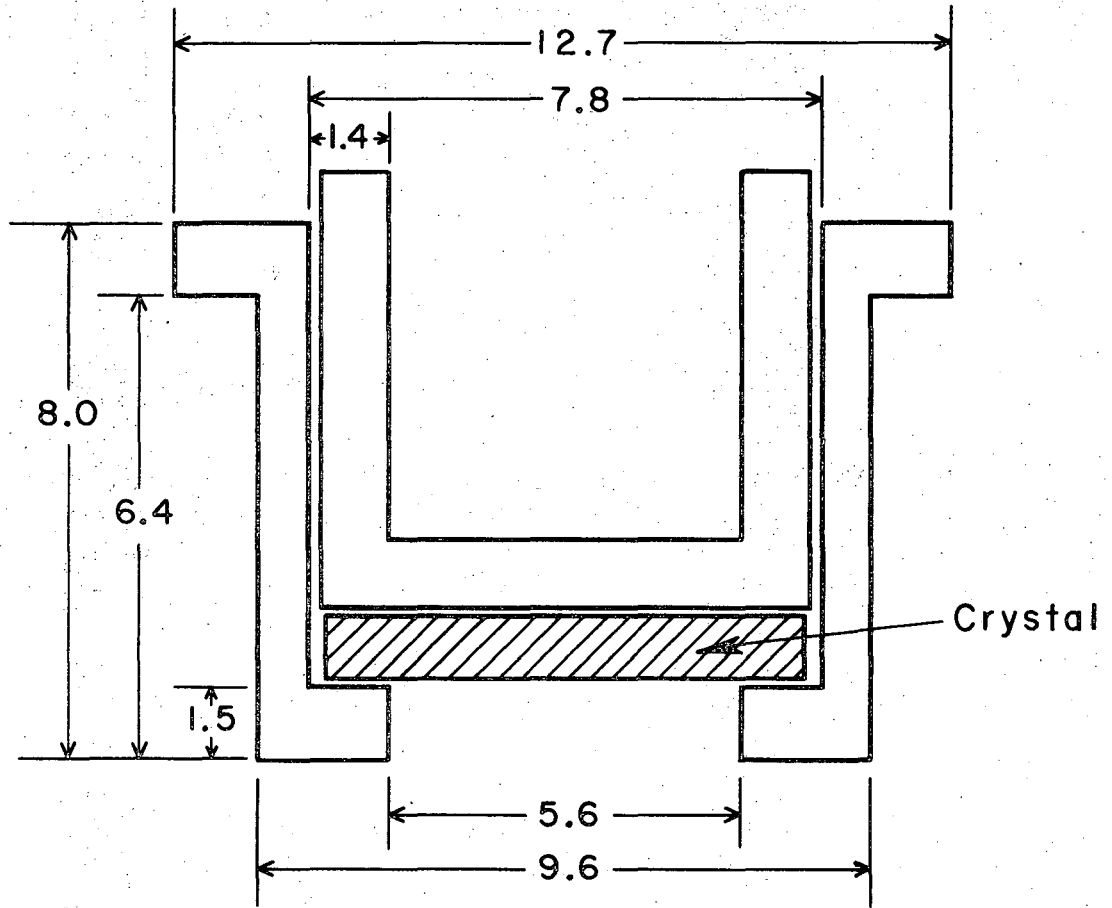
Dimensions in mm

XBL695-2624

Fig. 6. Aluminum Oxide Vaporization Cell

The cell was suspended by a 0.077 mm platinum wire from a quartz semi-micro balance (Fig. 7) so that the crystal vaporized downward. The all-quartz balance is manufactured by Worden Quartz Products, Houston, Texas. The cell is suspended from the sample hook with the appropriate counter-weight hung from the tare hook. The beam pointer, which is observed through a microscope with a movable crosshair, moves a total of 800 divisions from beamstop to beamstop. The sensitivity of the balance, i.e., mg/divisions, is adjusted by hanging weights on the sensitivity adjustment hook. The balance is very susceptable to vibrations and hence the sensitivity of the balance was set at 0.03 mg/division. This meant that if the measured center of the pointer was in error by three divisions, the datum point would be in error by only 0.09 mg. This error was not significant in relation to the weight losses observed in this study.

The balance was calibrated by means of small platinum weights weighed on a Mettler semi-micro electrobalance. The calibration was made across the entire scale and was checked frequently during use, and no change in calibration was found during this study.

The balance assembly was mounted atop a vertical quartz (fused silica) tube heated by a Kanthal coil in the system seem in Fig. 8. A series of quartz hooks hung from the sample hook of the balance and terminated opposite the cell loading port after passing through a slot in a heat shield which protected the balance from radiation from the furnace. The cell and its platinum suspension wire were inserted through this port and hung on the hook. About twenty minutes was required for the

DAMPING MAGNET
(OPTIONAL)

ALUMINUM DAMPING VANE
(OPTIONAL)

PALLADIUM STOPS

BEAM SUSPENSIONS

SAMPLE SUSPENSION

PROTECTION LOOP

APPROX. CENTER
OF MASS

PERMANENT MAGNET
FOR ELECTROMAGNETIC
BALANCING (OPTIONAL)

TARE WEIGHT
SUSPENSION

REFERENCE POINTER

BEAM POINTER

SENSITIVITY ADJUSTMENT
HOOK SUSPENSION

SAMPLE HOOK

TARE HOOK

SENSITIVITY ADJUSTMENT HOOK
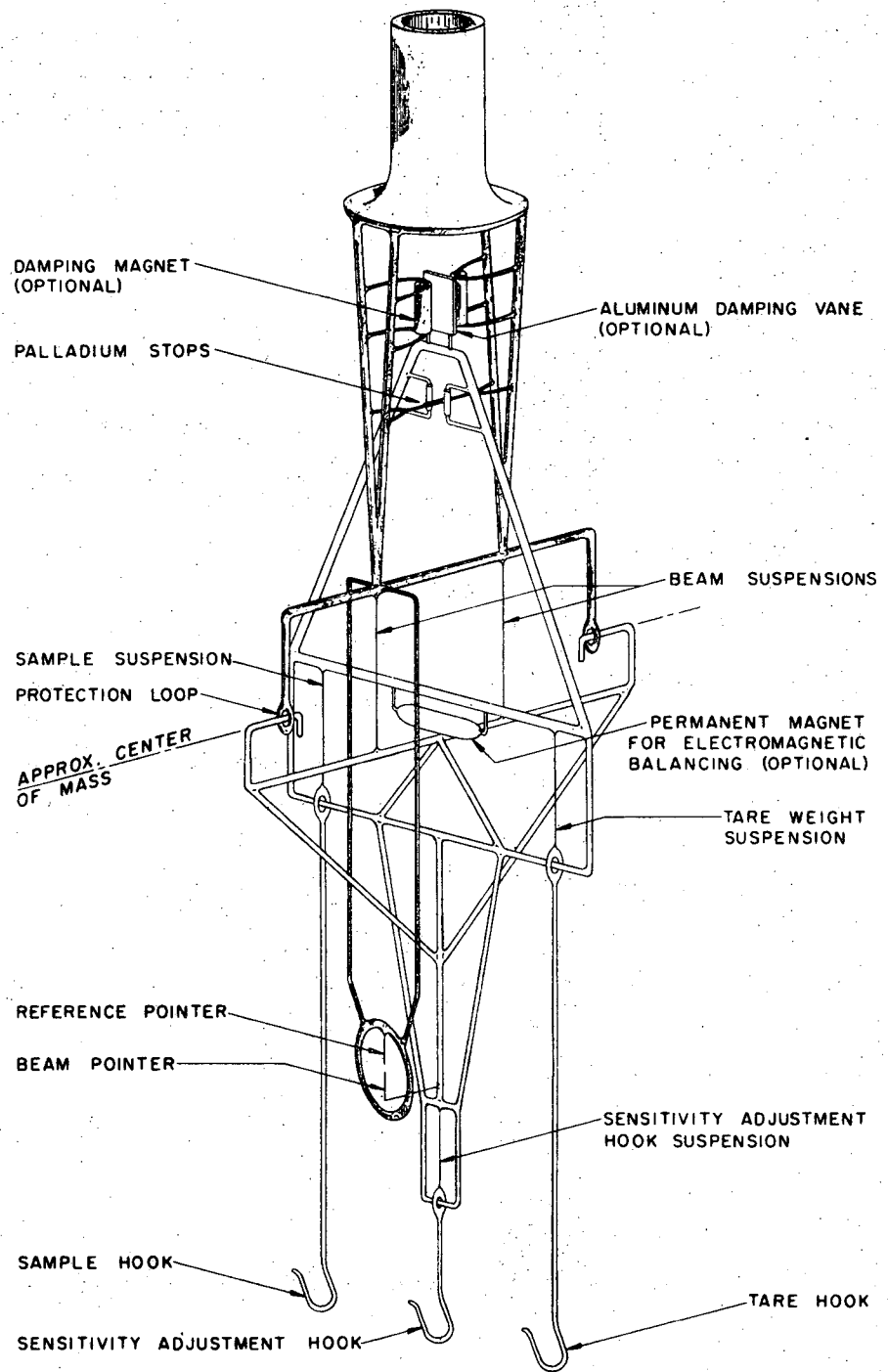
XBL 695-460

Fig. 7.   Quartz Semi-micro Balance

Balance reading microscope

Quartz balance

Radiation shield

Quartz hook

Ion gauge

Cell loading port

Cooling collar

Cell suspension wire

Quartz tube

Heat shields

Kanthal coil

Temperature control thermocouple

Vaporization cell

Leak valve

To vacuum pump

Quartz window
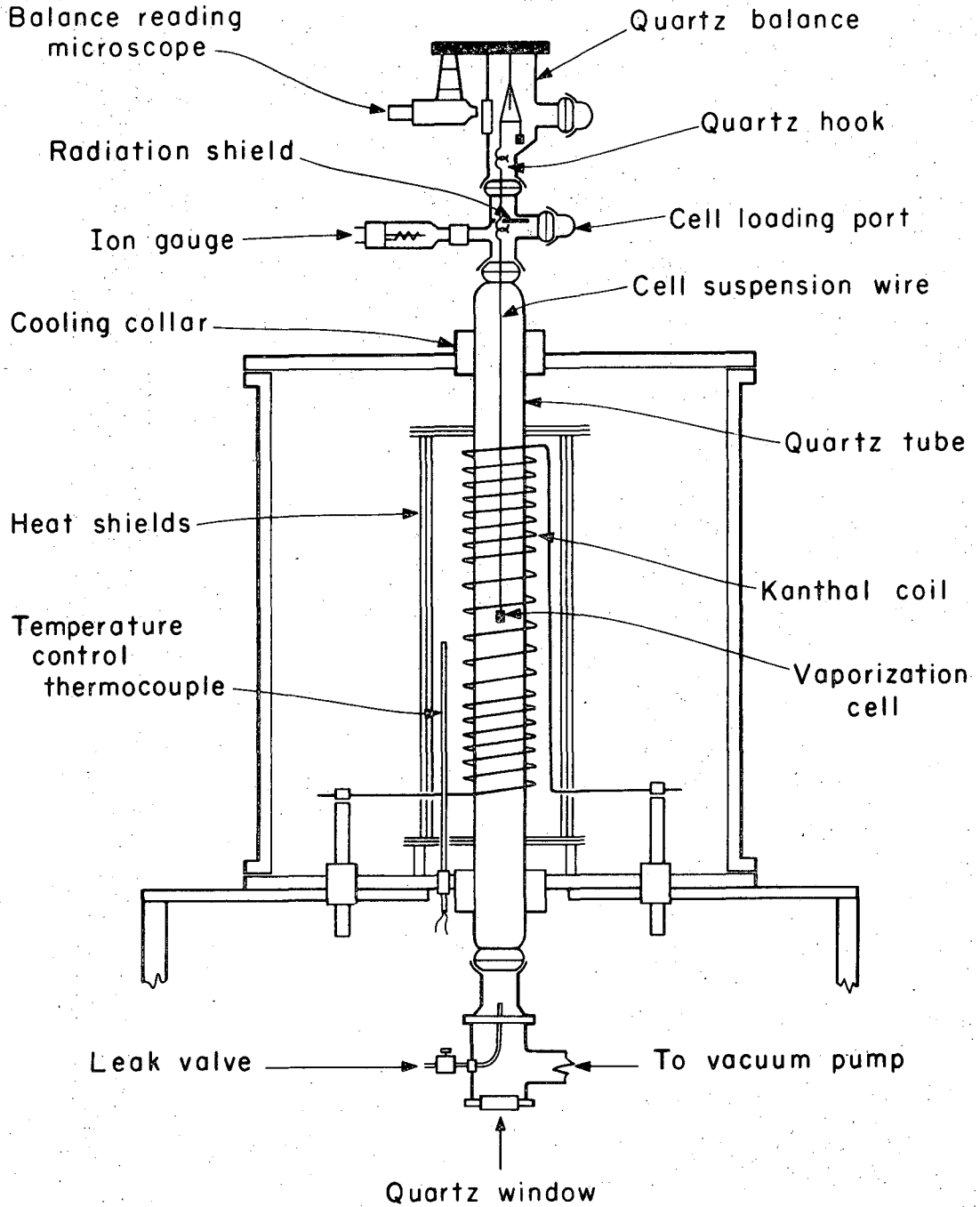
XBL695-2625

Fig. 8. Vacuum Furnace and Balance Assembly

balance vibrations to damp out after the cell was hung on the hook, then the beam pointer was set at about 150 (on the scale of 0 to 800) by hanging small platinum wires on either the tare hook or sample hook.

The quartz tube had an i.d. of approximately 50 mm and was cooled at each end by a water cooling collar which prevented heat conducted up the tube from melting the Apiezon T grease in the ball joints.

The heating coil, which was made of 3.4 mm diameter Kanthal A- 1 was tied to three slotted alumina support rods by 0.4 mm Kanthal wire. The coil was wound so that there were six turns 13 mm apart at the top and bottom and six turns 20 mm apart in the center which gave a constant temperature zone of 3.5 cm. The control thermocouple kept the temperature constant to $\pm 2°C$ at the vaporization temperature of $1107°C$. The furnace tank was filled with argon. The heat shields were initially made of 0.18 mm thick molybdenum, but later the inner shields were made of 0.18 mm thick nickel.

A maximum of 0.3 mg was lost during the 20 to 25 minutes which was required to reach the vaporization temperature.

The system was pumped with a four-inch diameter, three-stage MCF diffusion pump (Octoil-S) with a baffle and liquid nitrogen cold trap. Although the system could be pumped to 4×10^{-6} torr, the pressure rose to 1 or 2×10^{-5} torr during vaporization. The pressure was read with an ion gauge at the top of the system. Since this is at the opposite end of the system from the pumping port, the measured pressure represents a maximum value.

A Granville-Phillips leak valve at the bottom of the system allowed the introduction of various gases. The stainless steel tube aimed the incoming gases directly at the vaporizing surface and hence, because

of the furnace design, there was no opportunity for the gases to react
with the heat shields or the heating coil. Before a gas was introduced
into the system, the gas inlet system was flushed for an hour with the
gas. The carbon monoxide and methane were supplied by the Matheson Company and the oxygen by the Pacific Oxygen Company. The typical impurities,
as stated by the suppliers were as follows:

Gas	Impurities in PPM	
CO	CO_2	200
	O_2	20
	N_2	75
CH_4	N_2	< 50
	O_2	2
	CO_2	10
	C_2H_6	30
O_2	N_2	< 500
	CO_2	2
	Ar	2000

A Cambridge scanning electron microscope was used to examine the
various surfaces. It was operated at 20 kV and at an angle of $20°$ from
the normal to the surface. An excellent discussion of the principles
and operation theory has been given by Kimoto and Russ.[36] The crystals
had sufficient conductivity so that no metallic coating was required in
order to prevent sample charging.

The aluminum oxide cell (Fig. 6) has a channel length to radius
ratio of the oriface of $L/r = 0.54$, and a transmission probability of
0.83 (see the book "The Characterization of High Temperature Vapors"

John Wiley and Sons, Inc., 1967 edited by John L. Margrave. No oriface

correction was made for the vaporization of either zinc oxide of cadmium

sulfide because of their low vaporization coefficients.

IV. RESULTS OF ZINC OXIDE

A. Basal Faces

Figure 9 shows ten basal face vaporizations of eight crystals (both sides of crystals one and three were vaporized.) Although there is some variation of rates within the zinc-face group and within the oxygen-face group, there is a distinct difference between the rates for the two faces. This, and a concurrent, somewhat ambiguous, study by Wolff et al[52] who also studied zinc oxide, provides the first observations of such behavior for a congruently vaporizing compounds. The Ga(111) and As(111) faces of GaAs exhibit different vaporization behavior[47,48] but this compound vaporizes incongruently and liquid gallium remains on the surface.

While the Zn-face was being vaporized, the opposite O-face was being annealed, and vice versa for the vaporization of the O-face. However, there was no observable effect on the rates due to the order of vaporization of the two faces. Also, no difference in vaporization behavior was found between chemically etched and non-etched crystals. Table two gives the history of the crystals whose vaporization behavior is shown in Fig. 9.

Not only were rates of vaporization for opposite faces different, but also the steady-state morphologies were entirely different. Figure 10 shows the vaporization of a Zn-face and an O-face of two different crystals for which vaporization was interupted at the times indicated by arrows so that the developing morphology could be recorded photographically. Figures 11 and 12 show this development.

The Zn-face steady state morphology could not be resolved with the optical microscope at high magnifications because of its roughness, but at low magnifications (i.e. 60X) the surface appears gravel-like or like an "orange peel".

TABLE 2

Vaporization number	Zn-FACE Crystal number[*]	Comments
1	L307 No. 4	Oxygen face vaporized first; Zn face etched with 20 vol. % HNO_3 before vaporization
2	L40B51 No. 7	Previously unvaporized; Zn face etched with 20 vol. % HNO_3
3	L40B85 No. 6	Oxygen face vaporized first; zinc face vaporized with no etching
4	L40B85 No. 3	ZINC DOPED; zinc face had been previously vaporized for a total of eight hours
5	L40B85 No. 9	ZINC DOPED; zinc face had been previously vaporized for a total of seven hours
	O-FACE	
3	L40B85 No. 6	Previously unvaporized; no surface etching
6	L307 No. 3	Previously unvaporized; etched with 20 vol. % HNO_3
1	L307 No. 4	Previously unvaporized; no surface etching
7	L40B51 No. 2	ZINC DOPED; etched with 20 vol. % HNO_3 before zinc doping, not etched after doping
8	L40B85 No. 5	ZINC DOPED; As-received crystal, no surface etching

[*]L40 and L307 are Minnesota Mining and Manufactoring Company lot numbers and B51 and B85 are company batch numbers.

In Fig. 11b, one can easily observe the border between the free surface and the area of the crystal that was under the cell lip. Upon continued vaporization, the border advanced toward the edge of the crystal as can be seen in Figs. 11c and 11d. This slow increase in the effective vaporization area would eventually lead to vaporization rates that were calculated to be about 10% higher. Consequently, crystals that had been extensively vaporized were not used for quantiative measurements.

Occasionally small flat areas or "islands" would be left on the Zn-face after the steady state had been reached, as can be seen in Fig. 11d. It was thought that these "islands" might be caused by surface impurities, especially silicon or aluminum since these elements were present on the surface of the as-recieved crystals. Several crystals which had these "islands" were examined with an electron beam microprobe, but the extremely rough surface prevented quantitative measurements. Silicon and aluminum were found, however, not only on the "islands", but also on the rest of the surface and no corrolation could be made. Generally, surfaces that had many "islands" had vaporization rates that were lower by 15%-20% than those surfaces that had no "islands" but exceptions did occur. These "islands" disappeared after several hours of vaporization.

Figures 12a-d show the development of the steady state morphology on the oxygen face. This surface is clearly different from the Zn-face and can best be described as an array of hexagonal pits. Although the pits are at various depths, they can easily be examined by the optical microscope. In contrast to the Zn-face, no sharp border is produced between the free surface and the area under the cell lip.

Figure 13 through 17 are optical photographs of the Zn-face steady state morphologies on five crystals. Although there are differences in the degree of roughness (note the two magnifications in these five photos) the similarities are readily apparent. The Zn-face surfaces were too rough and irregular to be replicated for examination with the electron microscope, however, they could easily be examined with the scanning electron microscope (SEM). Figures 18 through 21 are SEM photos of four Zn-face steady state morphologies, three of which are seen in the preceding series of optical photographs. Figures 22 and 23 are scanning electron micrographs of the "islands" of Fig. 11d. The SEM "looks at" the surface at an angle of $20°$ from the normal, and flat areas that appear shiny under an optical microscope appear as various shades of gray with the SEM.

The surface of L40B51 No. 7 (SEM photo Fig. 18; optical photo Fig. 14) is somewhat atypical because of the large peaks which jut up from the surface. Otherwise, these Zn-faces can best be described as "mountain peaks separated by narrow valleys".

Figures 24 through 27 are optical photographs of the O-face steady state surfaces. The higher magnifications of Figs. 26 and 27 clearly show the hexagonal pits. Figure 28 is a low magnification SEM of the oxygen steady state surface, and Figures 29 and 30 clearly show the hexagonal pits on the O-face. Figure 31 shows steps on some small, steep-sided pits that developed on the surface that was under the cell lip.

B. Effects of Foreign Gases, Excess Zinc and Adsorbed Water

Three possibilities might account for the difference in vaporization rates between the Zn-face and O-faces:
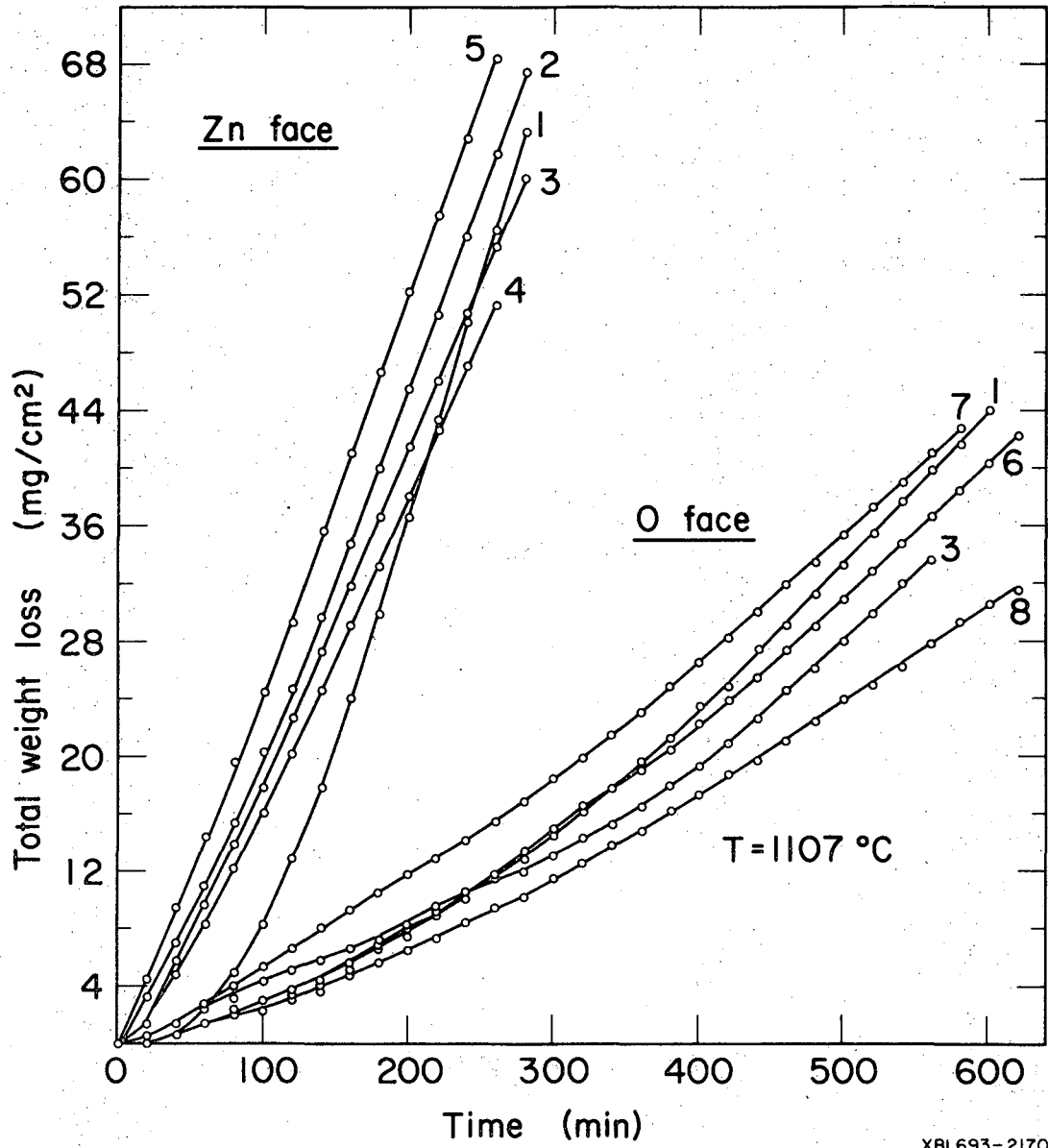
Fig. 9. Vaporization of Zn(0001) and O(000$\bar{1}$) Faces
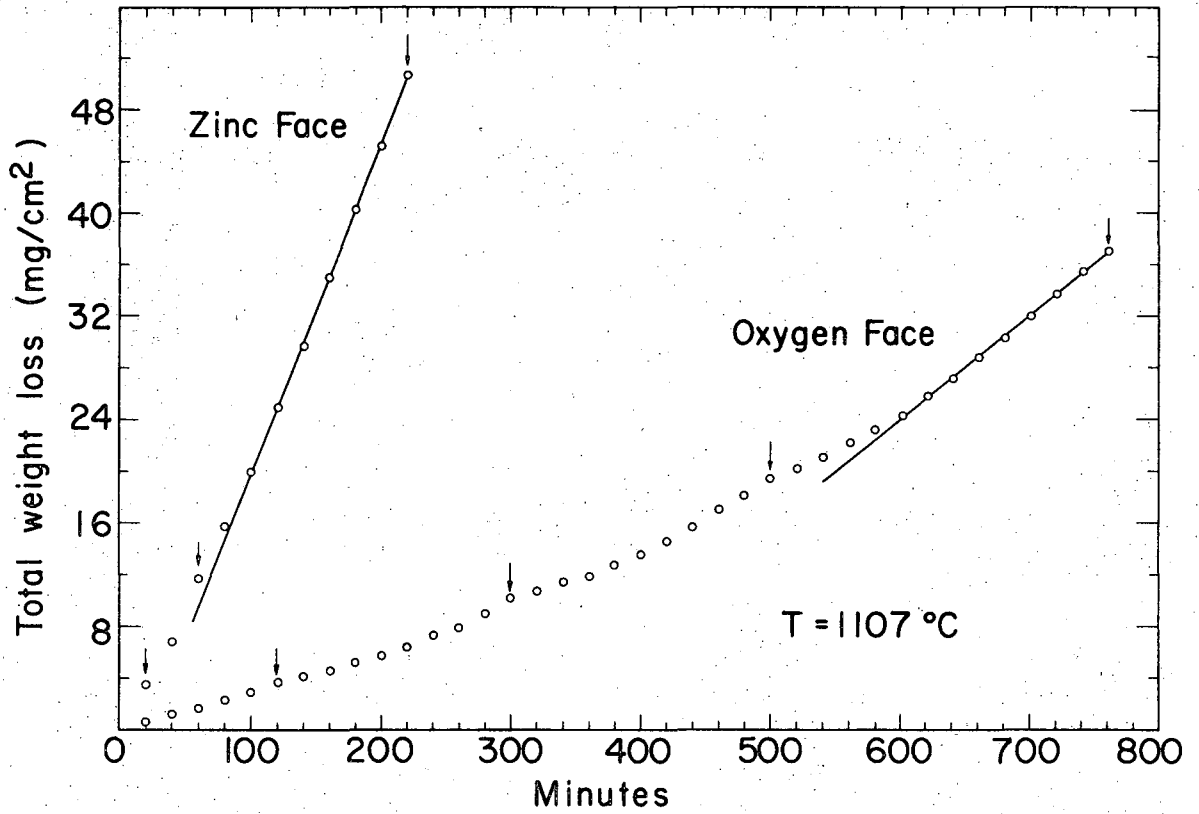
Fig. 10. Vaporization of a Zn-face and an O-face for Photographic
Sequences in Figs. 11 and 12.

XBB696-3617

Fig. 11a. Zinc-face as-received, before vaporization in Fig. 10.

.5 m m
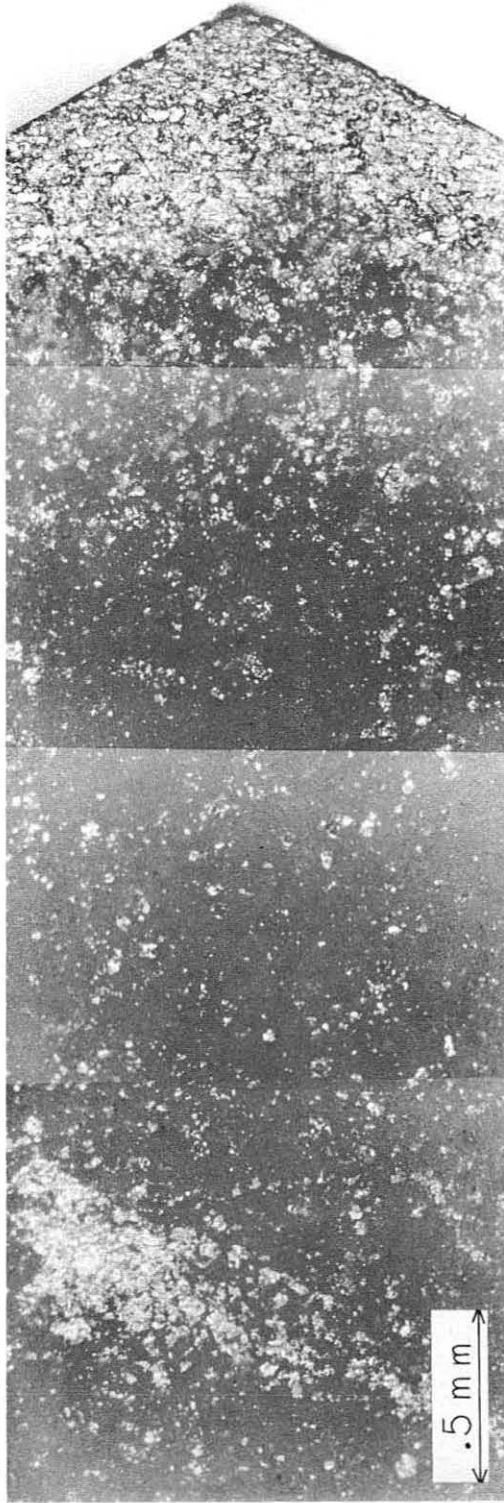
XBB696-3619

Fig. 11b. Zinc-face after 20 minutes (see Fig. 10).
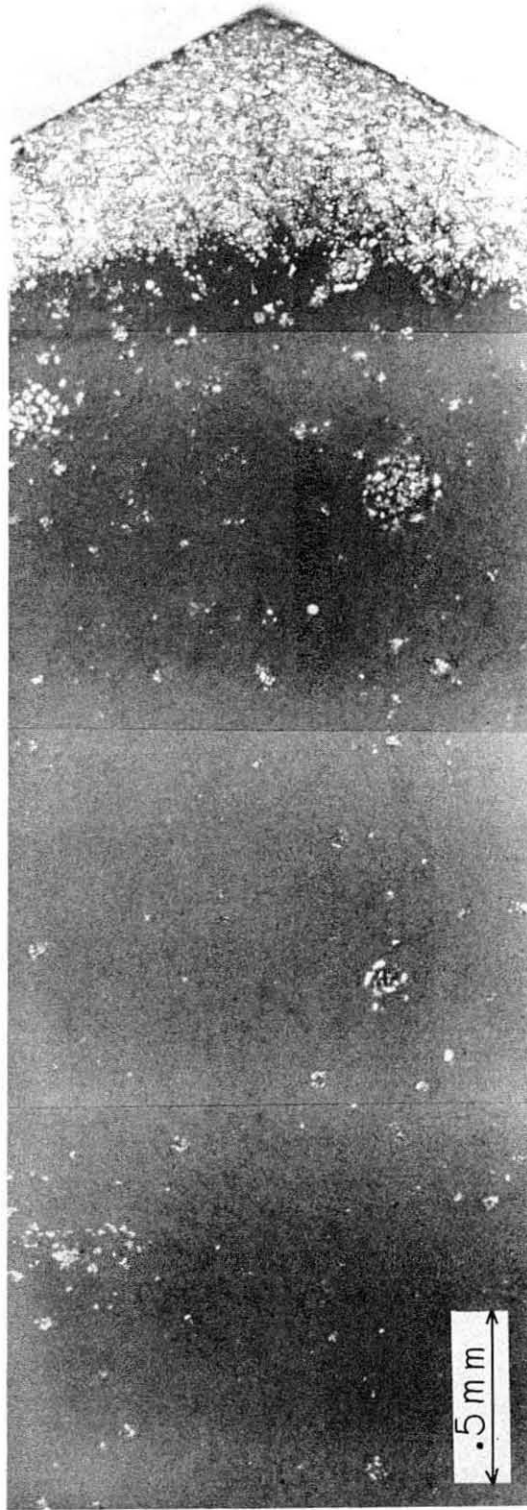
XBB696-3620

Fig. 11c Zinc-face after 60 minutes (see Fig. 10).
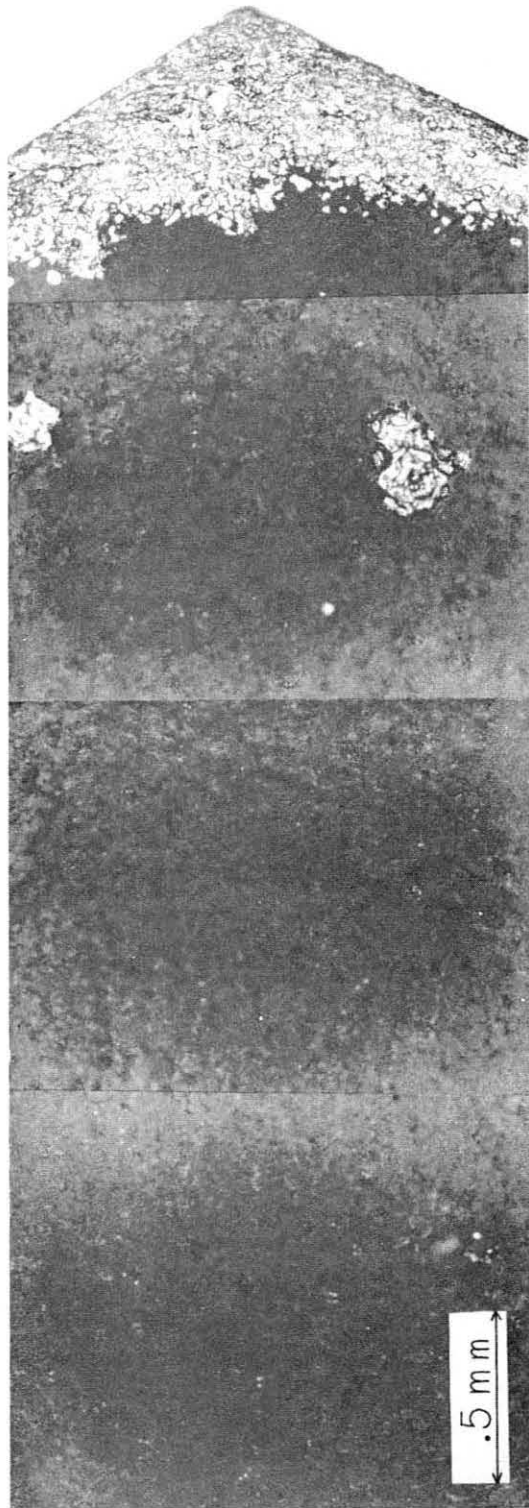
XBB696-3621

Fig. 11d. Zinc-face after 220 minutes (see figure 10).

XBB696-3618

Fig. 12a. Oxygen face as-received, before vaporization in Fig. 10.
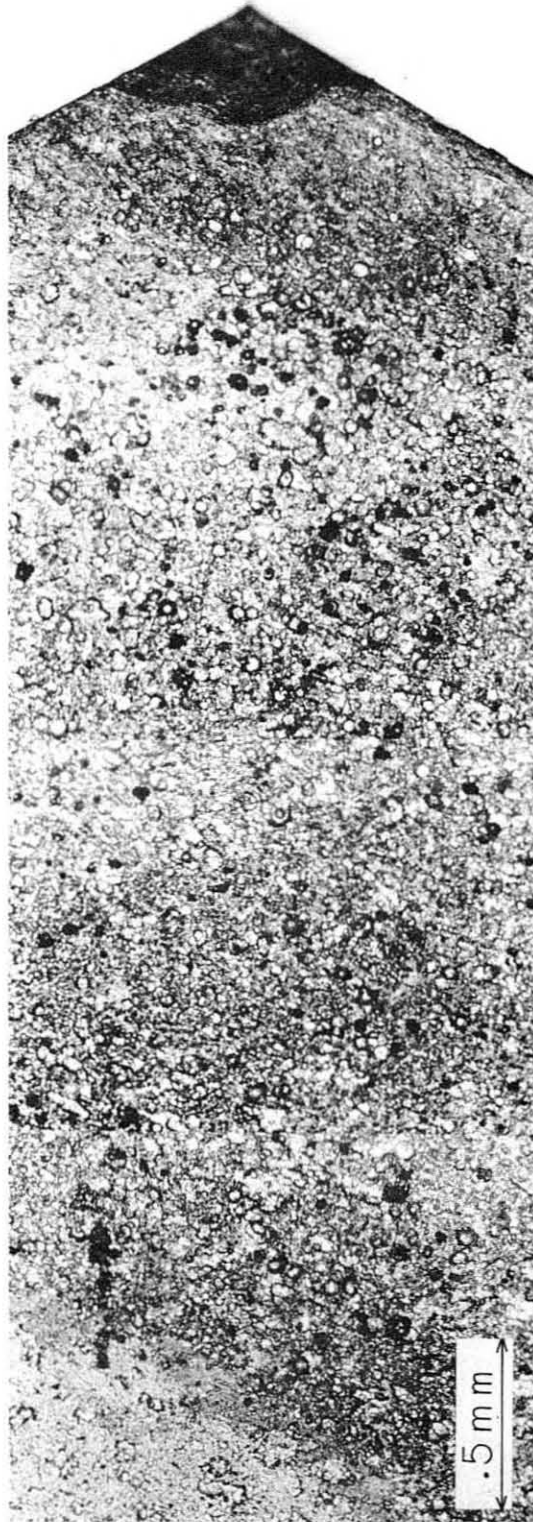
XBB696-3622

Fig. 12b. Oxygen face after 120 minutes (See Fig. 10).
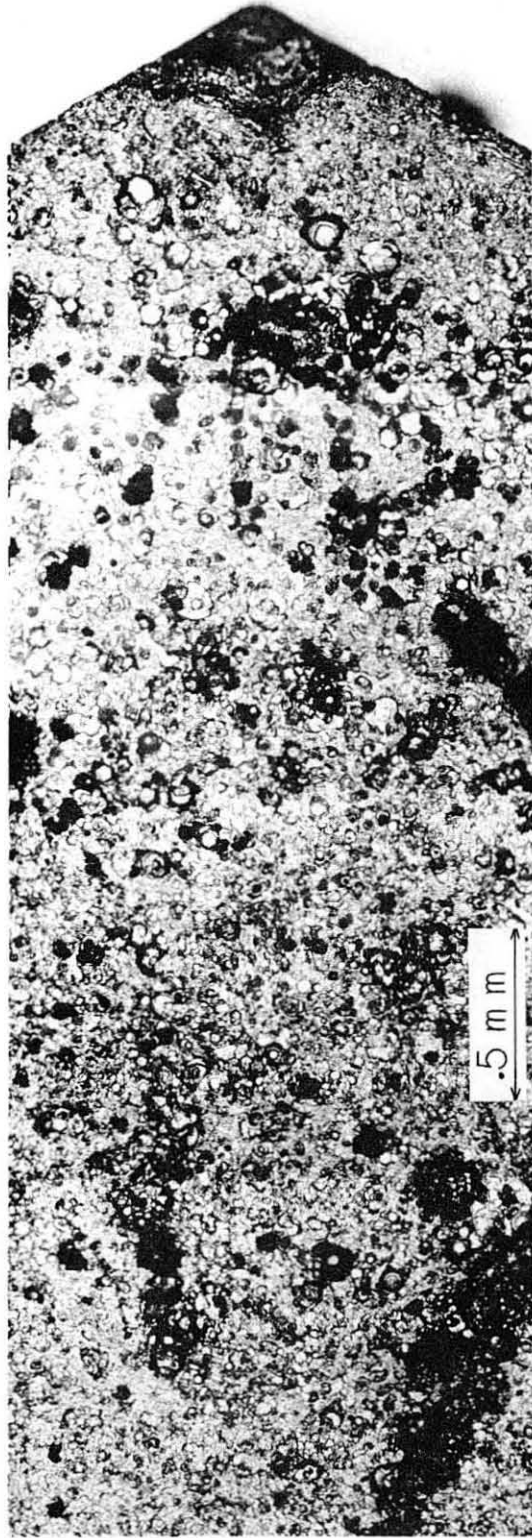
XBB696-3616

Fig. 12c. Oxygen-face after 300 minutes (See Fig. 10).
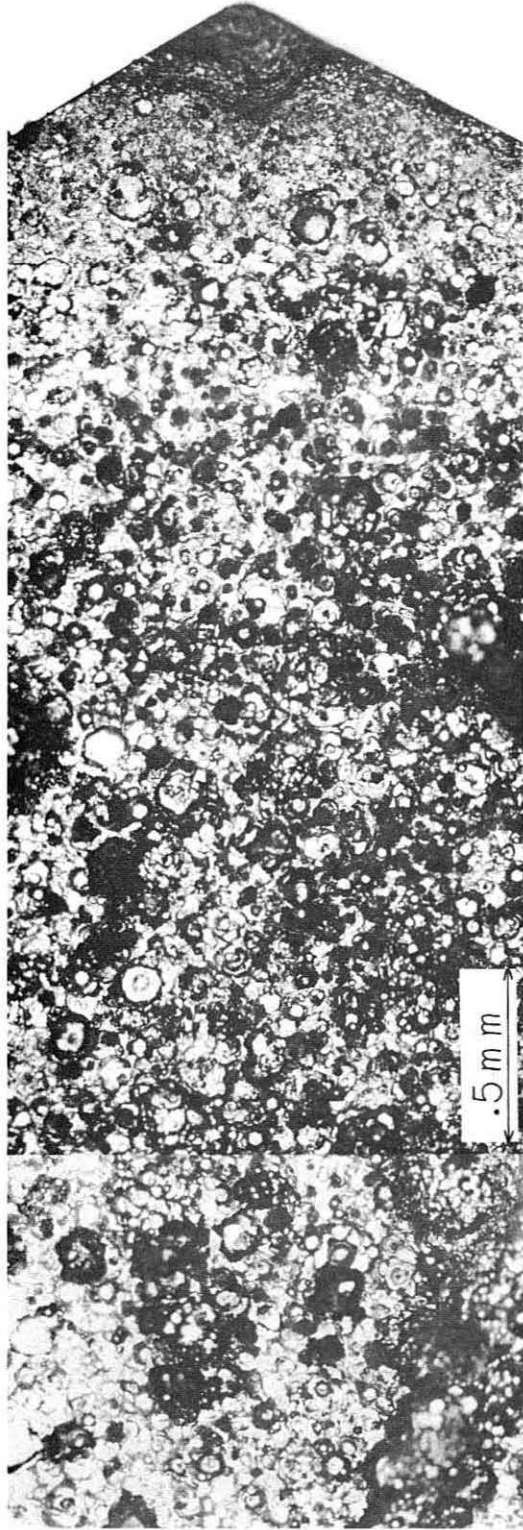
XBB696-3623

Fig. 12d. Oxygen-face after 500 minutes (see Fig. 10).
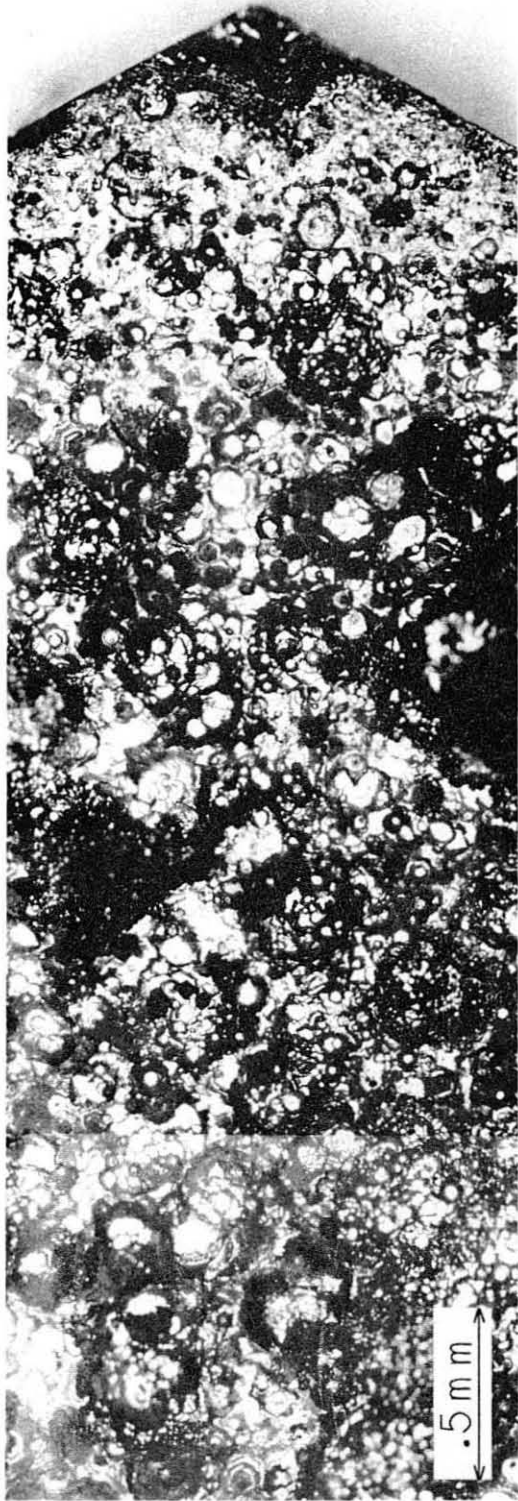
XBB696-3624

Fig. 12e. Oxygen face after 760 minutes (See Fig. 10).

.5 m m
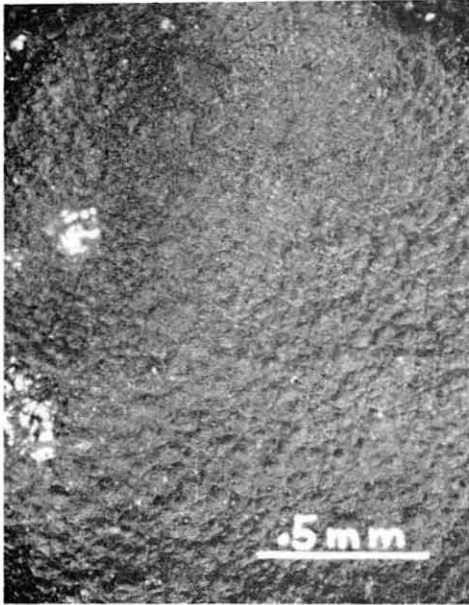
Fig. 13. Crystal L40B85 No.2
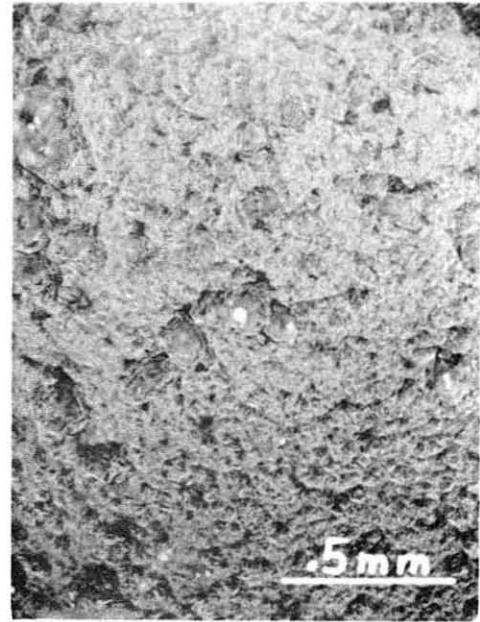
Fig. 14. Crystal L40B51 No. 7

XBB701-432

Zinc-face steady-state surfaces (optical photographs)
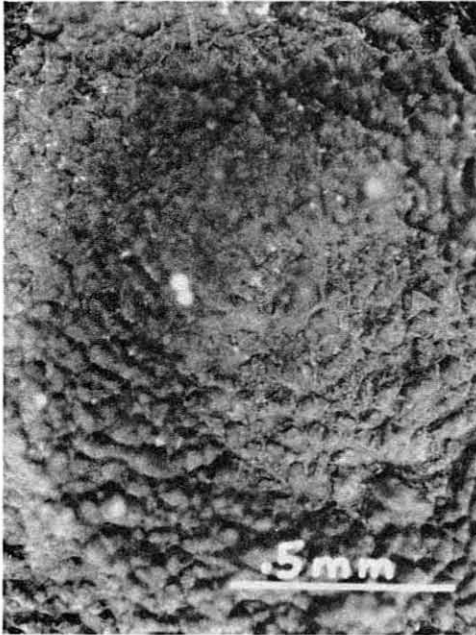
Fig.15. Crystal LAOB85 No.3
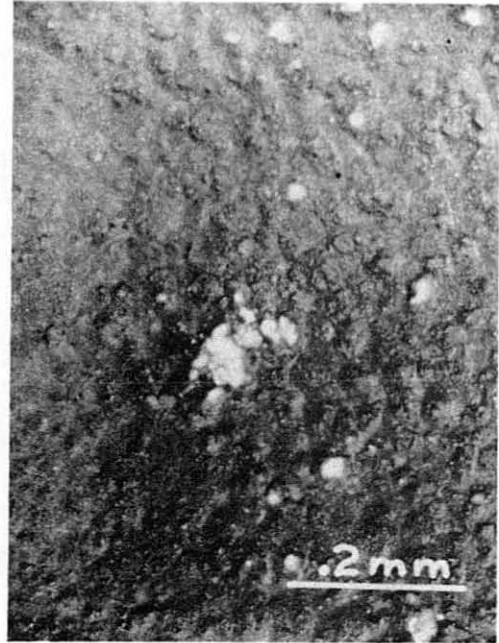
Fig.16. Crystal L307 No. 8

XBB701-434

Zinc-face steady state surfaces (optical photographs)
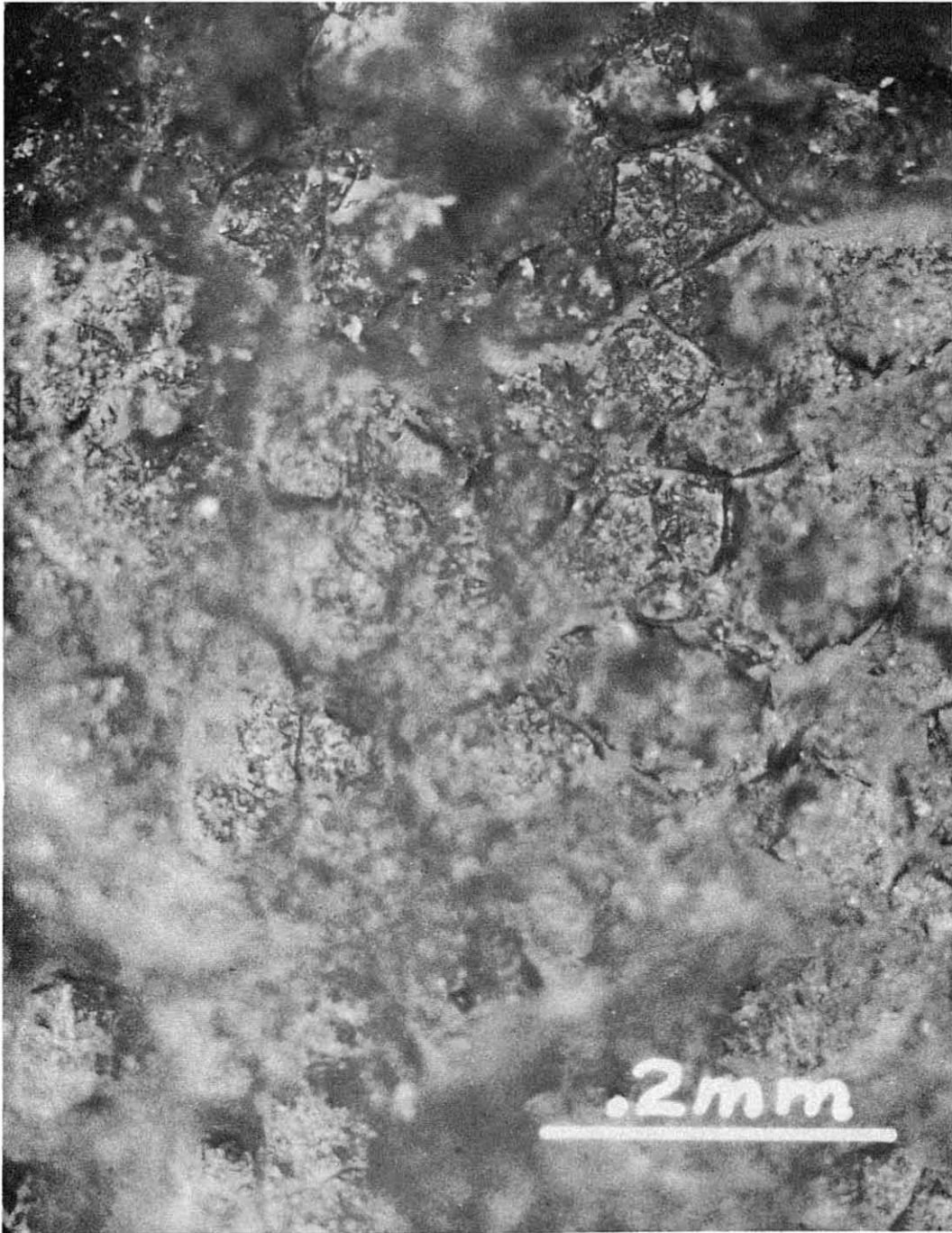
XBB701-440

Fig. 17. Crystal L307 No. 5. Zinc-face steady-state surface
(optical Photograph)
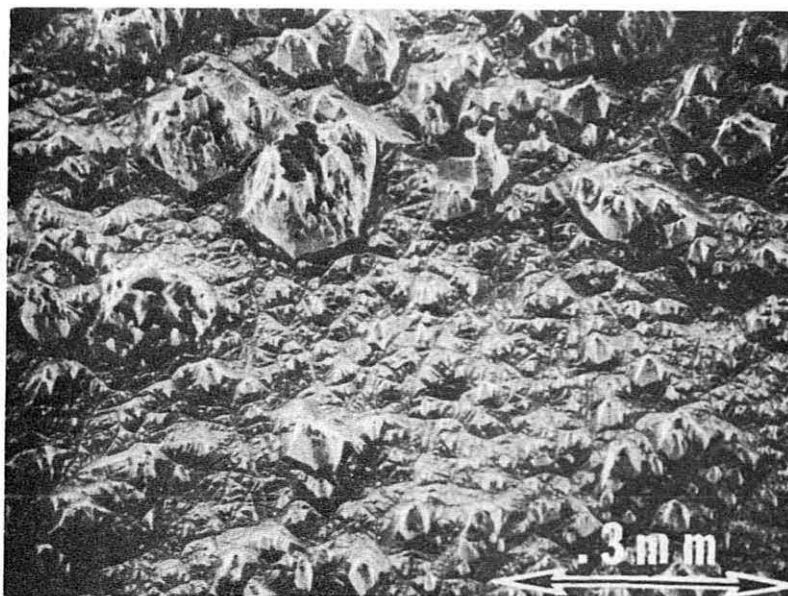
Fig. 18a. Scanning electron micrograph of zinc-
face steady-state surface in Fig. 14.

Fig. 18b. Detail of center of Fig. 18a.
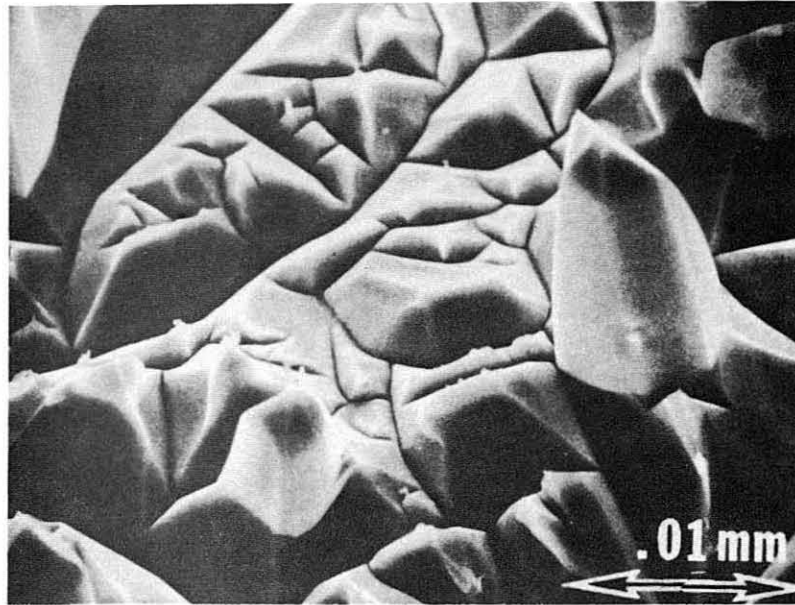
Fig. 18c. Detail of center of Fig. 18b.
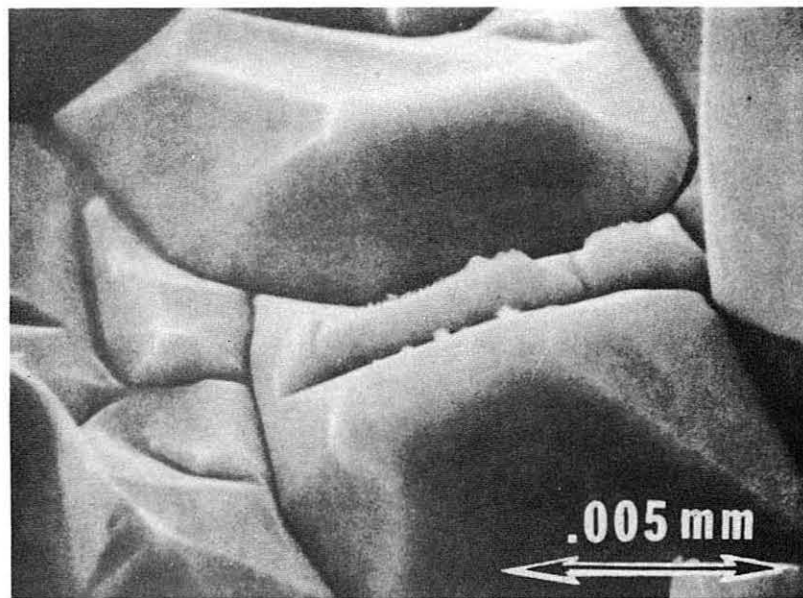
Fig. 18d. Detail of center of Fig. 18c.

XBB701-430
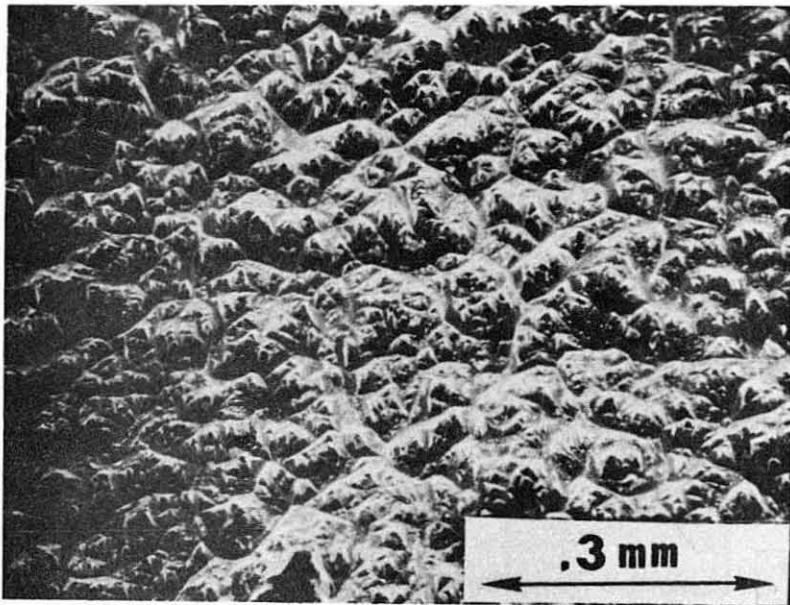
Fig. 19a. Scanning electron micrograph of zinc-
           face steady state surface in Fig. 13.
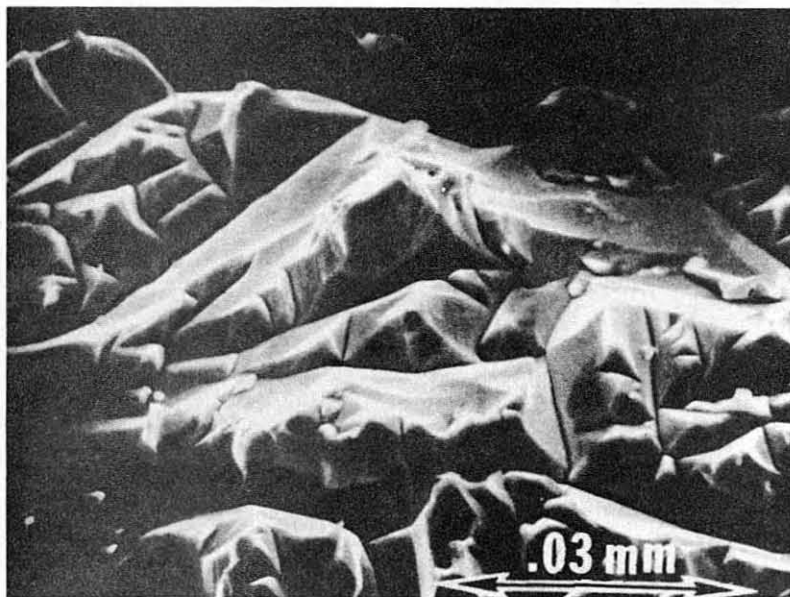
Fig. 19b. Detail of Fig. 19a.

XBB701-429
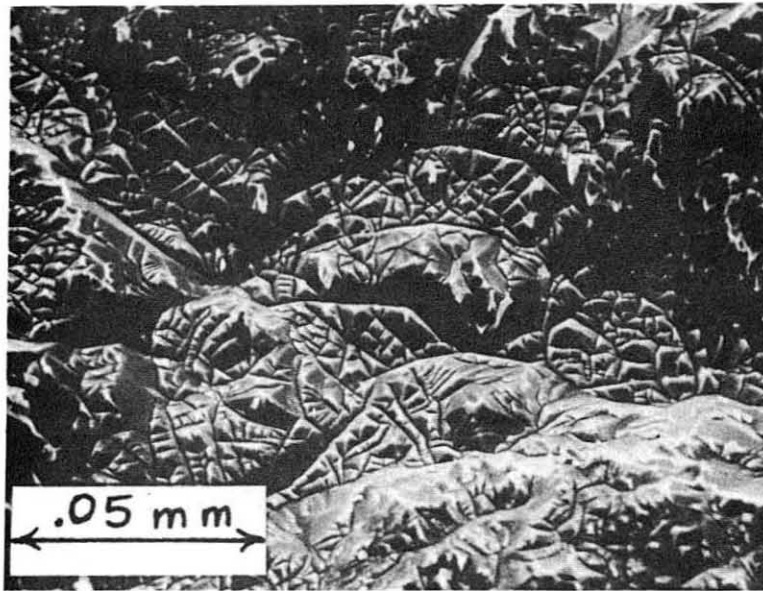
Fig. 20a. Scanning electron micrograph of zinc-
face steady-state surface in Fig. 17.
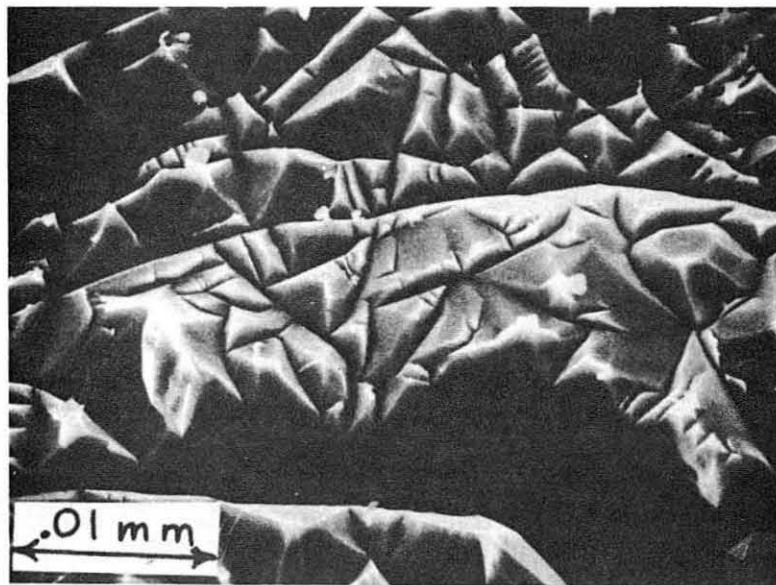

Fig. 20b. Detail of Fig. 20a.

XBB701-431
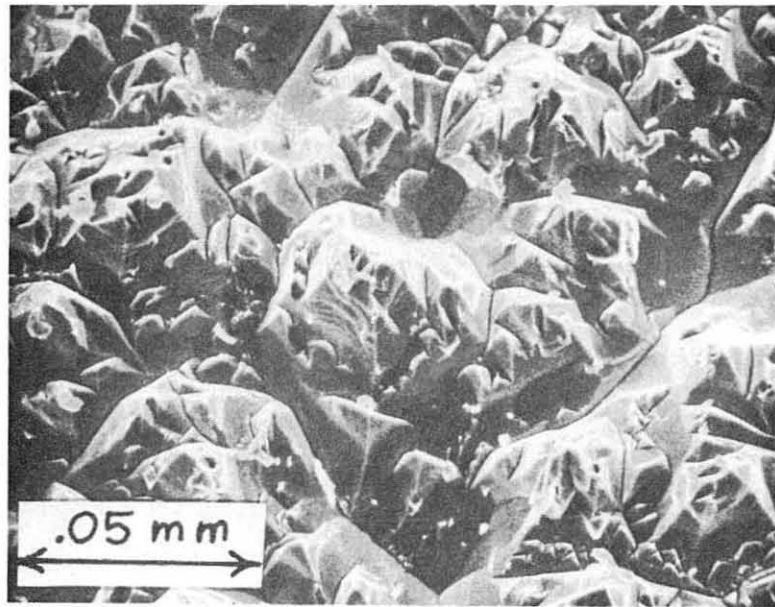
Fig. 21.   Scanning electron micrograph of zinc-
face steady-state surface of crystal
L40B85 No. 7.
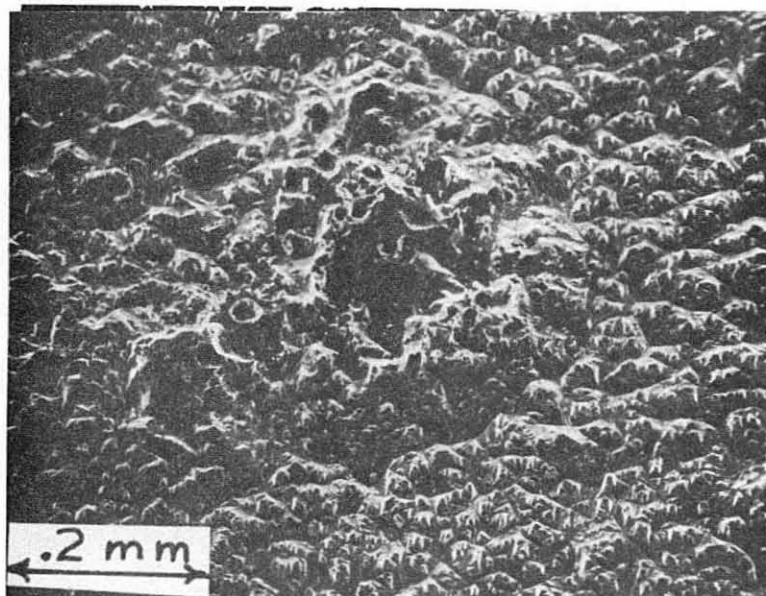
Fig. 22a.   Scanning electron micrograph of an
"island" on zinc-face steady-state
surface (crystal L40B85 No. 7).
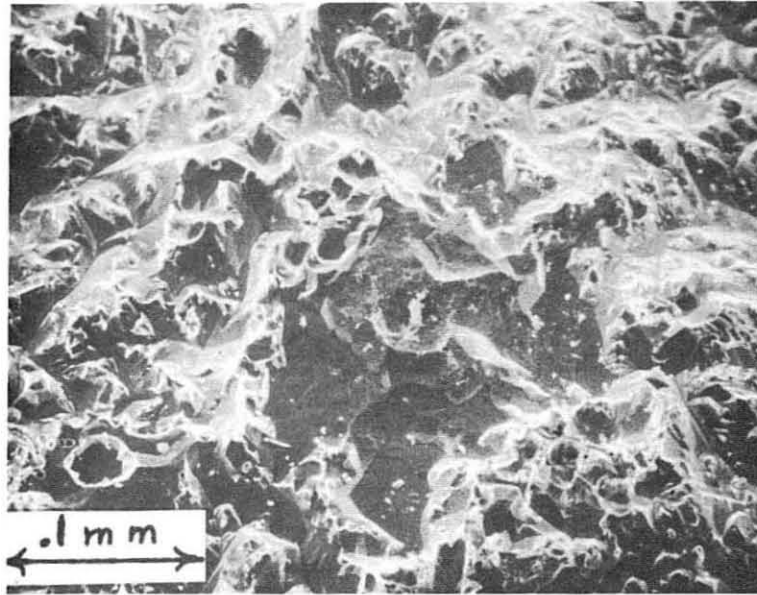
Fig. 22b. Detail of center of Fig. 22a.
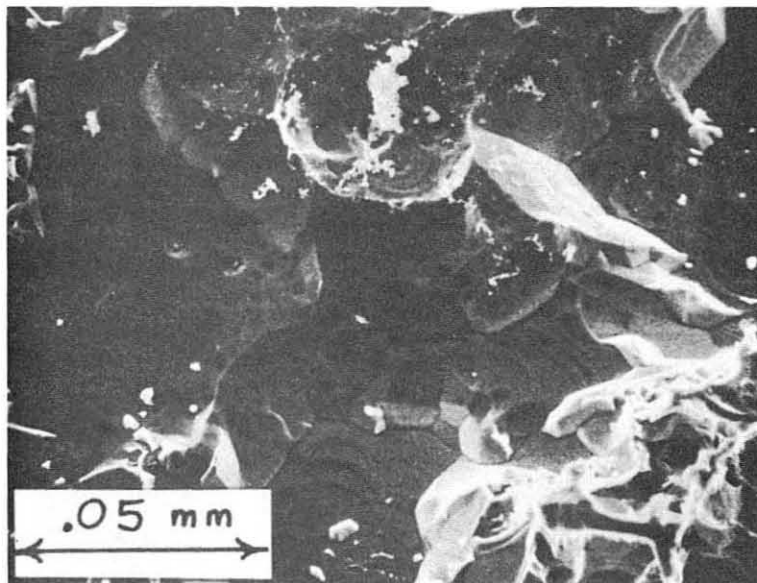
Fig. 22c. Detail of center of Fig. 22b.

XBB701-426
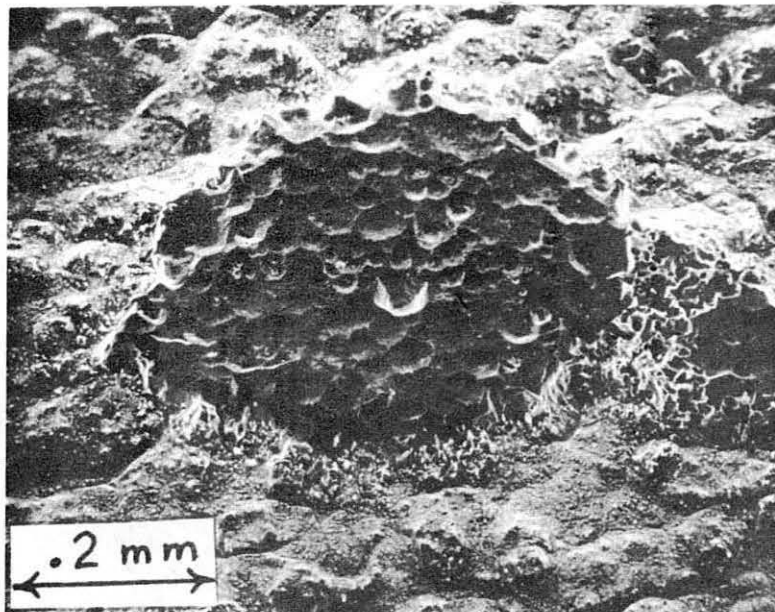
Fig. 23a. Scanning electron micrograph of an "island" on zinc-face steady-state surface (crystal L307 No. 5).
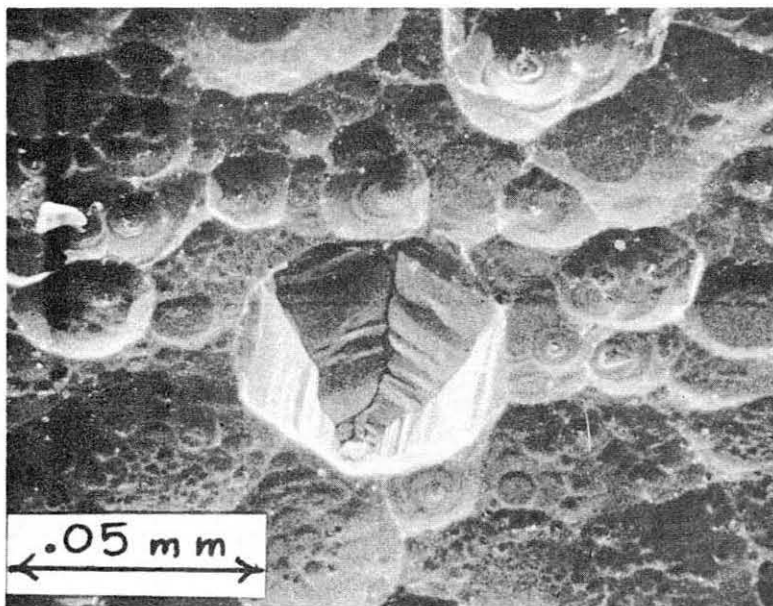
Fig. 23b. Detail of center of Fig. 23a.

XBB701-427
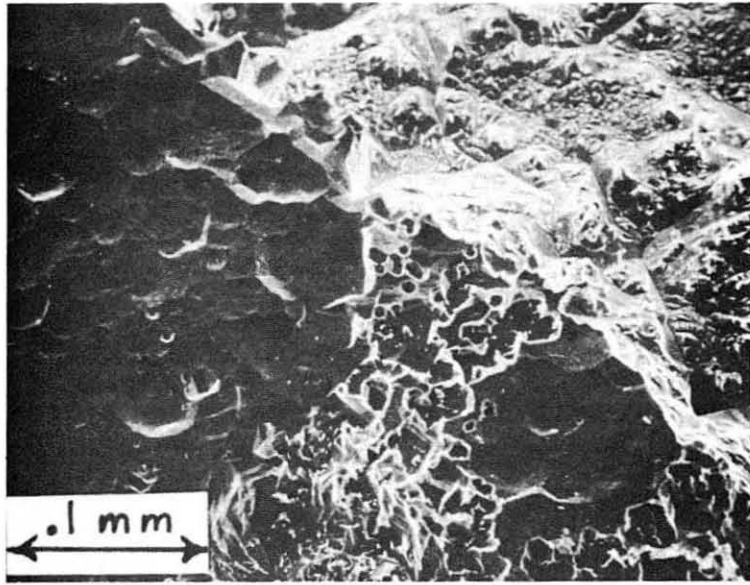
Fig. 23c. Detail of edge of "island" in Fig. 23a.
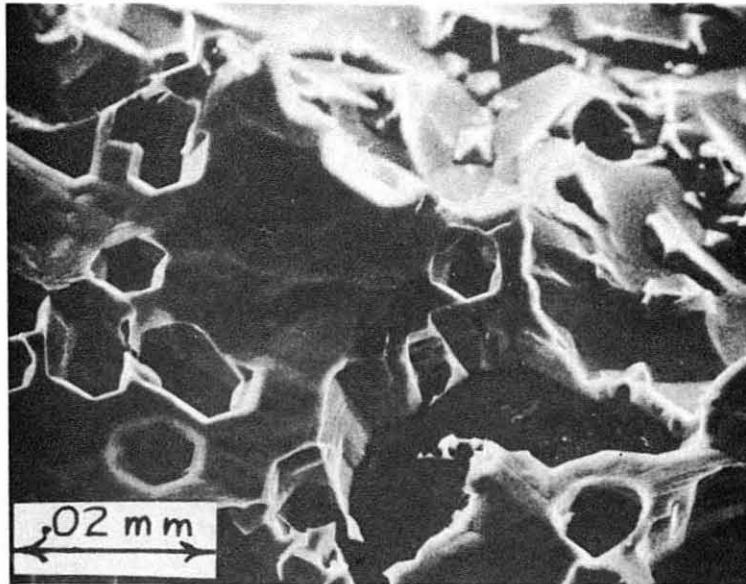
Fig. 23d. Detail of center of Fig. 23c.
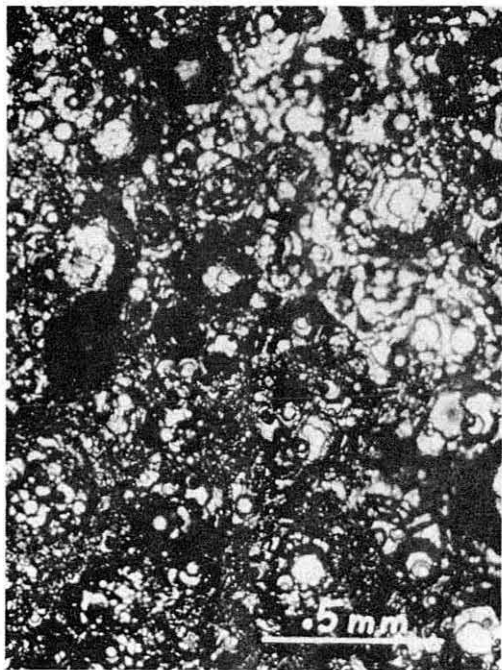
Fig.24   Crystal L307 No.3   Fig.25.   Crystal L40B51 No. 2
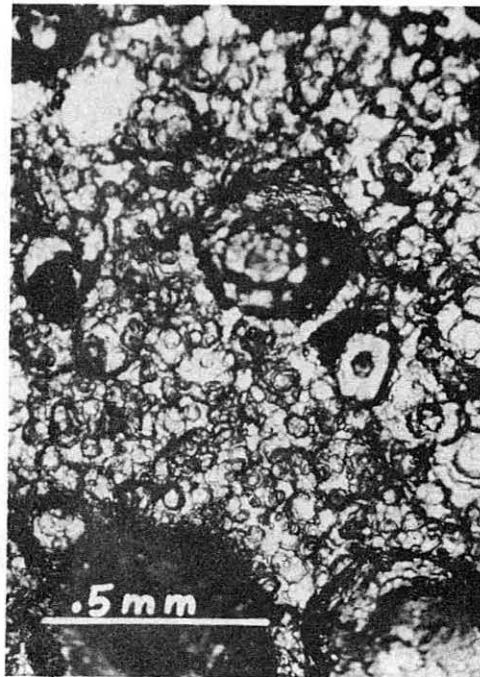
Oxygen-face steady-state surfaces (optical photographs)

XBB701-424
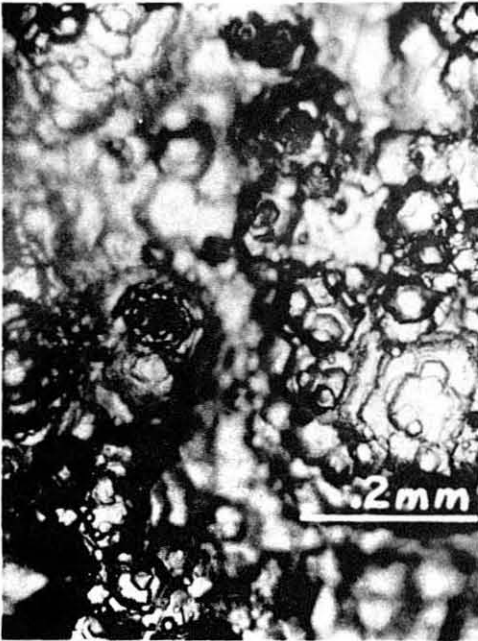
Fig.26.   Crystal L307 No. 3
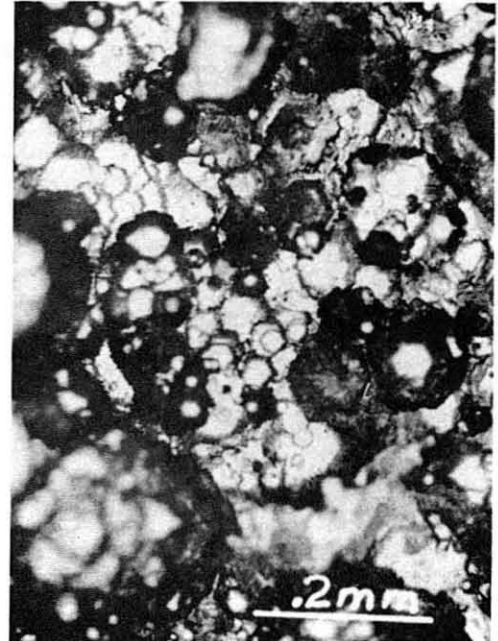
Fig. 27.   Crystal L307 No. 9

Oxygen-face steady-state surfaces (optical photographs)

XBB701-425
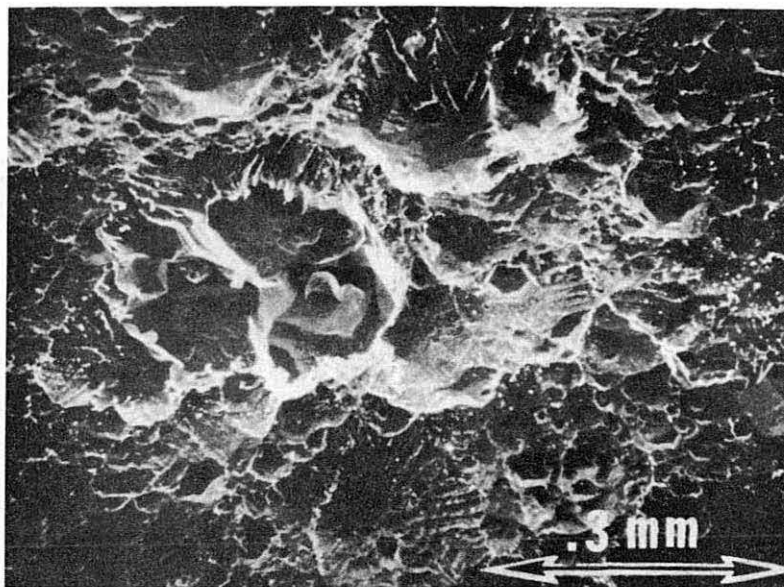
Fig. 28. Scanning electron micrograph of an oxygen-
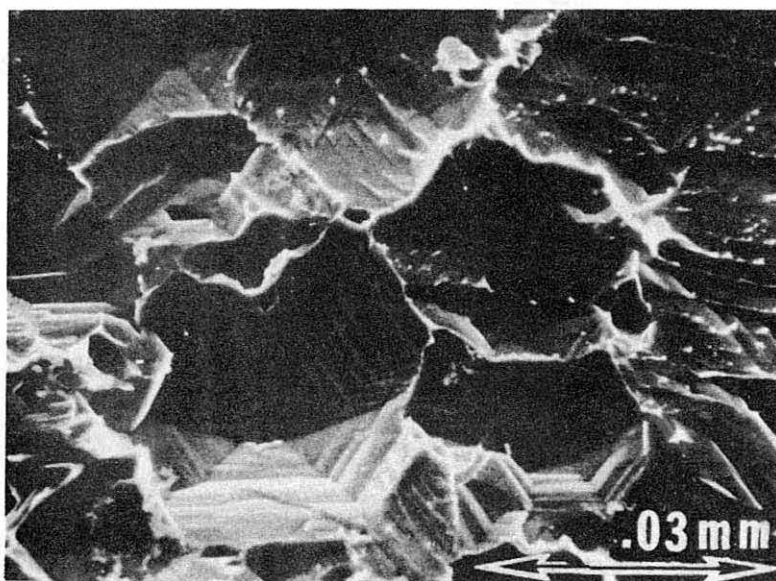   face steady-state surface (crystal L307 No. 3)

Fig.29.   Scanning electron micrograph of an oxygen-
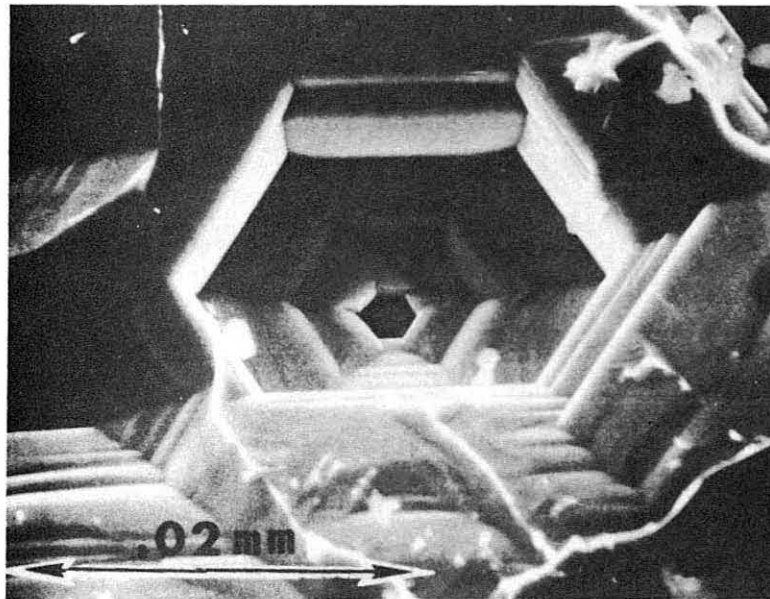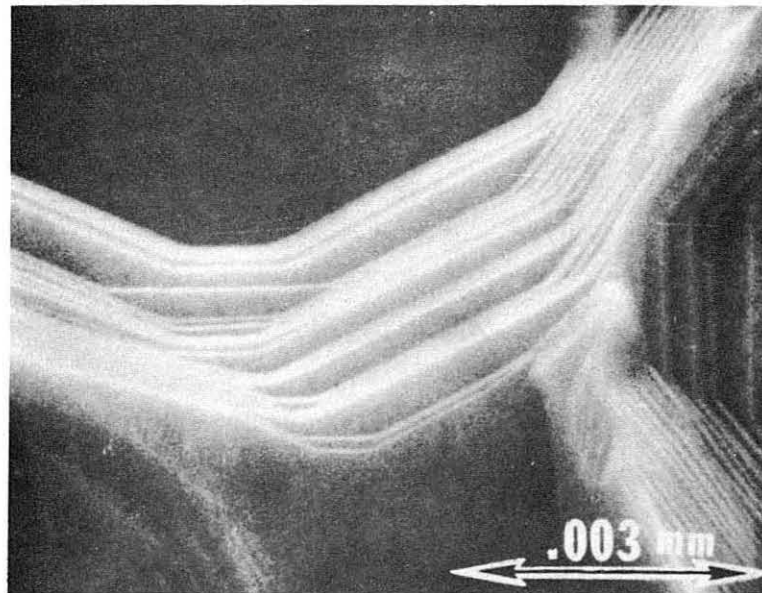   face steady-state surface (crystal L307 No.3).

XBB701-422

Fig.30. Scanning electron micrograph of an oxygen-
face steady-state surface (crystal L307 No.3)

Fig. 31. Scanning electron micrograph of ledges in
pits near edge of crystal under cell lip.

XBB701-438

(1) The asymmetry of the c-axis could directly influence the rate
of removal of surface atoms. That is, the rate at which the atoms leave
the lattice might be directly influenced by the different atomic arrange-
ment on the opposite basal faces.

(2) Impurities might be adsorbed on one face more strongly than
on the opposite face because of the different atomic arrangement. This,
in turn, could alter the kinetics.

(3) Residual gases in the system might react with the Zn-face at
a higher rate than with the O-face.

In order to test the latter possibility, the effect of additions
of about 8×10^{-4} torr of gases that might be expected to be in the back-
ground was tested. This pressure would produce a flux of about 10^{17} O_2
molecules/cm^2-sec onto the surface due to the background pressure of
oxygen as compared to a vaporization flux of about 10^{16} O_2 molecules/cm^2-sec
at the vaporization temperature of $1107°C$. Oxygen, methane, and carbon
monoxide were bled into the system through a leak valve as described in
the experimental section. The results for methane and carbon monoxide
on both the Zn-face and the O-face are seen in Fig. 32. The dashed
lines represent the maximum and minimum slopes for the vaporizations in
Fig. 9, which were done in the absence of background gases. No apparent
change in the vaporization rate of either the Zn-face or the O-face is
produced by either of these two gases.

The vaporizations of zinc oxide in the presence of a background
pressure of oxygen was measured both with powder samples and with a single
crystal. A platinum basket 2 mm deep and 6 mm in diameter was constructed

and filled with powder. A much higher vaporization rate was observed for the powder samples because of the much larger surface area, but the rate slowly decreases as the sample sinters. The introduction of 7×10^{-4} torr of oxygen produced no measurable change in vaporization rate for either the powder samples (Fig. 33) or for the single crystal (Fig. 34).

Vaporizations 4, 5, 7 and 8 in Fig. 9 were performed on crystals that had previously been zinc doped with enough zinc to give them a distinct red-orange color. When heated in vacuum at $1107°C$, the crystals lost the red color within 20 minutes or less and showed no apparent difference in subsequent vaporization rates from the rates of undoped crystals.

Several attempts were made to change the oxygen concentration by annealing the crystals in oxygen. Crystals were first annealed in a closed container for forty hours at $1120°C-1140°C$ to determine the effect of the annealing process itself. Annealing the crystals in an aluminum oxide container led to pronounced induction periods upon their subsequent vaporization. These induction periods were greatly reduced if the crystals were etched with nitric acid or cleaned in an ultrasonic cleaner after they were annealed. This strongly suggests that the annealing contaminated the surface. These induction periods were almost entirely eliminated when the crystals were wrapped in platinum foil before insertion into the alumina cell.

A cell for annealing the crystals in a flow of gas was fabricated from a one cm. diameter platinum rod. A 4 mm diameter alumina tube led the incoming gases to a slot in the center of the platinum cell which held the crystal.
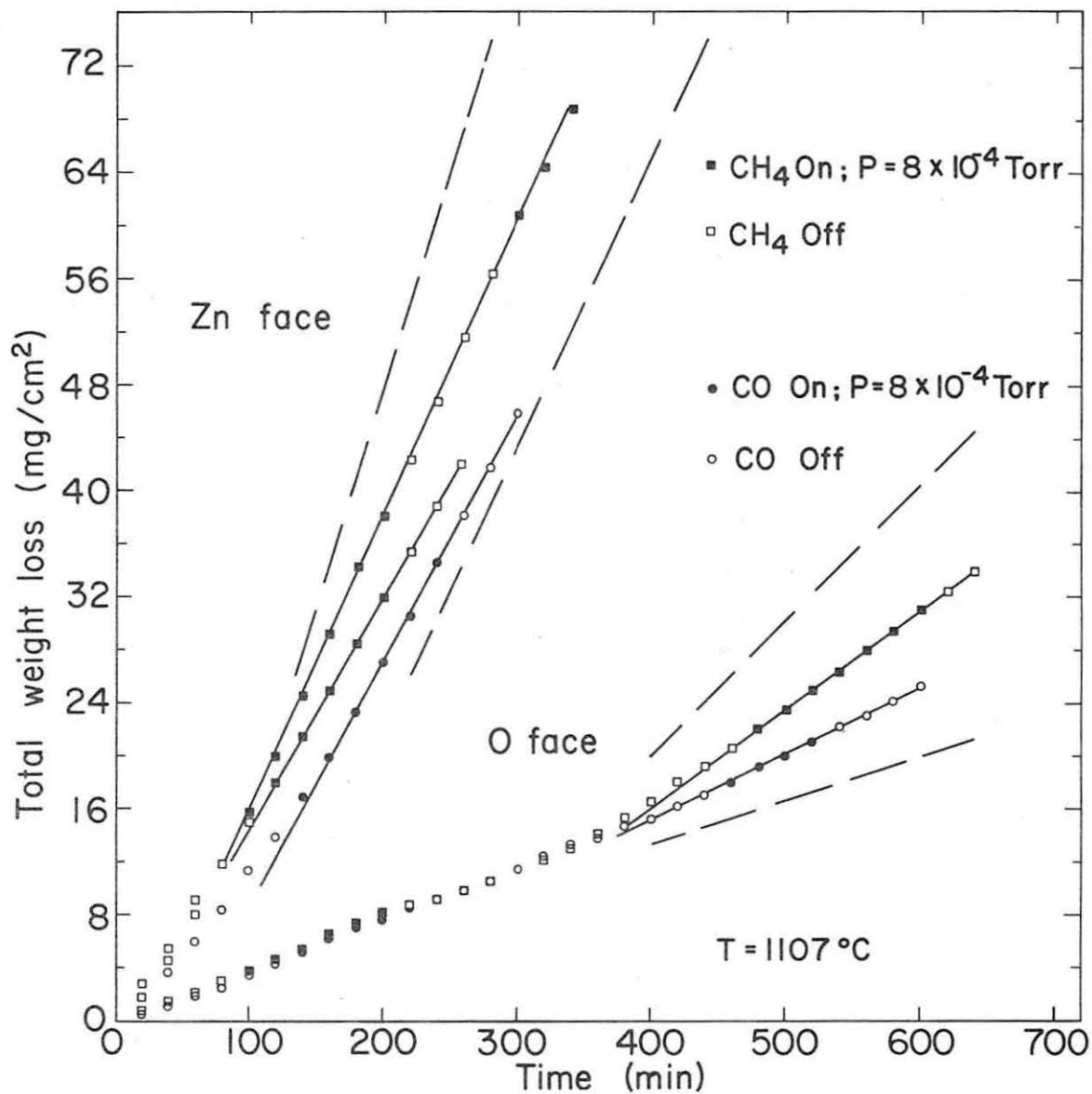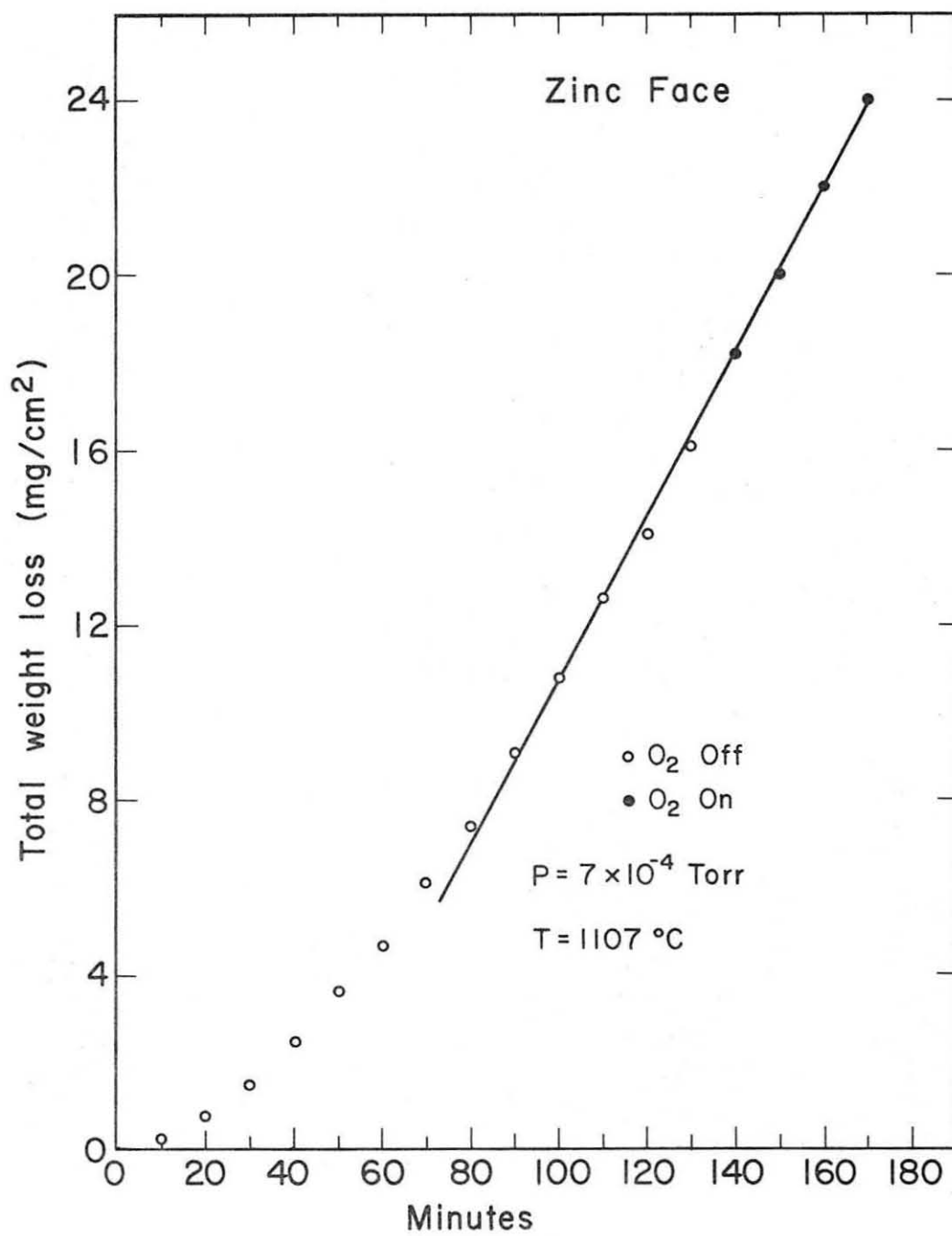
Fig. 32. Vaporization of Zn(0001) and O(000$\bar{1}$) faces in the presence of methane and carbon monoxide
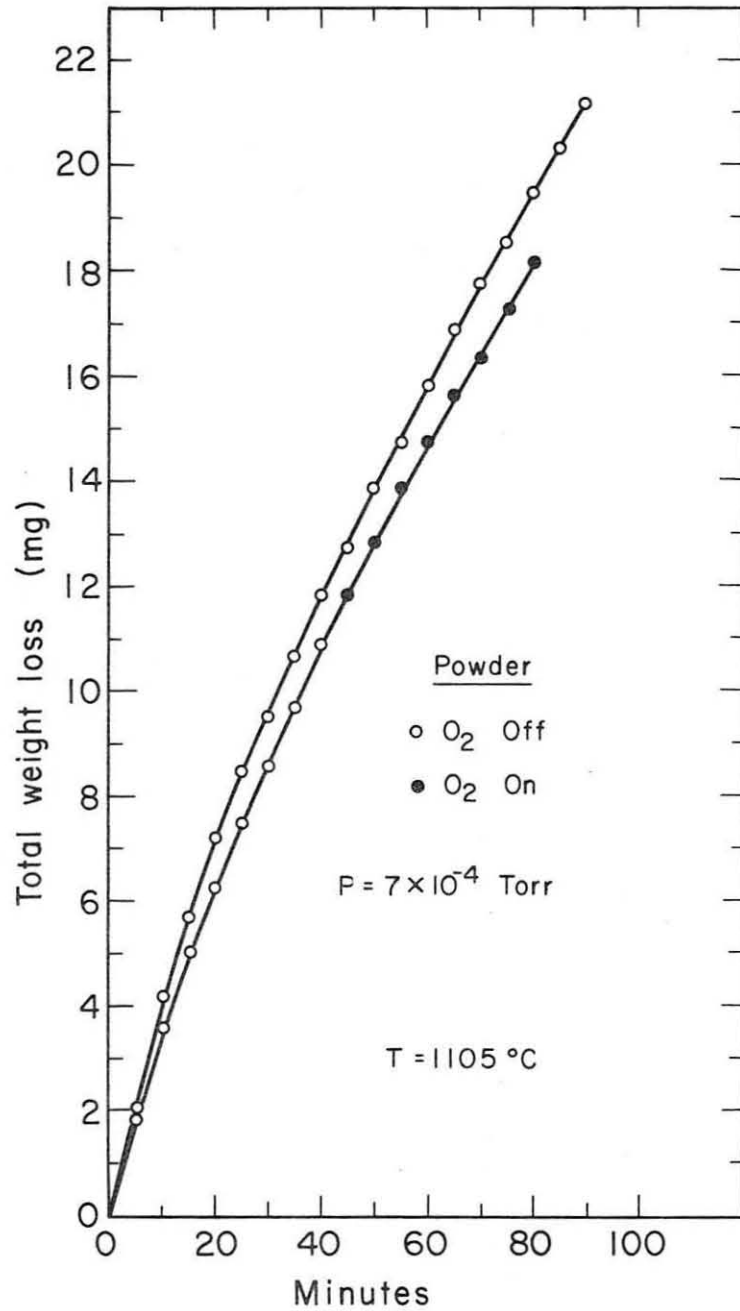
XBL701-2083

Fig.33. Vaporization of zinc oxide powder in vacuum
and in presence of oxygen

Fig.34. Vaporization of Zn-face in presence of oxygen

Crystals annealed for 70 hours at 1050°C in a flow of tank argon or oxygen showed pronounced induction periods upon subsequent vaporization. The weight loss of the crystal due to transpiration during the argon anneals was 50 times greater than during the oxygen anneals. This result is consistent with the expected influence of oxygen on the vaporization equilibrium ZnO(s) = Zn(g) + 1/2 O$_2$(g). Since both the tank argon and oxygen contained approximately 4 ppm water, it was suspected that the induction periods were due to reaction of water with the surface. Consequently, anneals were done in a flow of argon and oxygen which had been bubbled through water. The flow of wet gas was terminated before the crystals were cooled. These "wet anneals", however, eliminated the induction periods observed in vaporizations after the "dry anneals" although the weight losses observed for the crystals during their anneals were comparable.

The water in the annealing gases may have prevented the crystal surface from getting contaminated. Apparently the effects of the surface contaminants is greater than any effect of the oxygen annealing.

The vaporization curves in Fig. 9 exhibit induction periods, that is, periods of time during which the rate slowly changes before a constant steady state rate is reached. Part of this may be due to the formation of the final steady state morphology for crystals that had not been previously vaporized. However, such induction periods are also observed for crystals which had reached the steady state morphology but had been stored in air in glass containers.

Since zinc oxide vaporizes to gaseous zinc atoms and oxygen molecules, there is always zinc and oxygen present in the system. When a crystal is

cooled in the system after a vaporization is completed, the crystal might change in stoichiometry, at least on the surface. The subsequent vaporization would show an induction period until the stoichiometry changed to the steady state value if the rate depended on the zinc to oxygen ratio. Excess zinc has been shown to escape quickly, so **excess** oxygen is the more likely source of the induction periods. If oxygen is responsible, then quenching the crystal in oxygen at the conclusion of a vaporization should produce a large induction period in the subsequent vaporization.

The procedure followed was to close the valve to the diffusion pump at the conclusion of the vaporization, turn off the furnace, and then fill the system with tank oxygen to a pressure of about 700 torr. The system was then allowed to cool overnight and the following morning the system was evacuated and the vaporization was continued without removing the crystal. Figure 35 shows the results of two such oxygen quenches. In each case the induction period has been entirely eliminated and the vaporization has continued precisely from the point where it was halted. After 340 minutes total vaporization, the crystal was cooled in the system under a mechanical pump (MP) vacuum and remove for approximately one hour for examination. This procedure produced a small induction period, as can be observed.

In Fig. 36 the crystal was quenched in a similar manner with tank nitrogen and again the induction period was eliminated. Cooling the crystal in a static vacuum (i.e., closing the valve to the diffusion pump and reheating without exposure to air) also eliminated the induction period. Again, opening the system (when cool) to air produced a small induction period, and another oxygen quench eliminated it. Occasionally

the crystal could be removed for short times (less than one hour) with no subsequent induction period, but this was not the usual case. Finally, Fig. 36 shows a second nitrogen quench with no subsequent induction period.

Figure 37 shows the vaporization of an as-recieved crystal with the typical initial induction period. After 260 minutes it was removed and stored in air in a glass container for twelve weeks. The subsequent vaporization exhibits a pronounced induction period typical of a long exposure to lab air. A quench in argon followed by reheating without exposure to laboratory air also eliminates any induction period.

These results strongly suggest that the cause of the induction periods is adsorbed water. Hence, after 500 minutes (in Fig. 37) the crystal was nitrogen quenched and quickly removed from the system and stored for one week at room temperature in a dessicator containing water instead of a dessicant so that the air was saturated with water vapor. The crystal was in contact only with the water saturated air and not in contact with the liquid water. The subsequent vaporization exhibited the most pronounced induction period observed for any vaporization. At the conclusion of this vaporization, the crystal was stored for ten days in another dessicator containing fresh phosphorous pentoxide. This storage still produced an induction period, although much shorter as can be seen. These experiments with wet and dry storage were repeated, and the results were similar.
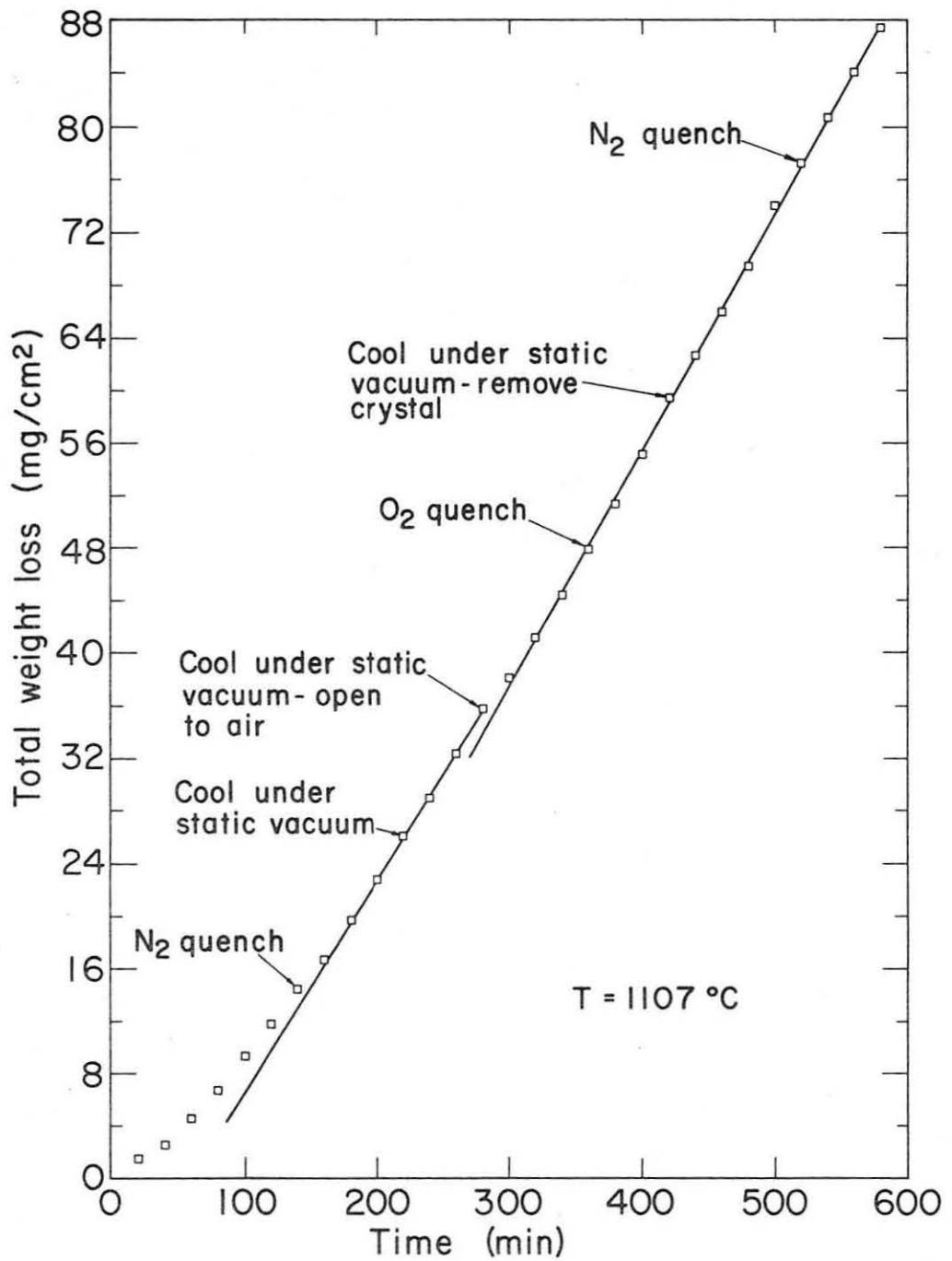
C. Prismatic Face Vaporizations

The six prismatic planes of the wurtzite structure are all crystallographically equivalent. Hence one should get similar vaporization rates and similar morphologies when a prismatic slice is vaporized in opposite
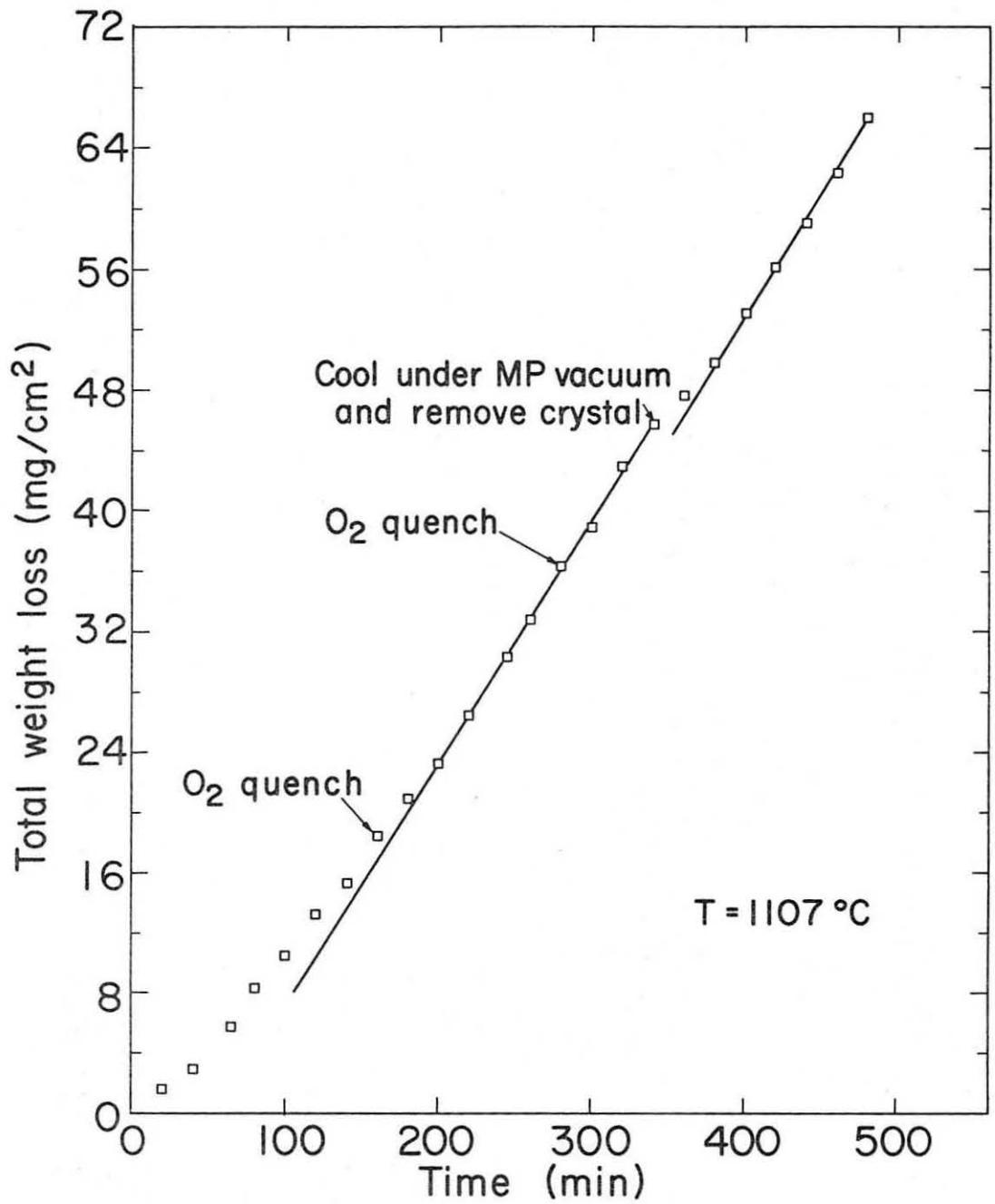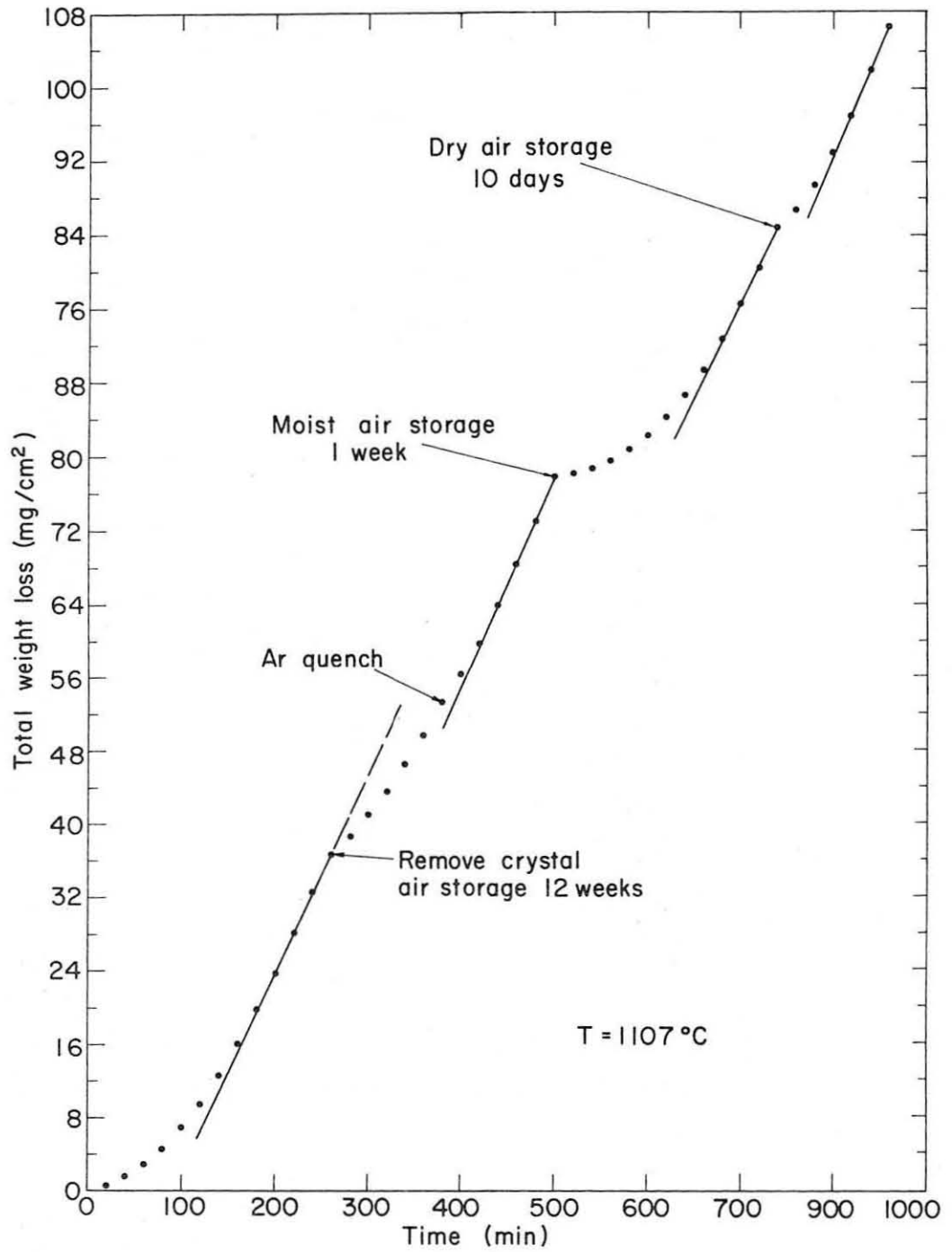
Fig.35. Vaporization of Zn-face and quenching experiments

XBL 698-3586

Fig.36. Vaporization of Zn-face and quenching experiments

Fig.37. Vaporization of Zn-face and quenching experiments

directions normal to the face. Figure 38 shows the vaporization of two prismatic slices. The A curves are vaporizations in opposite directions on one slice and the B curve is the vaporization of a second slice. The slice used for the A vaporizations was cut from the center of the crystal (see drawing of crystal slices in the experimental section) and hence the surfaces were produced by the diamond saw. On the other hand, the B vaporization was done on an as-grown prismatic face and the vaporization was stopped at the times marked by arrows so that the developing morphology could be photographically recorded. This development is shown in Fig. 39a through 39f. The lines seen in Fig. 39a are macroscopic growth ledges and scratches.

The prismatic slice that yielded the A curves was first vaporized for 660 minutes (open circles). It was then turned over and the opposite face vaporized for 620 minutes (solid circles), it was then turned over again and vaporization of the first side was continued (open circles) from 660 minutes to 1260 minutes. Induction periods are noted in these prismatic face vaporizations which are probably due to water adsorption such as was found for the basal faces.

The vaporization rates for opposite directions on a prismatic slice (A curves) are almost identical for the first two hundred minutes. The B slice showed an induction period following its first removal but little change in slope resulted from subsequent removals. All three curves show periods of nearly constant weight loss, but the trend is toward higher rates at longer times.

Figures 40 and 41 are optical photographs at the conclusion of vapori- zation B in Fig. 38. Two main features are evident in the morphologies on the

prismatic face: large irregular pits and pits which appear to be slits. These "slit pits" are parallel to the c-axis. A series of "slit pits" would occassionaly by very close together and thus form a larger pit, as seen in the center of Fig. 40. More "slit pits" seemed to develop as the vaporization continued. Figures 42 and 43 show "slit pits" developed at the conclusion of the 1260 minute $\underline{A}$ vaporization (solid circles). The opposite sides. **The prismatic slice developed similar morphologies (Fig. 44,45)**

The final morphology of the crystal used in vaporization $\underline{B}$ was examined with the scanning electron microscope (SEM). Figure 46 shows a typical large irregular pit, which was photographed optically in Fig. 41. Again, the reader is reminded that the SEM "looks at" the surface at an angle of 20° from the normal. Typical "slit pits" are seen in Fig. 47, with details of the lower left corner seen in Figs. 48 and 49. The difference between these two types of pits is striking. The large irregular pits show no crystallographic development, in complete contrast to the "slit pits". Another set of the large irregular pits is shown in Fig. 50, and another series of "slit pits" is seen in Fig. 51, with details of the areas between the slits seen in Figs. 52 and 53.

At this time there is no explanation as to why some areas of the prismatic face develop thermal pits that are irregular and others areas nearby develop the "slit pits". In contrast, the entire Zn-face developed the "mountain peaks", while the entire O-face developed the array of hexagonal pits.
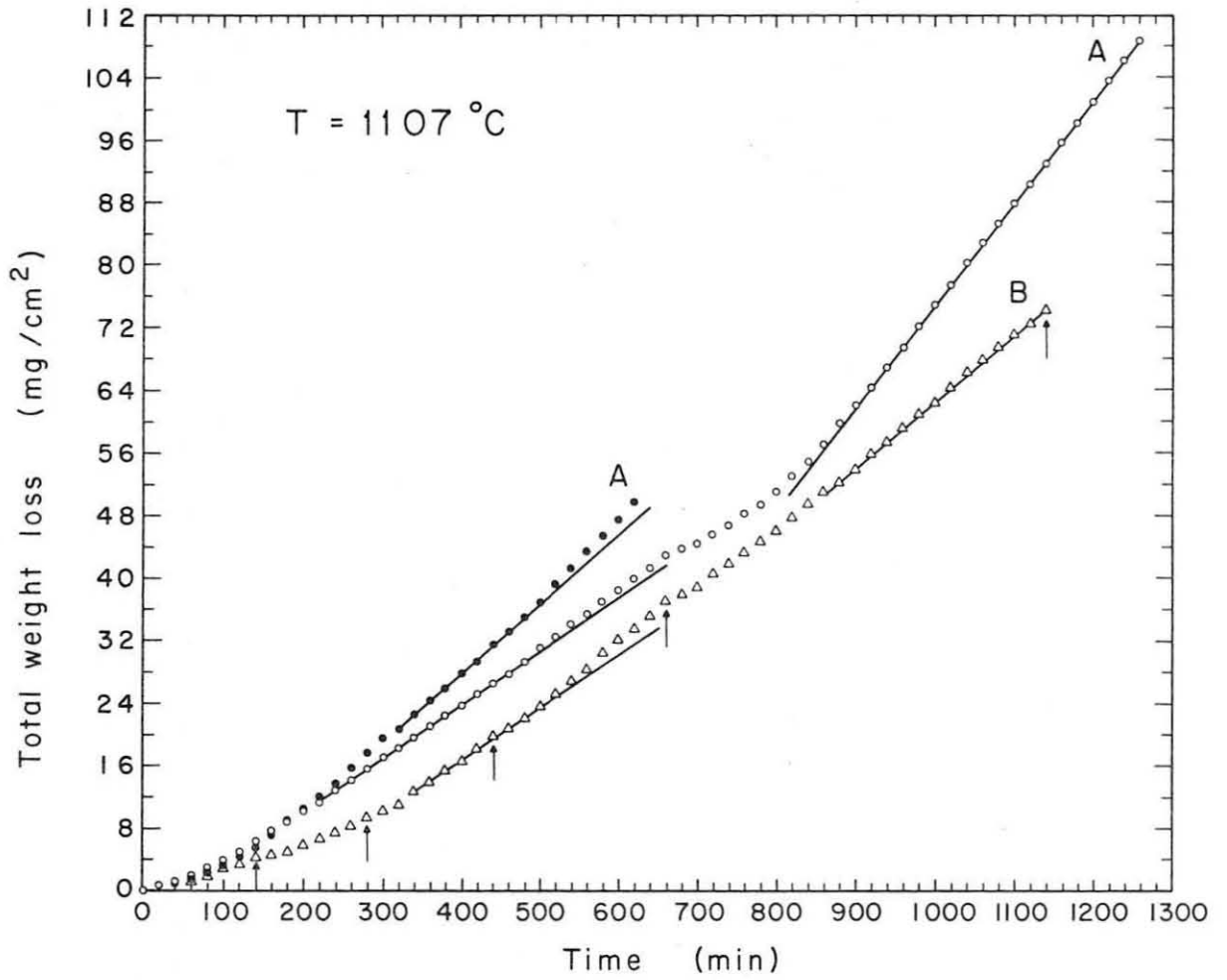
Fig.38. Vaporization of prismatic faces

XBL695-2623

Fig.39a. Prismatic face, as-grown, before vaporization (see Fig. 38).
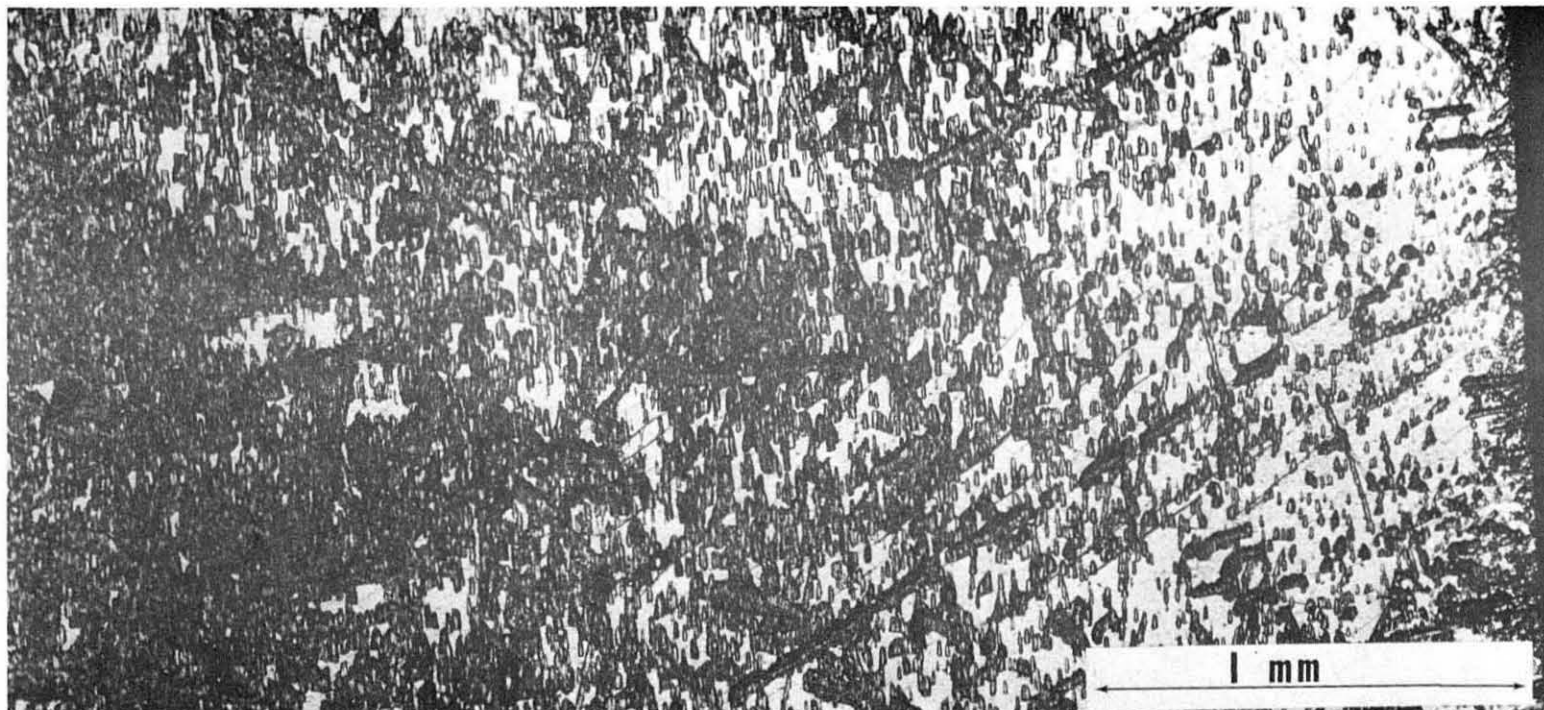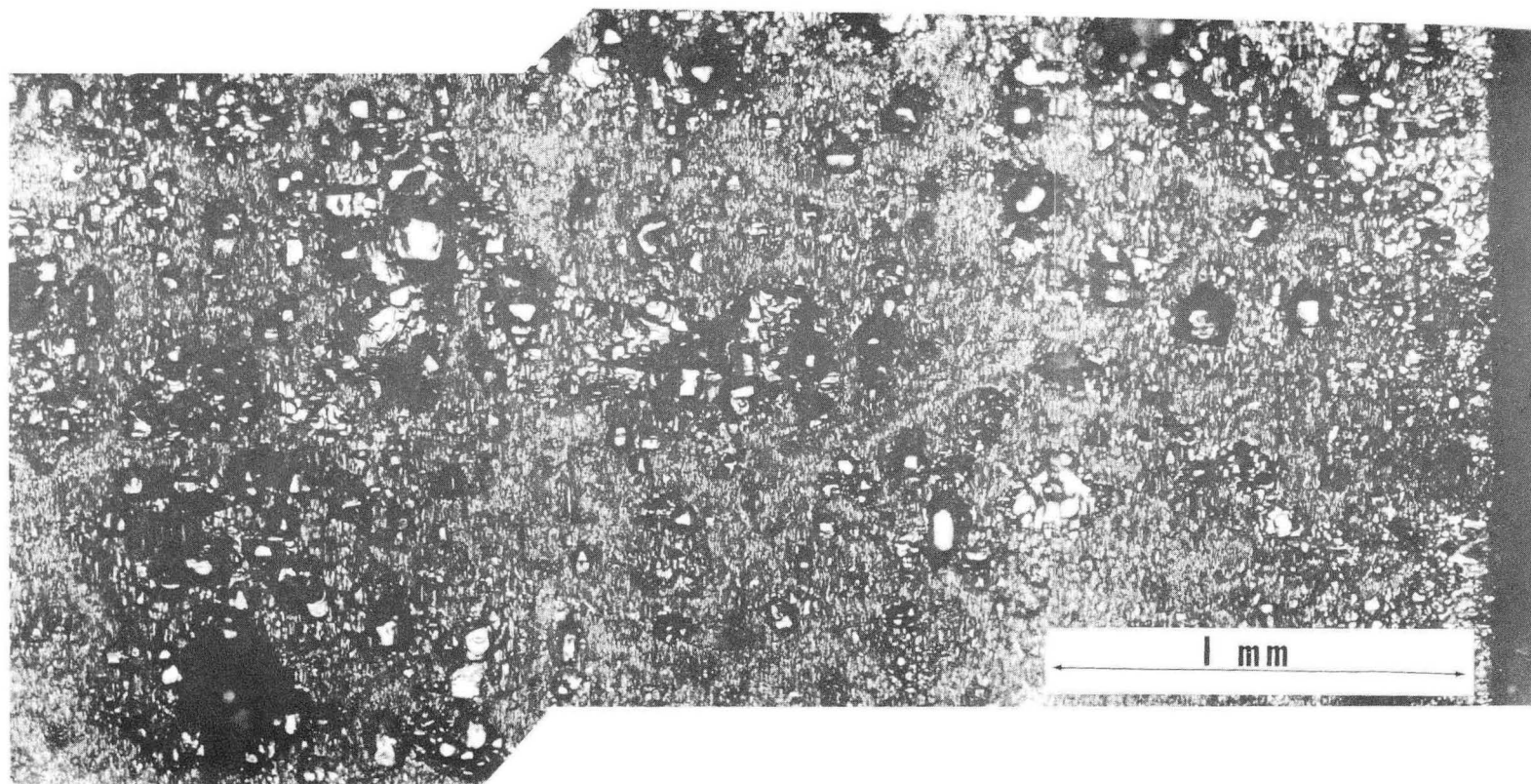
XBB693-2013

XBB693-2014

Fig. 39b. Prismatic face, after 140 minutes (see Fig. 38).
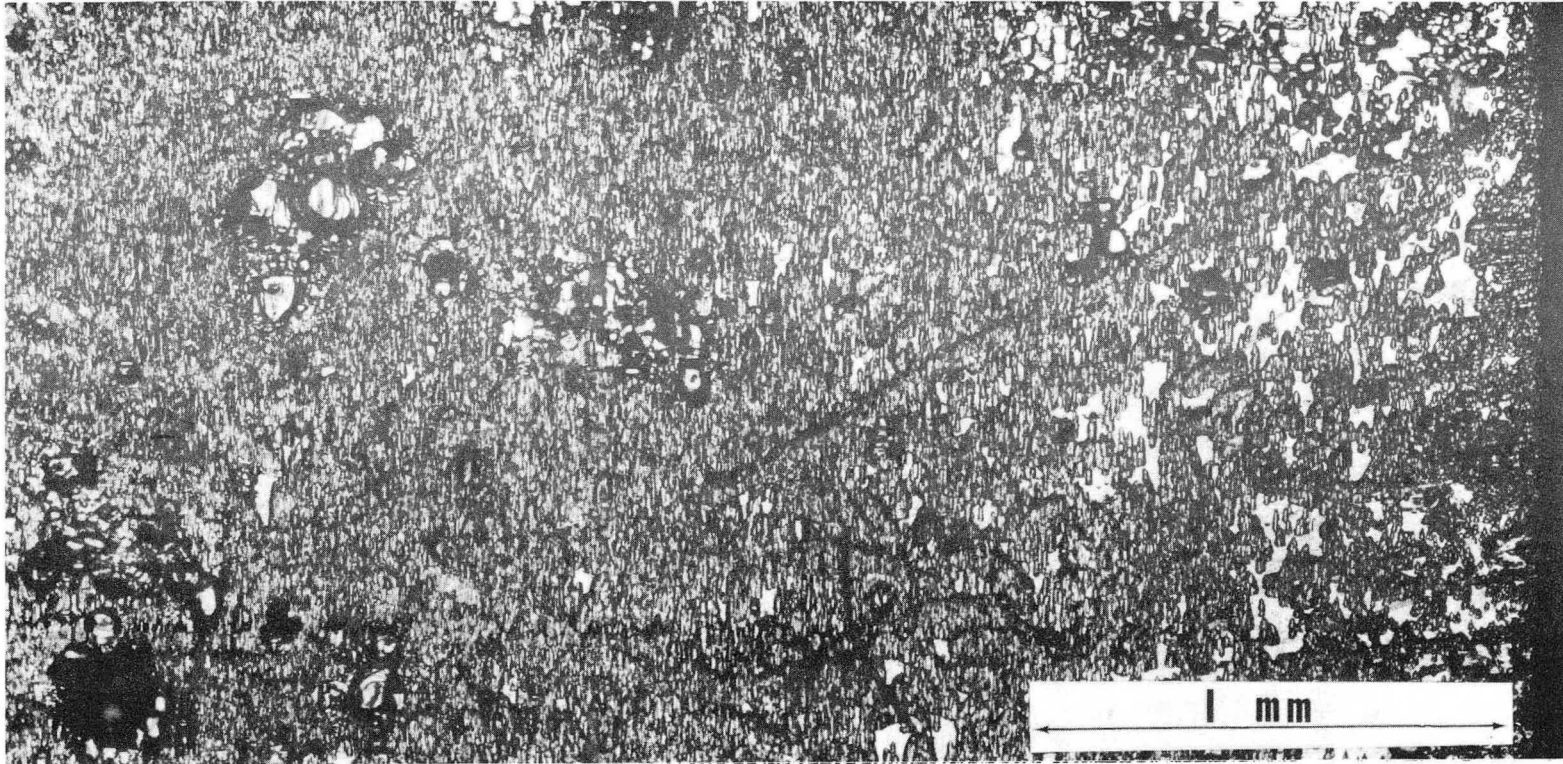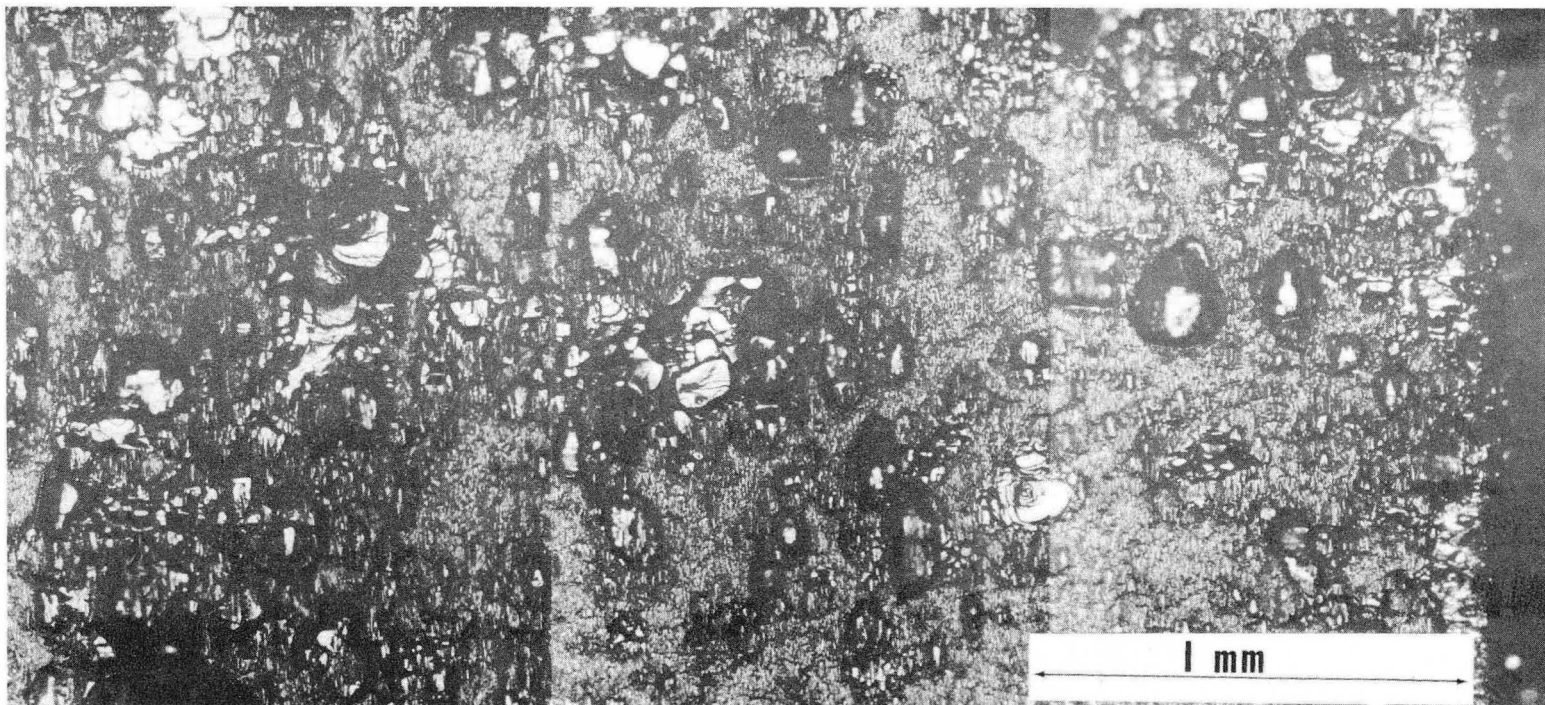
XBB693-2017

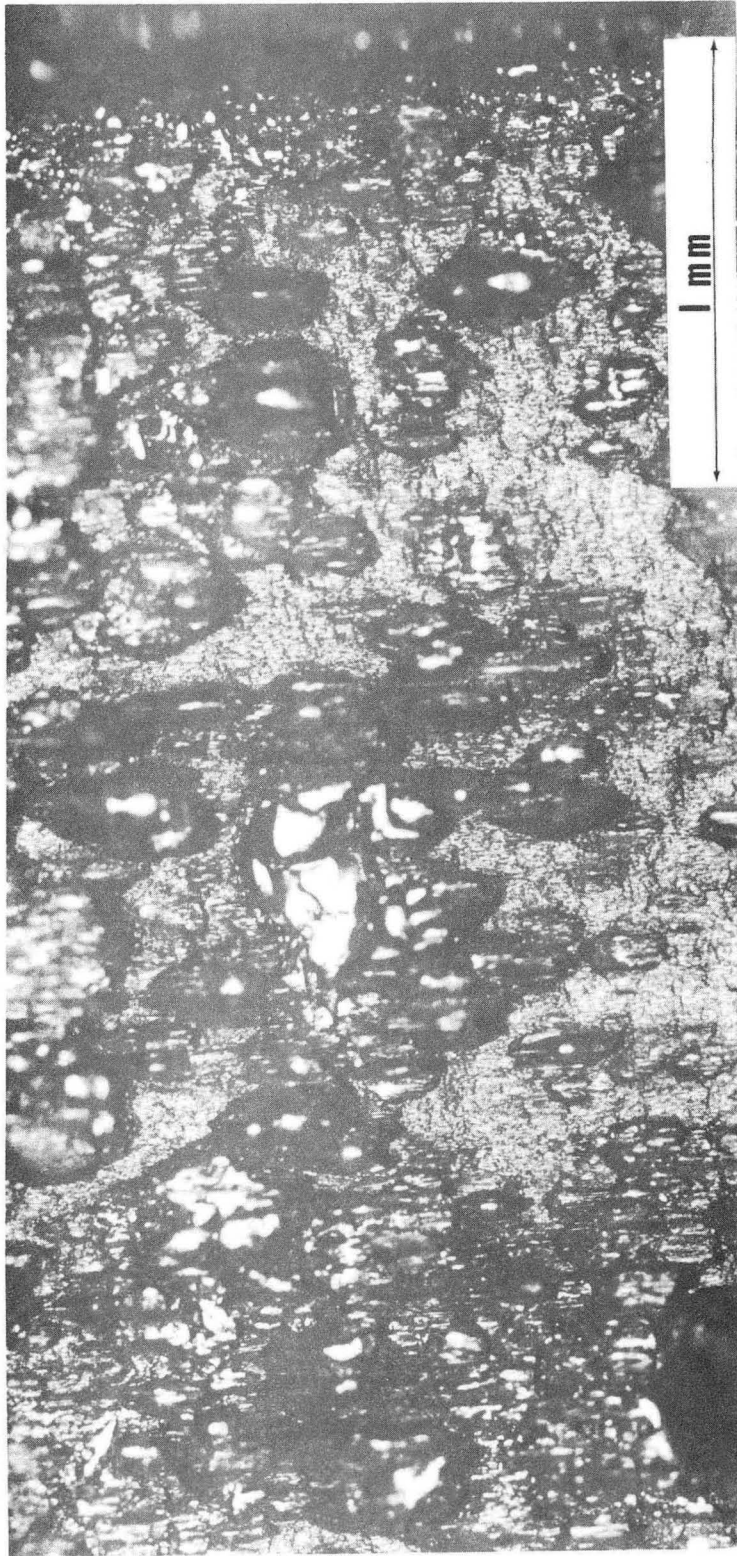Fig. 39c. Prismatic face, after 280 minutes (see Fig. 38).

XBB693-2015

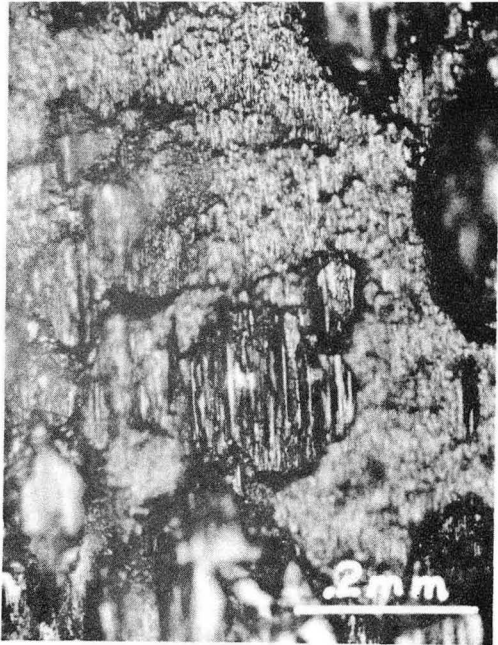Fig. 39d. Prismatic face, after 440 minutes (see Fig. 38).

XBB693-2018

Fig. 39e. Prismatic face, after 660 minutes (see Fig. 38).

XBB693-2016

1 mm

Fig. 39f. Prismatic face, after 1140 minutes (see Fig. 38).

Fig. 40   Fig. 41

Prismatic face steady-state surfaces (optical photographs)

XBB701-420
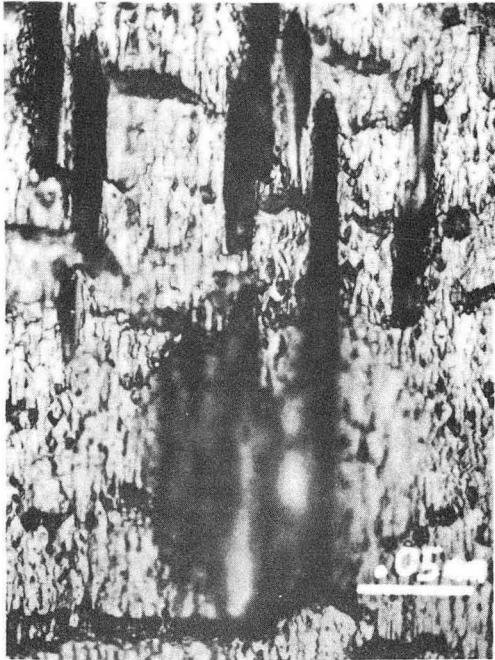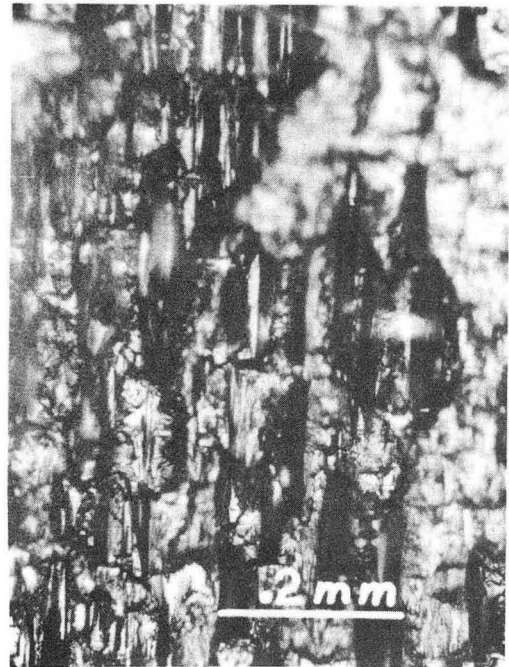
Fig. 42   Fig. 43

Prismatic faces steady state surfaces (optical photographs)

XBB701-421

Fig. 44   Fig. 45

Prismatic face steady-state surfaces (optical photographs)
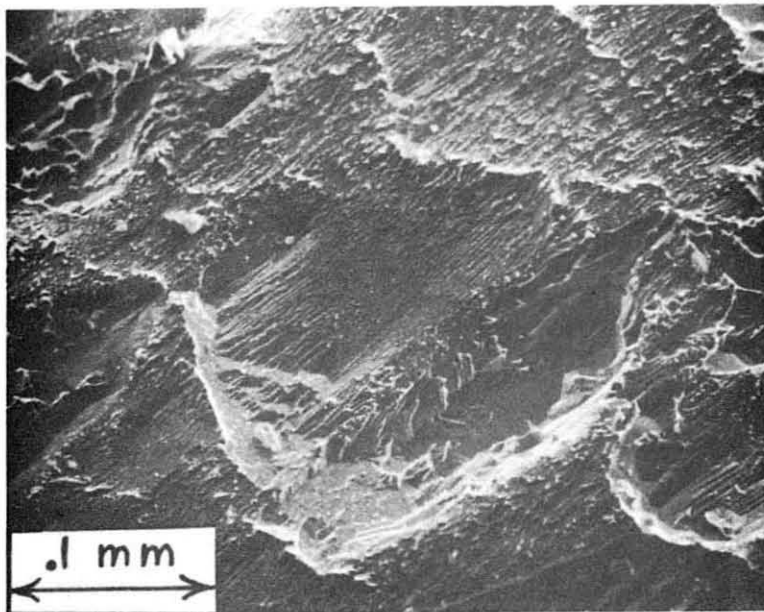
XBB701-418
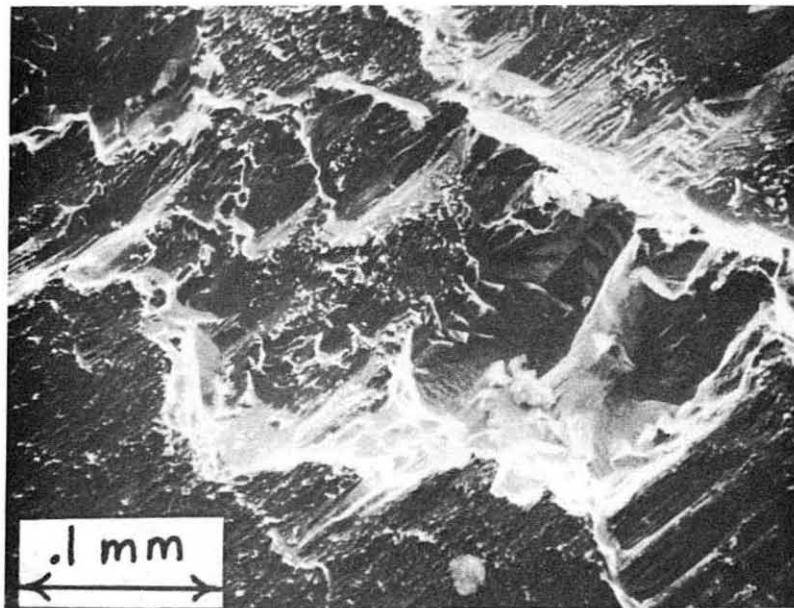
Fig. 46   Scanning electron micrograph of irregular
          pits on prismatic face steady-state surface
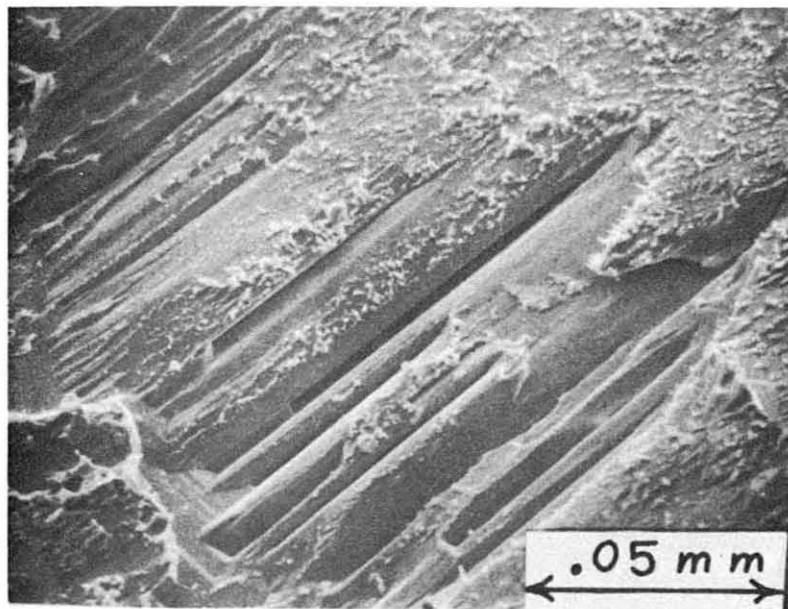
Fig. 47.   Scanning electron micrograph of "slit-
           pits" on prismatic face steady state
           surface
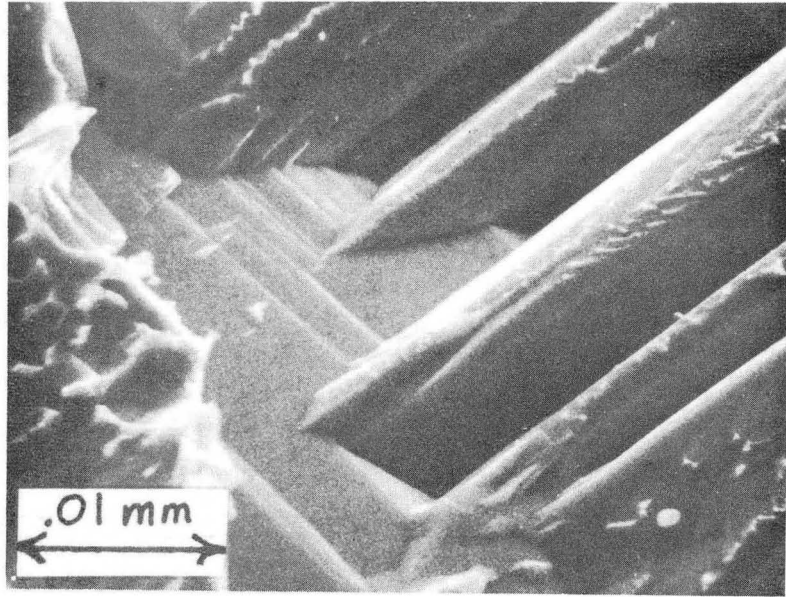
XBB701-415

Fig. 48.   Detail of "slit pits" in lower left corner
            of Fig. 47.
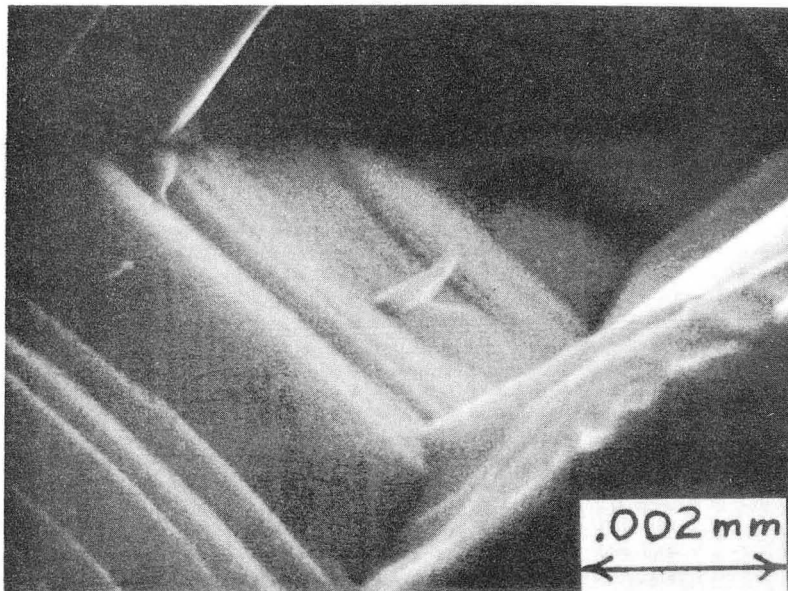
Fig. 49.   Detail of Fig. 48

XBB701-417

Figure 50. Scanning electron micrograph of
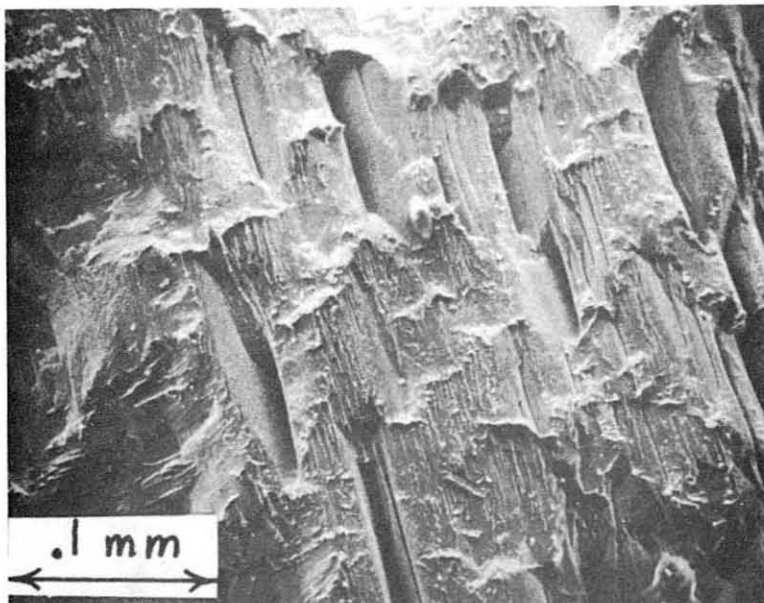irregular pits on prismatic face
steady-state surface

Figure 51. Scanning electron micrograph of
"slit pits" on prismatic face
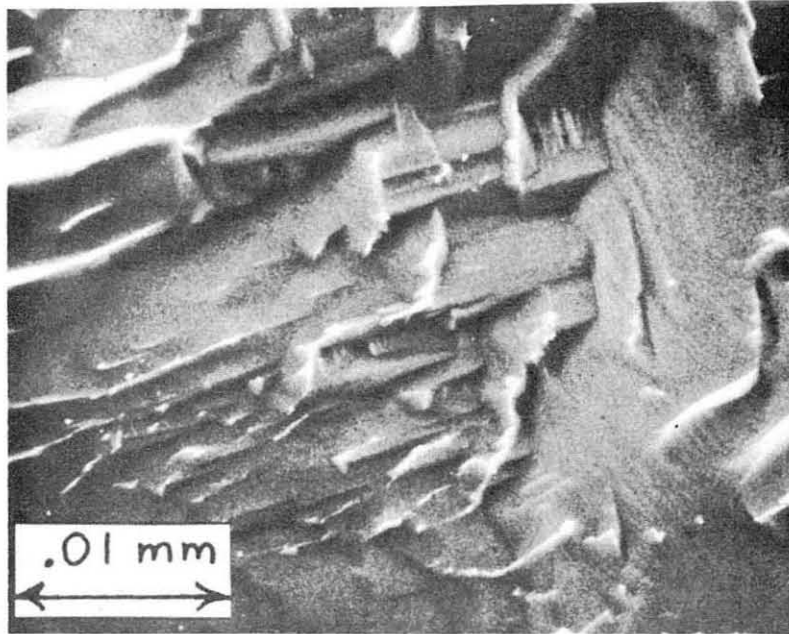steady-state surface

XBB701-416

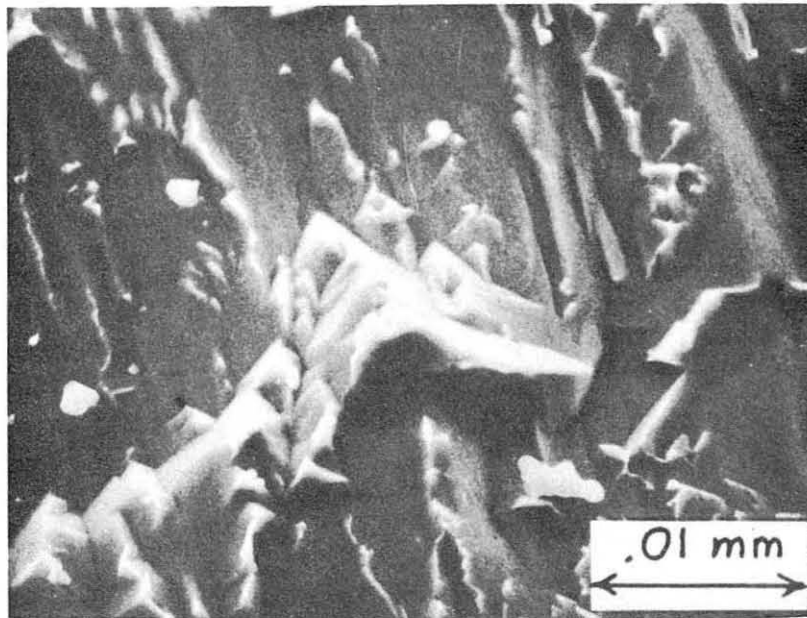Figure 52. Detail of left hand side of Figure 51, next to "slit pits"

Figure 53.   Detail of center of Figure 51, between the "slit pits"

XBB701-419

V. PREVIOUS CADMIUM SULFIDE VAPORIZATION STUDIES

Cadmium sulfide is a II-VI n-type semiconductor that crystallizes in the wurtzite structure. It is a much more useful semiconductor than is zinc oxide (it's room temperature band gap is 2.2 eV) and hence has been the subject of an immense number of investigations. The vaporization kinetics for cadmium sulfide have been more extensively studied than have the vaporization kinetics of any other materials; a brief summary of these investigations is given below.

1. Mass Spectrometric and Knudsen-Cell Vaporization Studies of Group 2B-6B Compounds[37]

This paper reports vaporization studies of the nine compounds of Zn, Cd, and Hg with S, Se and Te. They observe only $Cd_{(g)}$ and $S_{2(g)}$ above CdS from 850° to 1450°K and obtain, for the equilibrium vaporization reaction, $\Delta H^{\circ}_{1000} = 157.6$ kcal and $\Delta H^{\circ}_{298} = 163.6$ kcal for the reaction $2CdS_{(s)} \rightarrow 2Cd_{(g)} + S_{2(g)}$.

2. Orientation Dependence of the Evaporation Rate of CdS Single Crystals[38]

Results of vaporization studies of the prismatic and basal faces of cadmium sulfide single crystals are reported in the temperature range 680° to 760°C. No time dependence was observed for the basal faces and the authors stated that they did not observe any difference in rates between Cd(0001) and S(000$\bar{1}$) faces. The vaporization rate of the prismatic faces was lower than that for the basal faces, but after "many hours" it approached the basal face rate. No description was given of the basal face morphologies, but the prismatic faces developed deep channel-shaped crevices.

3. Evaporation Mechanism of CdS Single Crystals

    a. Surface Concentration and Temperature[39] Dependence of the Evaporation Rate

This paper reports the results of the vaporization of basal faces of cadmium sulfide into a beam of cadmium atoms or sulfur diatomic molecules. It was found that the vaporization rate was proportional to the inverse square-root of the impingement rate of the sulfur flux for fluxes greater than 10^{-3} g/cm^2-min. whereas the rate was unaffected by a cadmium beam.

The results were complicated by the fact that the cadmium and sulfur beams changed the stoichiometry of the crystals, which, in turn, lowered the vaporization rate (see paper 3.b below.). However, the authors concluded that stoichiometry changes were not important for vaporization periods of less than one hour. A kinetic scheme was derived that fit the observed inverse square-root dependence on the sulfur flux, but this scheme also required an inverse square dependence on the cadmium flux. Since no such dependence was found for vaporization into a cadmium beam, it was suggested that the incoming cadmium atoms did not ionize and hence did not come into equilibrium with the surface.

The study yielded an activation enthalpy and entropy of $\Delta H^* = 50.3 \pm 1$ kcal/mole and $\Delta S^* = 3.8 \pm 1$ eu at 1000°K for the reaction $CdS_{(s)} \longrightarrow Cd_{(g)} + 1/2\ S_{2(g)}$ when the activated complex is assumed to be an activated CdS molecule.

    b. Diffusion Controlled Evaporation of Cadmium-[40] and Sulfur-doped CdS

Crystals that had been doped with either cadmium or sulfur had evaporation rates that were lowered by as much as a factor of ten, the

magnitude depending on the amount of dopant. The crystals returned to
their "normal" rates as the excess dopant diffused out. The authors
concluded that the dopants caused the lower rates by changing the surface
hole and electron concentrations rather than by direct interference with
the surface cadmium or sulfur concentration.

4. Charge-Transfer-Controlled Vaporization of Cadmium Sulfide Single
    Crystals

    a. Effect of Light on the Evaporation Rate of the (0001) Face[41]

It was observed that light of greater-than-band-gap energy (6400Å)
increased the vaporization rate of cadmium sulfide basal faces by a
factor of five for high-resistivity crystals. The effect was believed to
be due to the influence of light on the rate of charge transfer between
the cadmium and sulfur lattice ions at the surface.

Evidence from studies of electrical properties of cadmium sulfide
indicates that the conductivity of cadmium sulfide is due to ionized
sulfur vacancies.[42,43] The sulfur vacancy concentration is lowered by
sulfur doping and hence the resistivity is increased. Since the incident
light produces hole-electron pairs, illumination of a sulfur-doped
crystal significantly increases both the hole and electron population.
These increases can affect both of the following reactions:

$$(1) \quad S^{-2}_{surface} + 2p = S^{\circ}_{surface}$$

$$(2) \quad Cd^{+2}_{surface} + 2n = Cd^{\circ}_{surface}$$
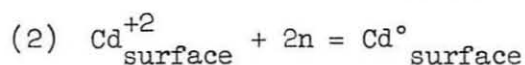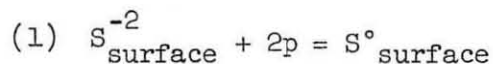
For high-conductivity crystals, only the hole concentration can be
significantly increased, with the result that only the rate of the first
reaction could be increased. This preferential increase, in turn, would
tend to make the crystal cadmium rich. As was noted before, cadmium

doped crystals showed a lower vaporization rate until the excess cadmium diffused out. Illumination of a cadmium doped crystal prevented the crystal from attaining its "normal" vaporization rate, an effect which was apparently due to the constant enrichment of the surface with cadmium.

b. Effect of Copper Doping on the Evaporation Rate of the[44] (0001) Face

Copper is an acceptor in cadmium sulfide and hence reduces the conductivity by trapping electrons. It also causes self-compensation, that is, for every ionized acceptor an ionized donor is produced. No direct interaction occurs because the copper acceptor center removes an electron from the valence band and the sulfur vacancy donor gives an electron to the conduction band.

Copper was deposited on the back faces of cadmium sulfide crystals and the front faces were then vaporized. The vaporization rates initially increased and then fell to values below the "normal" vaporization rate. This effect was thought to be due to rapid diffusion to the front surface of the mobile carriers produced by the self-compensation. The carriers could accelerate the charge transfer of the surface cadmium and sulfur lattice ions. When the slower diffusing copper ions reached the front surface, they trapped the electrons, thus lowering the vaporization rate.

5. Evaporation Mechanisms of Solids[45]

This review article examines vaporization theories and reviews various experimental results. The cadmium sulfide studies outlined above are discussed in detail.

6. Studies on the Sublimation of IIB-VIA Compounds[46] (Part II)

a. The Dependence of the Sublimation Pressure of Cadmium Sulfide on Crystalline Orientation

Based on the reaction $2CdS_{(s)} \longrightarrow 2Cd_{(g)} + S_{2(g)}$ the apparent

equilibrium constant for the sublimation of basal faces over the temperature range of 909° to 1083° K was found be:

$$\log K^{\ddagger}_{basal} = (18.057 \pm 1.270) - (3.811 \pm 0.126)10^4/T$$

while for prismatic planes it was found to be:

$$\log K^{\ddagger}_{pris} = (19.655 \pm 1.004) - (3.509 \pm 0.100)10^4/T$$

The equilibrium studies gave the following expression for the equilibrium constant in the temperature range of 882° to 1107° K:

$$\log K_{equil.} = (18.050 \pm 0.400) - (3.139 \pm 0.040)10^4/T$$

The calculated third-law enthalpies for the basal planes, prismatic planes, and equilibrium measurements were found to be 177.0, 168.7 and 159.3 kcal/mole respectively. The basal face pressures were a factor of three lower than those reported by Somorjai (see papers outlined above for references). No investigation was made of the behavior of opposite basal faces, but a large amount of scatter was observed in the basal face measurements. It was surmised that the asymmetry of the c-axis was a possible explanation.

* * * * * * * * * * * *

None of the kinetic studies of cadmium sulfide reported any measurement of different vaporization rates from opposite basal faces, but a search for possible differences seemed desirable in light of the difference found for zinc oxide. The higher vapor pressure of cadmium sulfide would make possible the determination of the temperature dependence of the vaporization rates.

VI.   EXPERIMENTAL SECTION FOR CADMIUM SULFIDE

An ultra-high purity cadmium sulfide single crystal with a face cut perpendicular to the c-axis was obtained from Eagle-Picher Industries, Miami, Oklahoma. A Laue back-reflection x-ray photograph showed that the face was within 1° of the desired orientation. The stated impurities of the crystal were (in parts per million):

Ag	.01	Mg	.10
Si	.90	Cu	.22

Basal slices 0.75 to 1.4 mm thick were cut from the crystal using a wire saw and a 1:1 water: glycerol slurry of 600 grit silicon carbide. The slices were etched with a nitric acid-acetic acid-water etch as described by Warekois et al.[34] One side of the basal slices etched to beautiful hexagonal pits (Fig. 54) while the opposite face produced a non-distinct surface (Fig. 55). These are the same results reported by Warekois et al. and, accordingly, Fig. 54 is identified as the Cd(0001) face and Fig. 55 is identified as the S(000$\bar{1}$) face.

Annealing a crystal wrapped in platinum foil for three days at 700°C in an evacuated quartz container produced no visible change in the crystal color, and produced no observable difference in vaporization behavior from unannealed crystals. (See section on results). Thereafter, crystals were not annealed prior to their vaporization.

The total pressure is the sum of the cadmium and sulfur pressure and was calculated from the slopes of the total weight loss versus time plots. The partial pressure in atmospheres for each component can be obtained from weight loss measurements by use of the equation:

$$P(atm) = \frac{\Delta W}{44.33} \ (T/M)^{1/2}$$
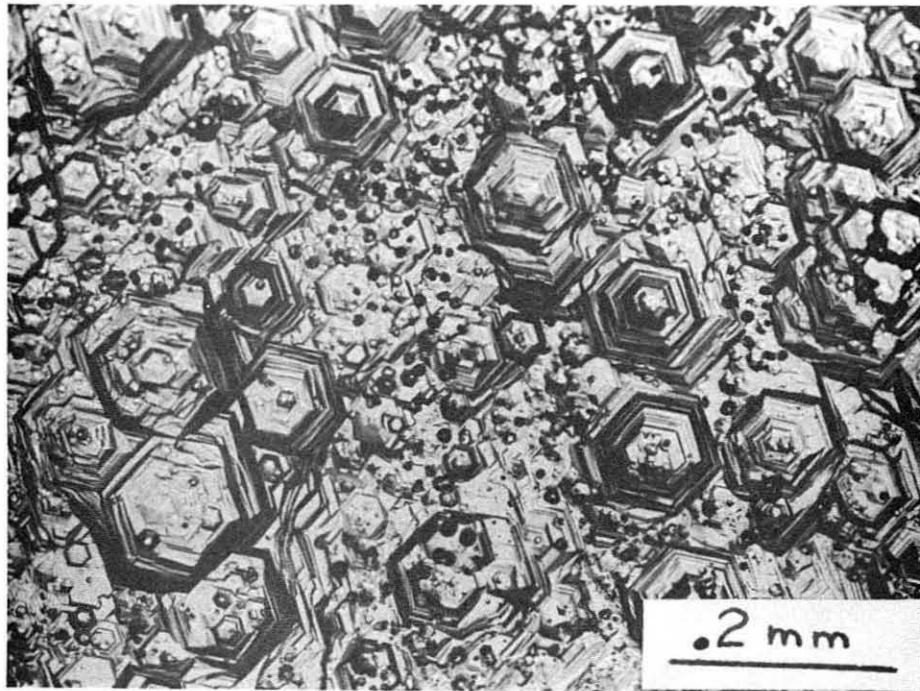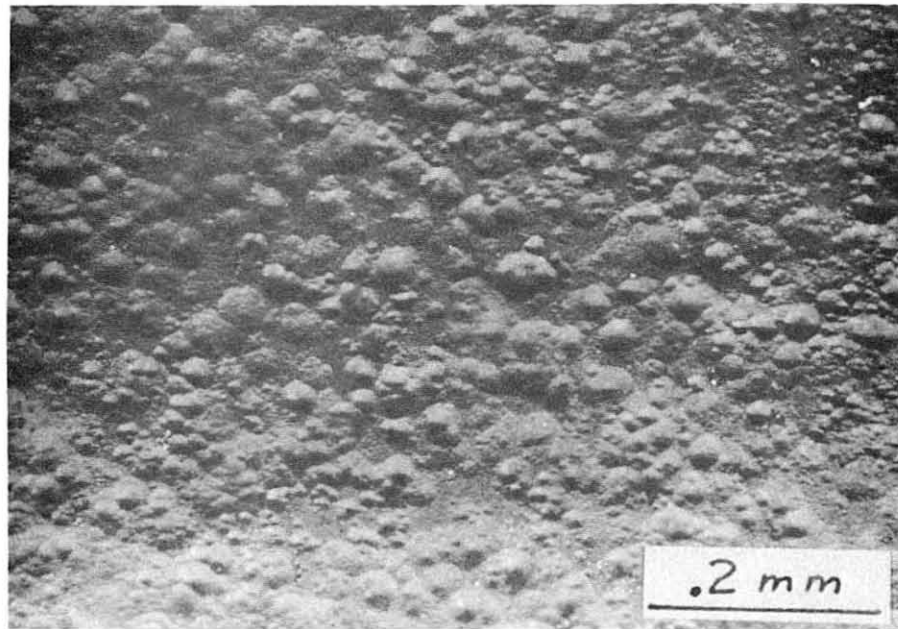
Figure 54.   Gd(0001) Face After Chemical Etch

Figure 55.   S(000$\bar{1}$) Face After Chemical Etch

XBB703-1333

where ΔW is the rate of weight loss in g/cm^2-sec, T is in °K and M is the molecular weight of the component. A derivation of this is found in the book "Characterization of High Temperature Vapors" chapter two, edited by J. L. Margrave.

The same aluminum oxide cell, quartz balance and furnace (Figs. 9, 10, and 11) were used for the cadmium sulfide vaporizations as were used for the zinc oxide vaporizations. A new quartz tube was used so that there would be no danger of contamination by zinc from previous zinc oxide vaporizations. A platinum tube 15 cm long, 4 cm in diameter and 0.5 mm thick was inserted into the hot zone in order to obtain a better constant temperature zone for the range of temperatures used (609°C-676°C). This produced a 5 cm long zone where the temperature was constant to ± 1/2°C.

It was possible to measure vaporization rates as a function of temperature because the vaporization rate is higher than for zinc oxide. This investigation was confined to the $Cd(0001)$ and $S(000\bar{1})$ basal faces.

Two wafers could be produced from each slice of the bulk crystal. If a concentration gradient of impurities was produced in the crystal during its growth, this method of selecting wafers should insure, insofar as is possible, identical impurity contents.

A crystal was not removed from the cell until vaporization had been studied over a range of temperature. This procedure minimized the amount of contaminants that could come into contact with the surface and eliminated any possible error that might be introduced by changes in placement of the crystal.

VII. RESULTS OF CADMIUM SULFIDE

Figure 56 compares the results for the annealed crystal at three temperatures with the dashed curves that represent more extended studies with unannealed crystals. For measurements with the annealed crystals, the $S(000\bar{1})$ face was vaporized first, with one point taken at each temperature. The crystal was then turned over and two points taken at each temperature from the $Cd(0001)$ face. Returning to the $S(000\bar{1})$ face, three points were again taken at each temperature, after which it was turned over and one more point taken at each temperature from the $Cd(0001)$ face. No slopes were determined for these vaporizations because only three temperatures were used.

Figures 57 and 58 are results for two 0.8 mm thick wafers (identified as number one and number two), made from one slice. Both crystals were etched before vaporization.

Not only are the vaporization rates of the $Cd(0001)$ and $S(000\bar{1})$ faces different, but also the enthalpies and steady-state morphologies are different. However the results differ from those found for zinc oxide in that it is the $Cd(0001)$ face that develops the hexagonal pits, while the $S(000\bar{1})$ face has a morphology that resembles rounded mountain peaks separated by narrow valleys (in zinc oxide, the $Zn(0001)$ face steady-state morphology resembled mountain peaks and the $O(000\bar{1})$ had the hexagonal pits).

The $Cd(0001)$ face of the crystal number one (Fig. 57) was vaporized first, with two points taken at each temperature in a random manner. The crystal was then turned over, and the $S(000\bar{1})$ face was vaporized. It was observed that the second of two pressures measured at a given
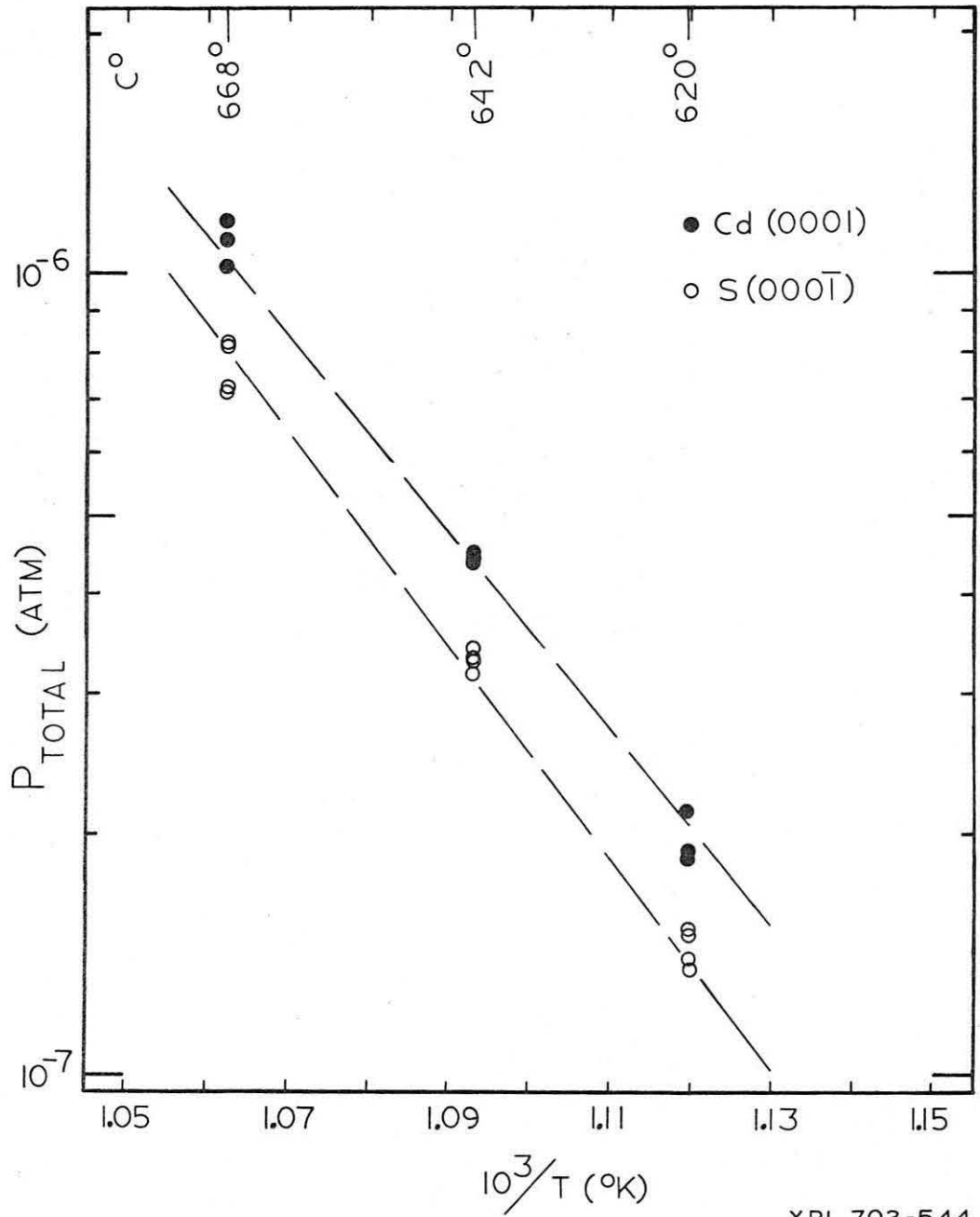
Figure 56. Total Pressure vs. Reciprocal Temperature for an Annealed Crystal
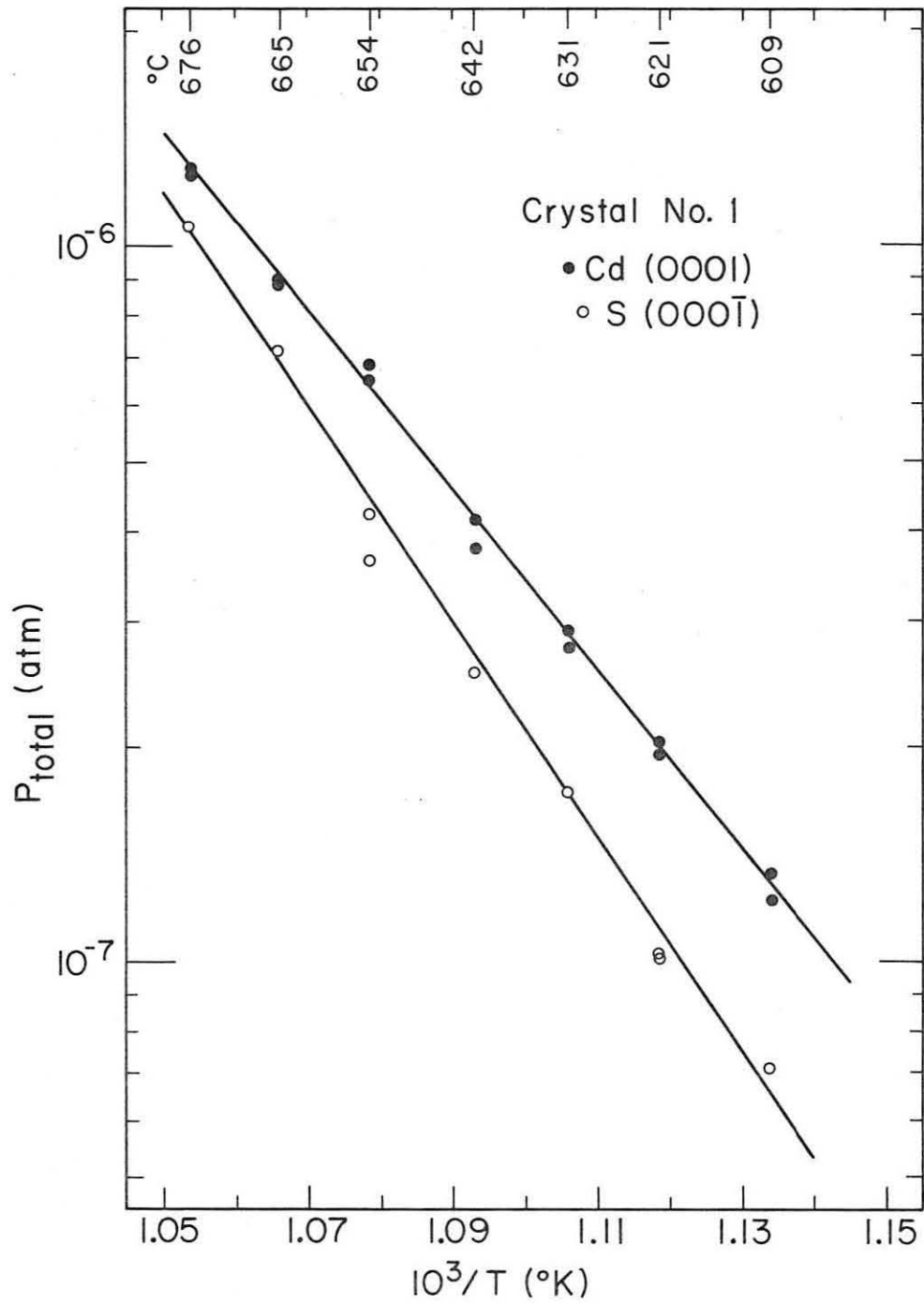
Figure 57. Total Pressure vs. Reciprocal Temperature
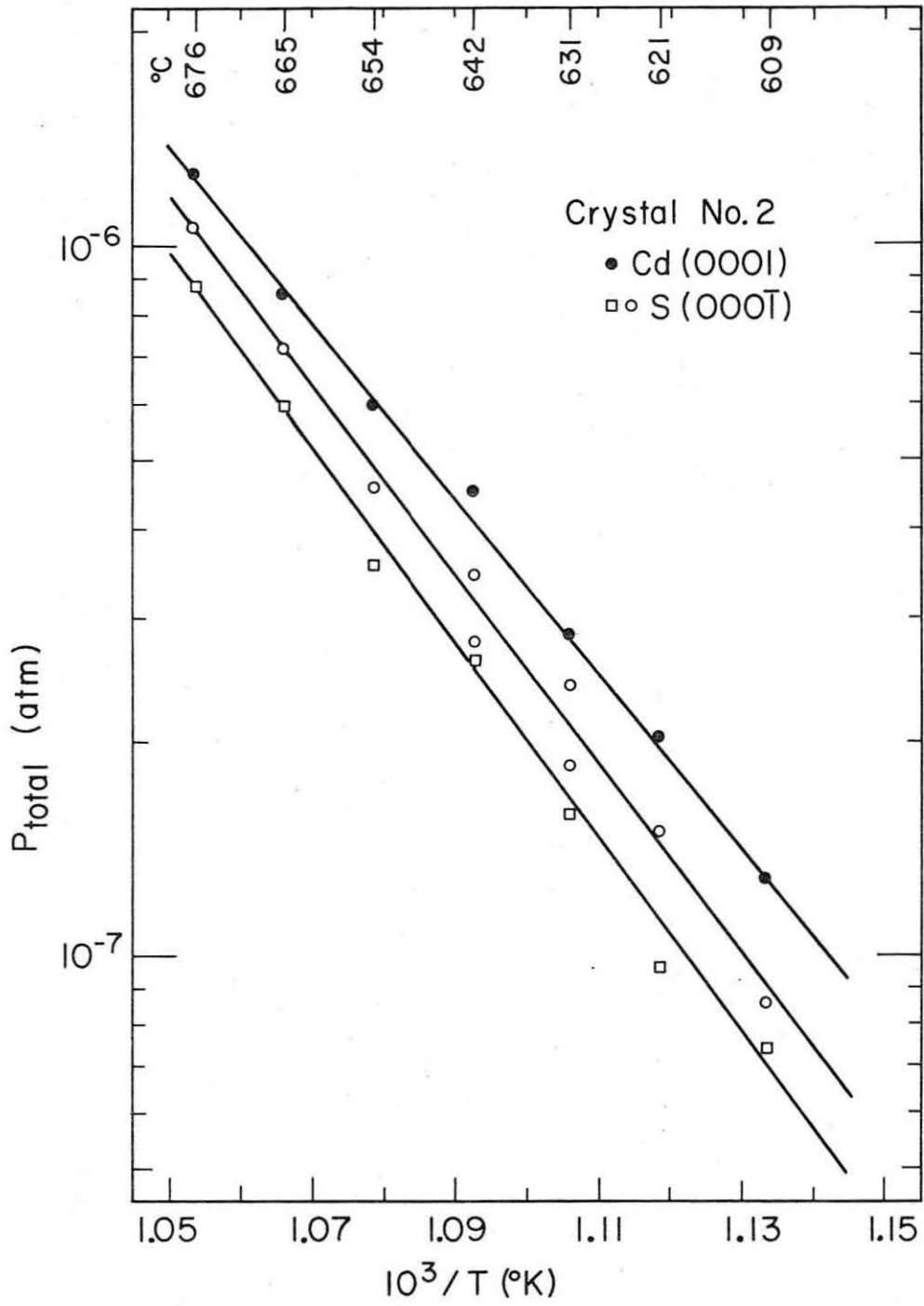
XBL702-2337

XBL702-2336

Figure 58.   Total Pressure vs. Reciprocal Temperature

temperature from the $S(000\bar{1})$ face was lower than the first. The crystal was removed, but no obvious irregularities were noted.

The $S(000\bar{1})$ face of crystal number two (Fig. 58) was vaporized first (circles) with one point taken at each temperature. The crystal was then turned over for vaporization of the $Cd(0001)$ face. After vaporization of this face was finished, a second set of points was taken on the $S(000\bar{1})$ face (squares). As can be seen, the second set of points is lower than the first. However, for both crystal one and two, the $Cd(0001)$ face exhibits a higher rate and lower slope than the $S(000\bar{1})$ face, regardless of the order of vaporization of the two faces.

Figure 56 through 58 are total pressure versus reciprocal temperature, that is, $P_{total} = P_{Cd} + P_{S_2}$. For the vaporization reaction into vacuum

$$CdS_{(s)} \longrightarrow Cd_{(g)} + 1/2 S_2(g)$$
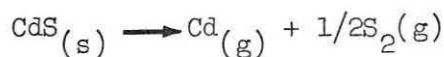
one can write an apparent equilibrium constant:

$$K^{\ddagger} = P_{Cd} P_{S_2}^{1/2}$$

The slope of $\ln K^{\ddagger}$ versus reciprocal temperature then yields an apparent activation enthalpy of vaporization. By assuming that the flux of cadmium atoms (Z_{Cd}) is twice the flux of sulfur molecules (Z_{S_2}), we have:

$$P_{Cd} = (2\pi M_{Cd} RT)^{1/2} Z_{Cd}$$

$$P_{S_2} = 1/2 (2\pi M_{S_2} RT)^{1/2} Z_{Cd} \tag{1}$$

hence

$$P_{Cd} = \left(\frac{4 M_{Cd}}{M_{S_2}}\right)^{1/2} P_{S_2} \tag{2}$$

therefore

$$\ln P_{Cd} P_{S_2}^{1/2} = \ln \left[\frac{4 M_{Cd}}{M_{S_2}}\right]^{1/2} P_{S_2}^{3/2} \tag{3}$$

Since
$$P_{total} = P_{Cd} + P_{S_2}$$

from (2) we have
$$P_{total} = P_{S_2}\left[\left(\frac{4M_{Cd}}{M_{S_2}}\right)^{1/2} + 1\right] \tag{4}$$

or
$$P_{S_2} = \left[\frac{1}{\left(\frac{4M_{Cd}}{M_{S_2}}\right)^{1/2} + 1}\right] P_{total} \tag{5}$$

Putting (5) into (3), we get:
$$\ln K^{\ddagger} = \ln P_{Cd} P_{S_2}^{1/2} = \ln\left[\left(\frac{4M_{Cd}}{M_{S_2}}\right)^{1/2}\left(\frac{P_{total}}{\left(\frac{4M_{Cd}}{M_{S_2}}\right)^{1/2} + 1}\right)^{3/2}\right] \tag{6}$$

The total pressures were converted to an apparent equilibrium constant by equation (6), and the slopes were determined by least squares and are given in the table below in kcal (errors are one standard deviation):

	Crystal #1	Crystal #2	Sum of points of Crystals #1 & #2
Cd(0001)	86.12±1.40	83.98±1.85	85.41±1.09
S (000$\bar{1}$)	103.04±3.57	(1st)91.62±4.01	96.66±3.39
		(2nd)95.12±3.60	

Munir (see previous summary of papers) reports
$$\log K^{\ddagger} = 18.057 - 3.811 \times 10^4/T$$

which yields $\Delta H^{\ddagger} = 175.3$ kcal for the reaction:
$$2CdS_{(s)} \longrightarrow 2Cd_{(g)} + S_{2(g)}$$
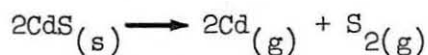
or 87.7 kcal for the reaction
$$CdS_{(s)} \longrightarrow Cd_{(g)} + 1/2S_{2(g)}$$
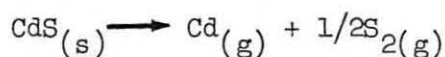
The latter reaction being the one used in the calculation of the apparent activation enthalpies of vaporization in the above table.
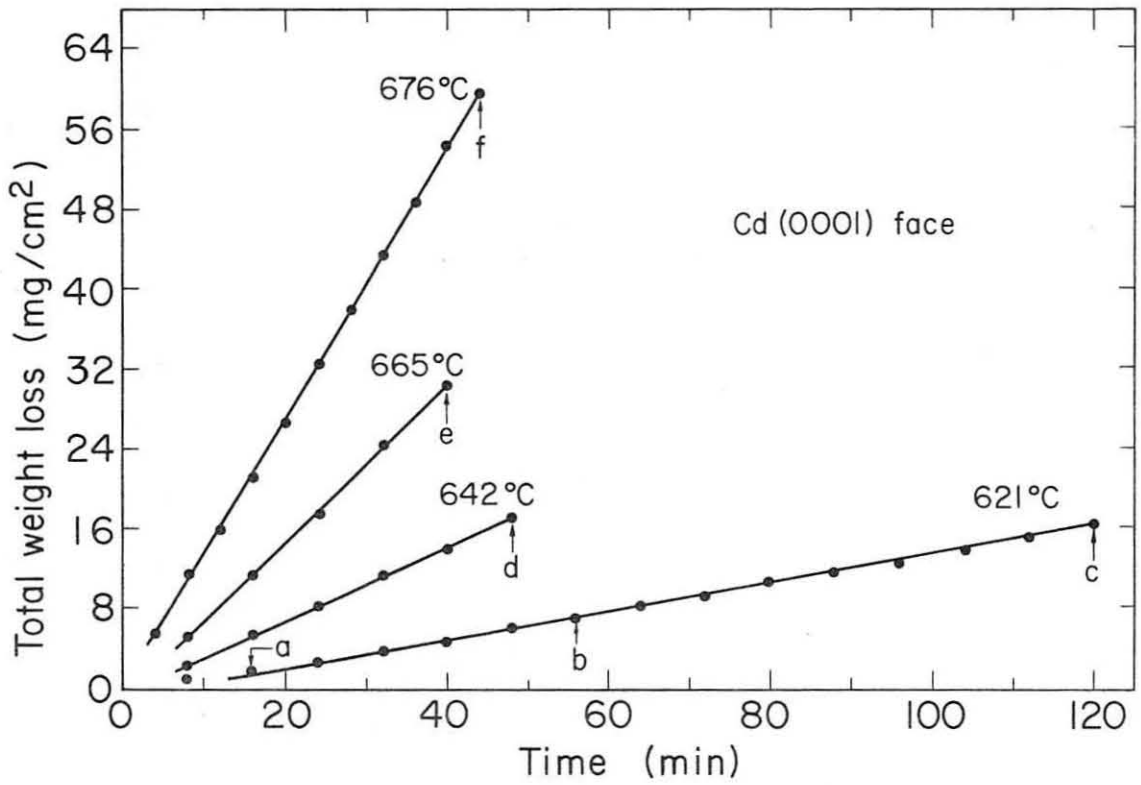
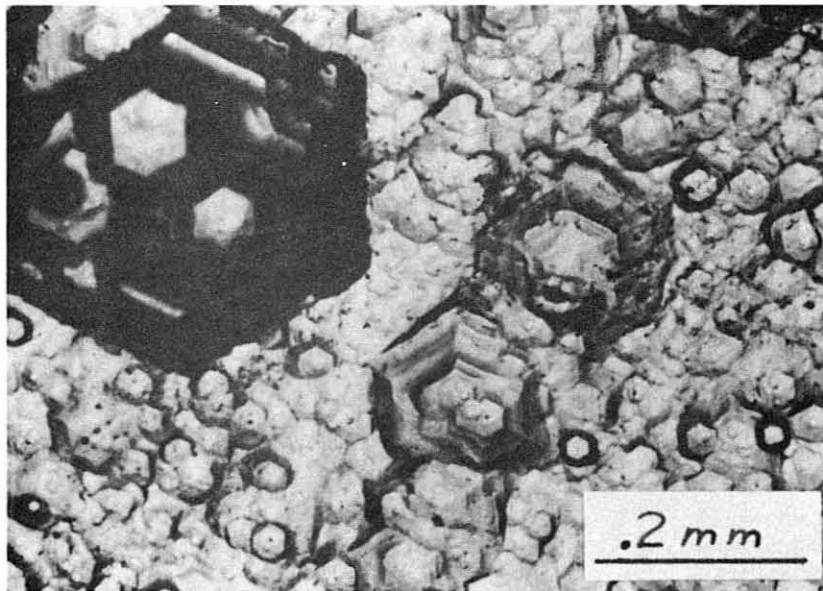Figure 59. Total Weight Loss vs. Time (see Figures 60 thru 66)
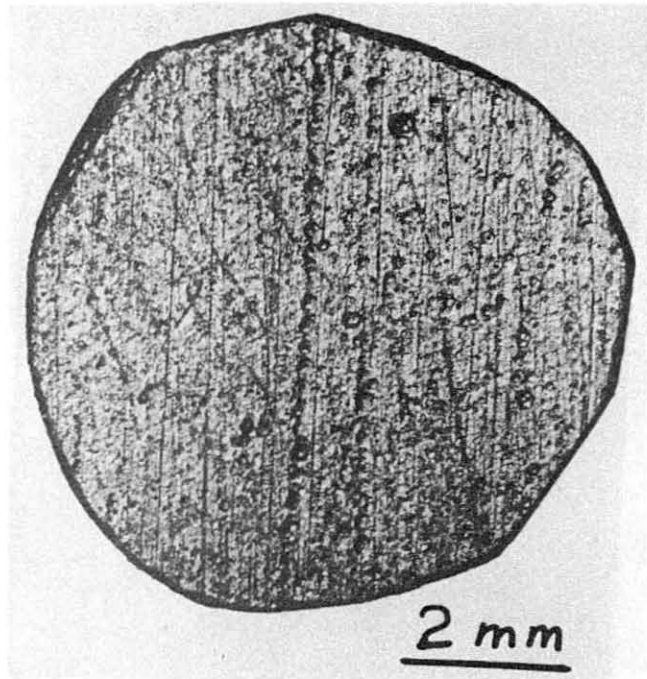
(a)
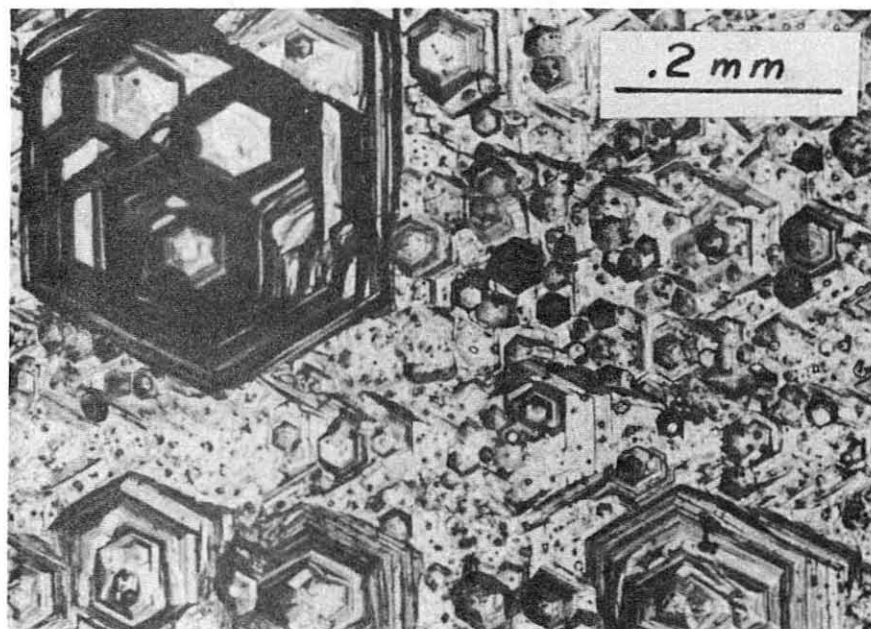
(b)

Figure 60.   Optical Photograph of Chemically Etched
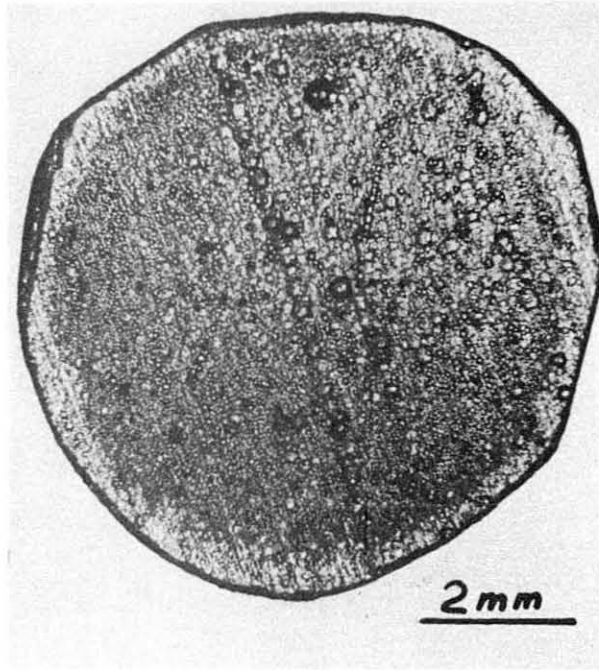   Cd(0001) Face before Vaporization at 621°C
              in Fig. 59
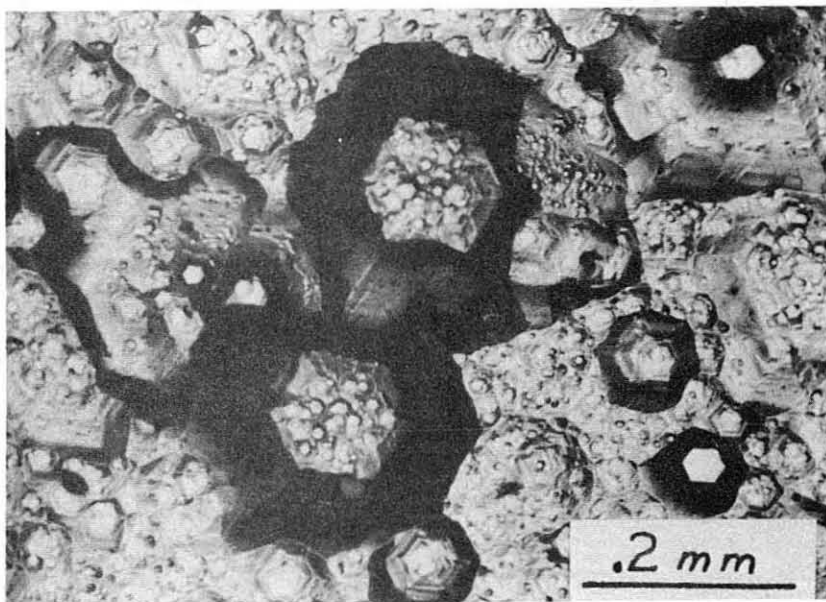
XBB703-1340

2mm

(a)

.2 mm
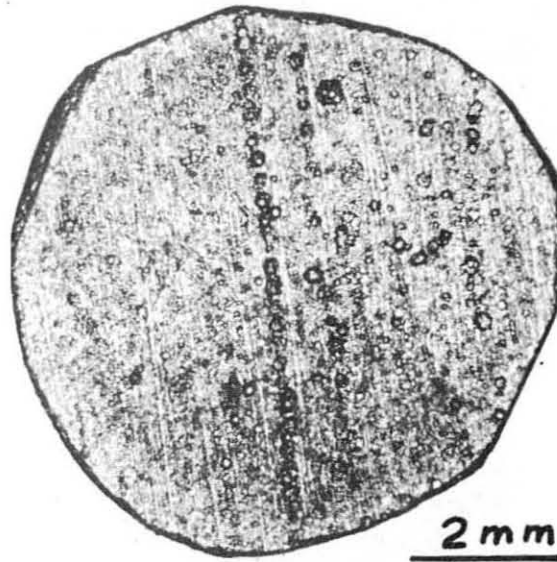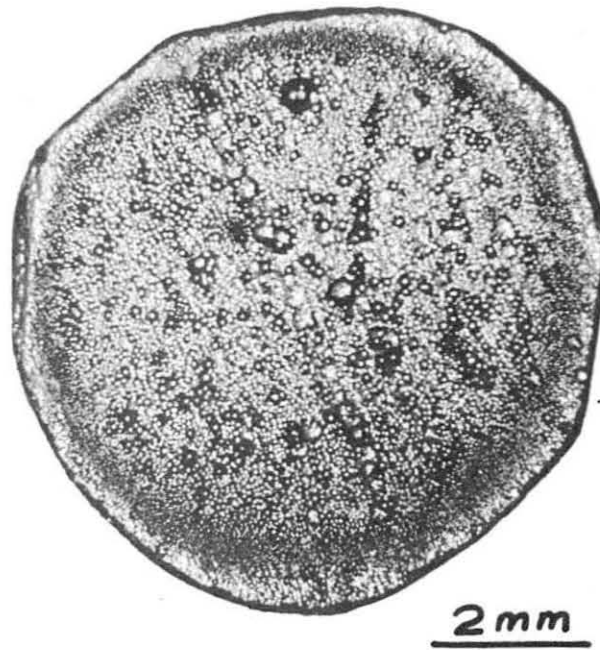
(b)

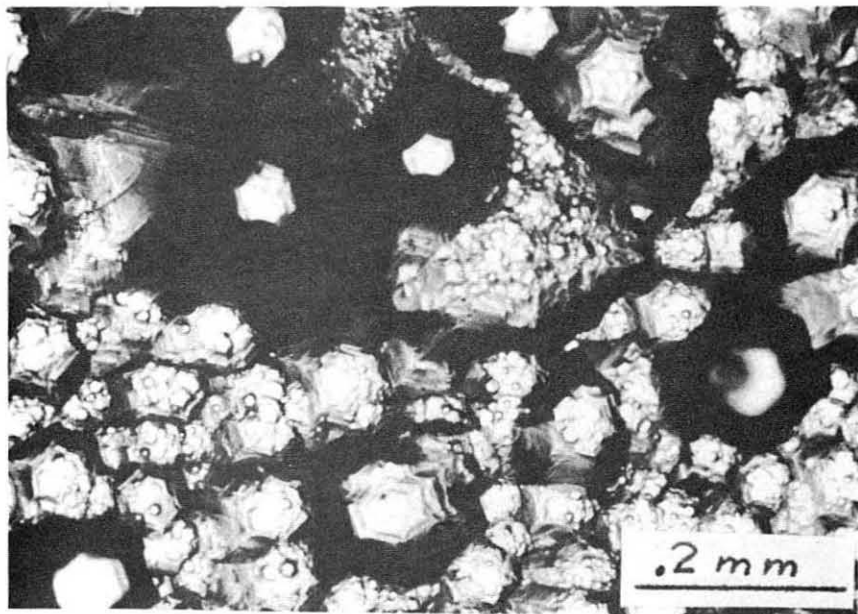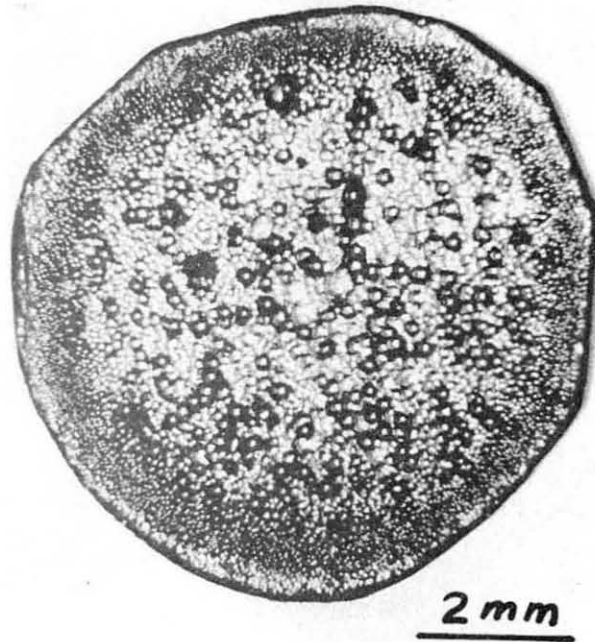Figure 61. Cd(0001) Face at Point a in Fig. 59

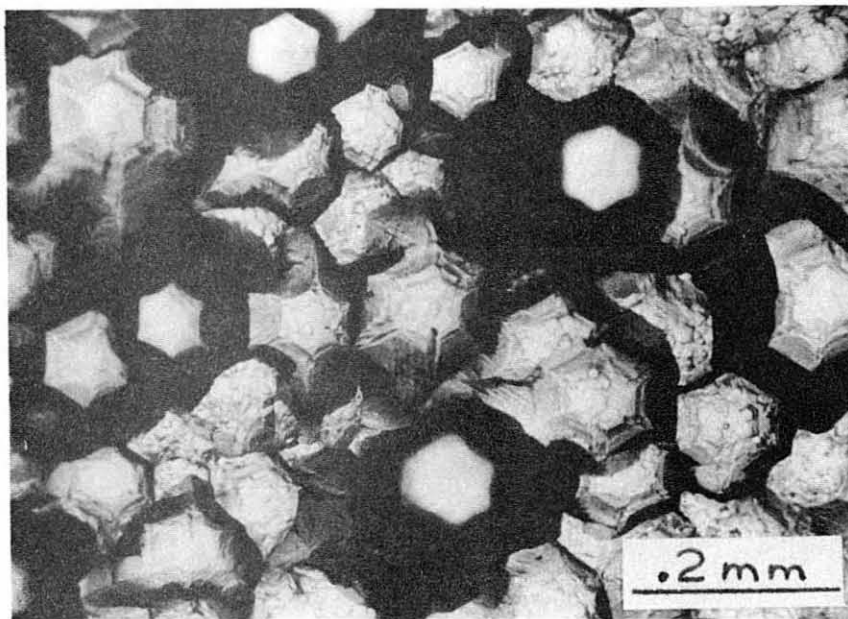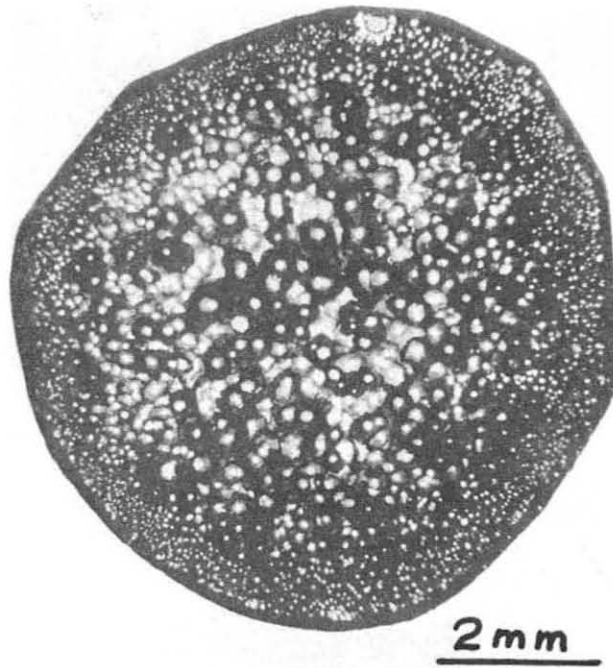XBB703-1338

(a)

(b)

Figure 62. Cd(0001) Face at Point <u>b</u> in Fig. 59

XBB703-1335

2mm

(a)

.2 mm

(b)

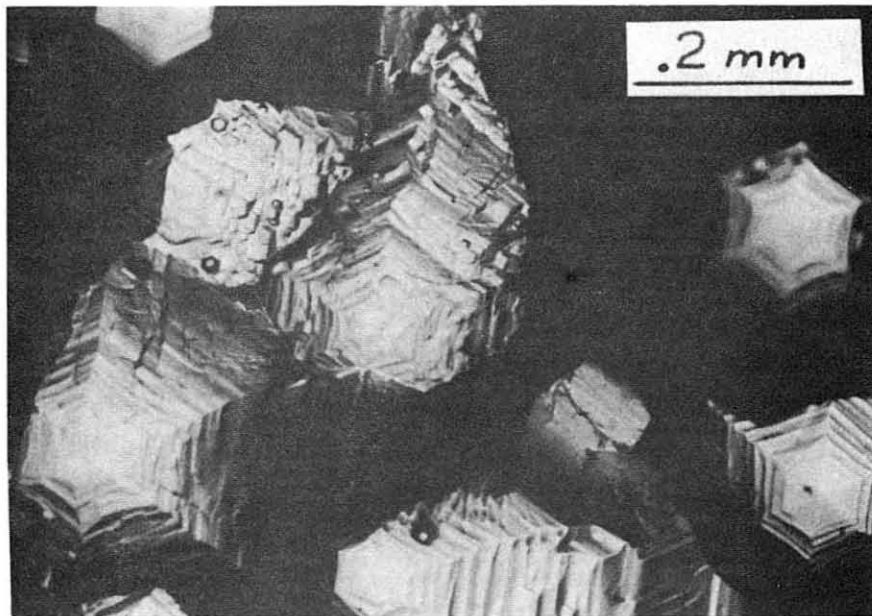Figure 63. Cd(0001) Face at Point c in Fig. 59

XBB703-1342

2mm

(a)

.2mm

(b)

Figure 64. Cd(0001) Face at Point <u>d</u> in Figure 59
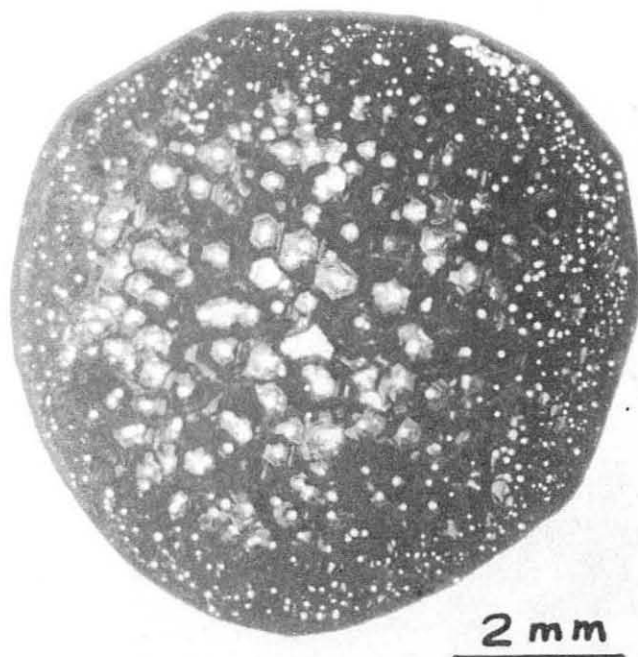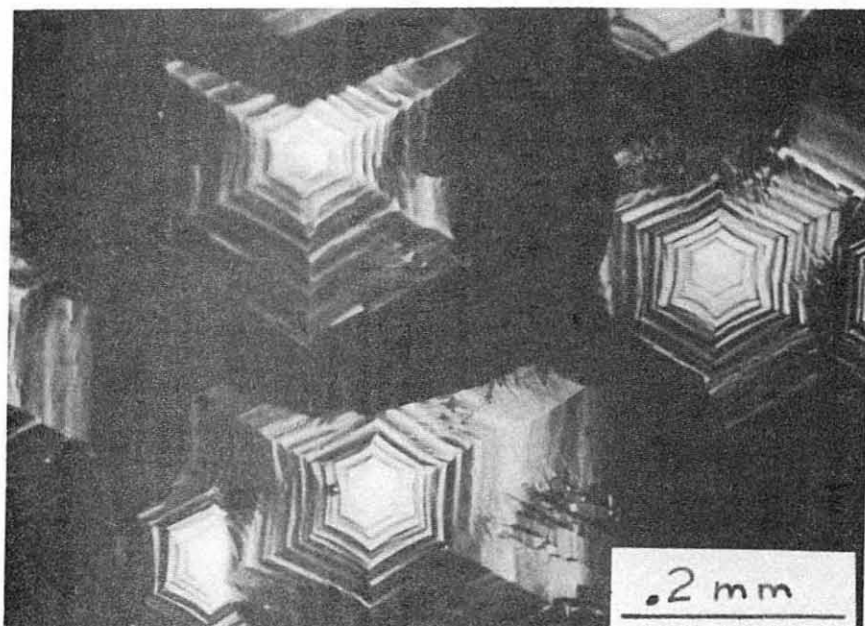
XBB703-1341

(a)

(b)

Figure 65. Cd(0001) Face at Point e in Fig. 59

XBB703-1337

(a)

(b)

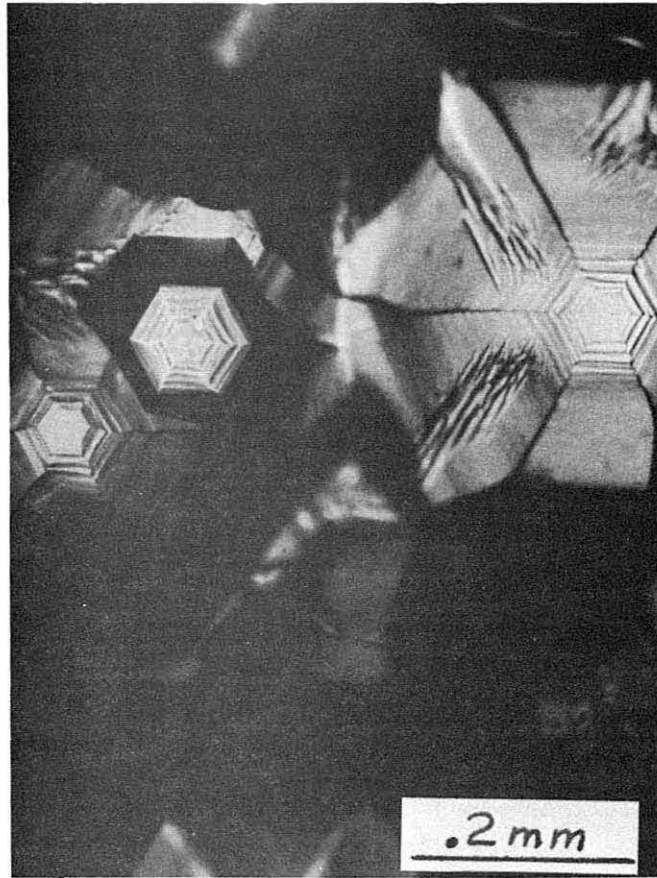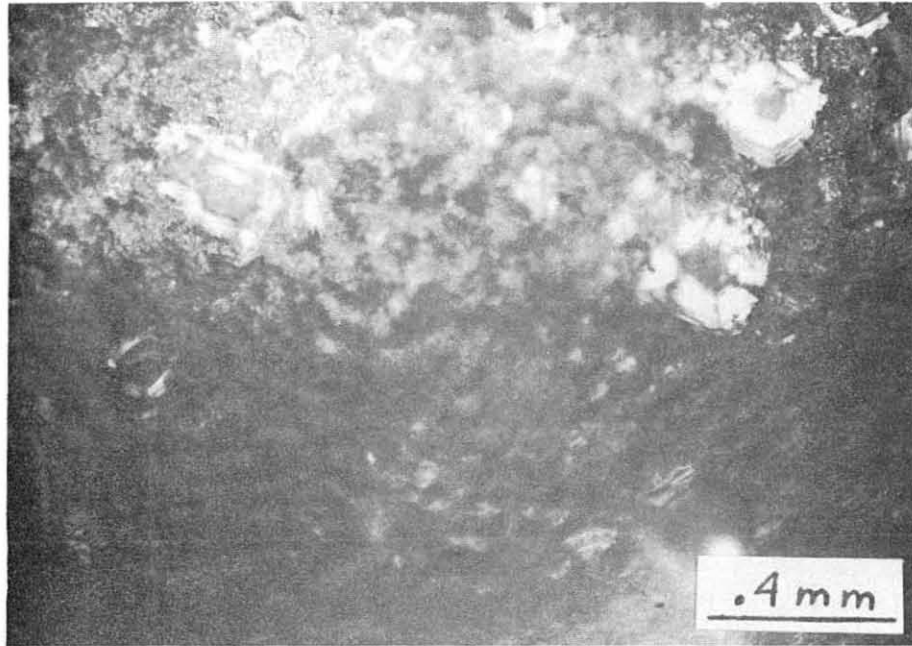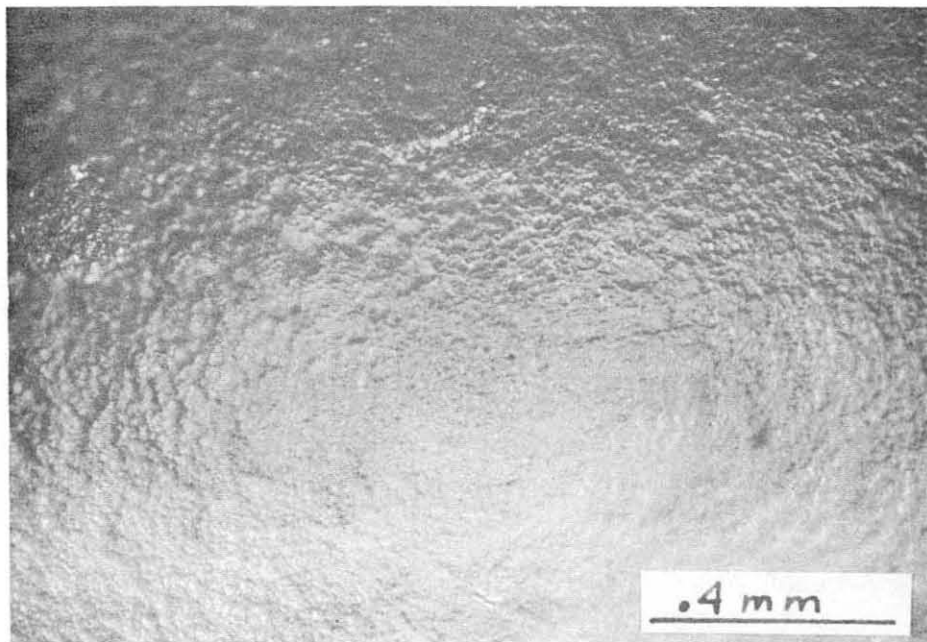Figure 66. Cd(0001) Face at Point _f_ in Fig. 59

XBB 703-1344

Figure 66-c. New Thermal Pit Emerging
within Older Pits in upper
left-center

XBB703-1332

(a)

(b)

Figure 67. Optical Photographs of S(000Ī) Steady-State
Surfaces

XBB703-1334

It is evident that in this temperature range the $S(000\bar{1})$ face has a lower rate and a higher enthalpy of activation for vaporization than the $Cd(0001)$ face.

Crystal number two was vaporized to the extent that one of the pits just penetrated the crystal. Hence it would not seem that the difference in vaporization behavior for the two faces could be due to a concentration gradient.

Figures 60 through 66 show the development of the steady state morphology on a $Cd(0001)$ face and the corresponding vaporization data are shown in Fig. 59. Figure 60 shows the $Cd(0001)$ face after it was etched, and Figs. 61, 62, and 63 show the crystal after 16, 56 and 120 minutes of vaporization at 621°C. Apparently vaporization continues from pits developed by the chemical etching, but it is very difficult to follow the actual development of such small pits. Figures 64, 65 and 66 show the crystal after vaporization at 642°C, 665°C and 676°C respectively. As can be observed, the thermal pits grow in size, with some pits seemingly engulfing others, as is seen in Fig. 66b. However, Fig. 66c apparently shows a smaller pit developing within previously formed pits.

One can observe, in Fig. 62a the border between the free surface and the area of the crystal that was under the cell lip. Upon continued vaporization, the border advanced slightly toward the edge of the crystal as can be seen in the subsequent photographs.

The $S(000\bar{1})$ face developed a non-distinct surface with no features that could be observed with the optical microscope. Figure 67b is an optical photograph of crystal number two taken with oblique lighting. A coarser, but similar surface, from a different crystal is seen in Fig. 67a.

The crystal surfaces were examined with the scanning electron microscope (SEM) and Fig. 68a is a general view of the Cd(0001) steady state surface, where the hexagonal pits are clearly visible. Figure 68b is a detail of the steps on the steep sides of the two upper pits. In Fig. 68a one can see a smaller pit that is apparently forming on the floor of a larger pit in the lower left corner.

The crystal was remounted before the photos in Figs. 69 through 71 were taken. The white particles seen on the surface are silver conducting paint used to mount the samples on the original mount.

Figure 69a is a higher magnification of the pit in the lower left corner of Fig. 68a. Many of these hexagonal pits seem to have very steep sides with gently sloping floors. (See Figs. 68a, 70a and 71a). Figure 69b shows the new pit seen in Fig. 69a which is forming on the floor and one can observe the steps on the floor of the pit.

Figures 70a and 71a are general views of the Cd(0001) face, where one, again, observes that the pits have steep sides and gently sloping floors. Figure 70b is a higher magnification of the center pit in Fig. 70a.

Figure 71b shows the pit in the upper left-hand corner which seems to be a "younger" pit with no observable steps on the sides. Figure 71c shows the floor of the pit in the upper right-hand corner, where the steps on the floor are readily observable.

Figure 72a, b and c are SEM photographs of the $S(000\bar{1})$ face of crystal number one where it is obvious that this face developes an entirely different morphology than the Cd(0001) which can best be described as rounded mountain peaks separated by narrow valleys. Figures 73a, b and c are similar SEM photographs of crystal number two and, again, a similar

morphology is noted. The features seen in Fig. 73c at 8000X exhibit

ledges which are not so evident in Fig. 72c. Also, one can observe some

very fine particles "sprinkled" about. A yellow powder was obtained

when the $S(000\bar{1})$ steady state surface was brushed or rubbed. The yellow

powder was removed by pressing a piece of masking tape against the surface

which was then examined with an electron beam microprobe. Quantitative

measurements could not be made on the powder because it did not present

a solid mass to the electron beam and because the electron beam tended to

burn the tape; however, the powder contained both cadmium and sulfur.

The ratio of the counts/sec of Cd to S in the powder was within 10% of

the ratio of Cd to S in a sample cadmium sulfide crystal. Hence the "powder"

on the surface apparently is made up of small pieces of cadmium sulfide

that is somehow produced by the vaporization process.

Comparison of the SEM photographs of the Cd(0001) face and the

$S(000\bar{1})$ seems to indicate that the sulfur face has the larger surface area.

However, it is also this face that had the smaller vaporization rate, hence

it seems unlikely that the surface area difference is responsible for

the difference in vaporization rate, especially since the two sides

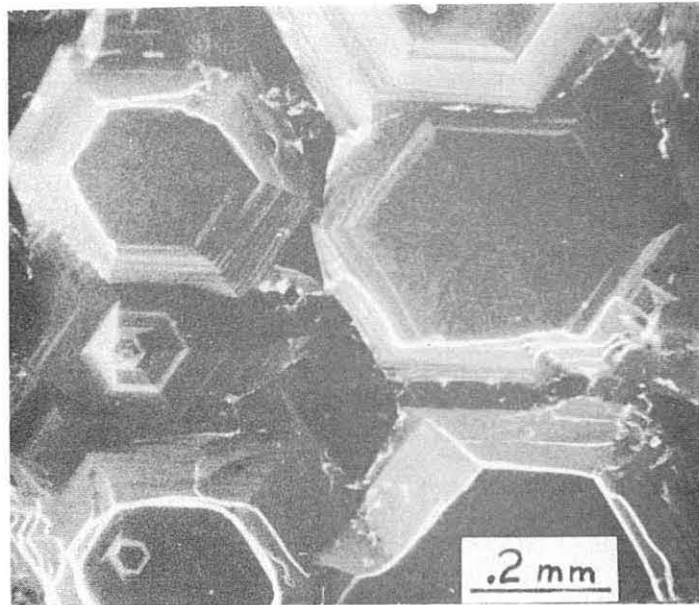exhibit different enthalpies.

Figure 68-a. Scanning Electron Micrograph (SEM)
of Cd(0001) Steady-State Surface
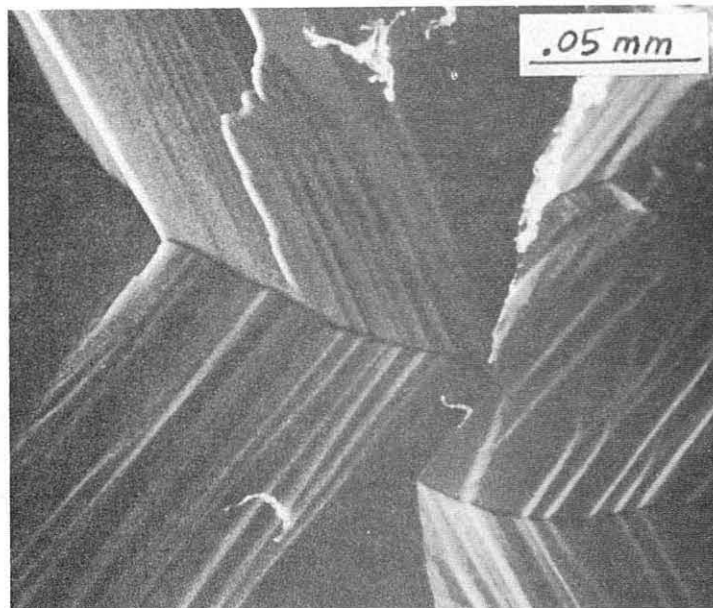

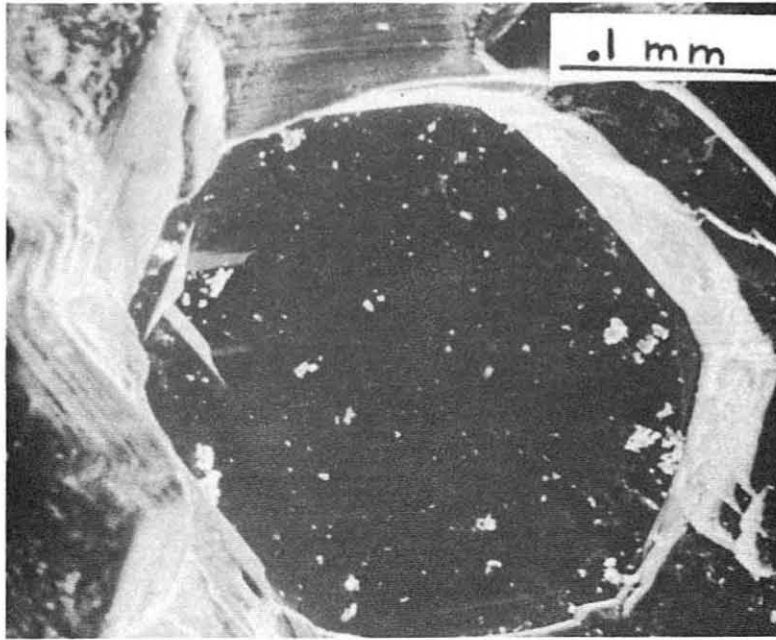Figure 68-b. Detail of Fig. 68-a.

XBB703-1347

Figure 69-a.   SEM of Pit in Lower Left Corner
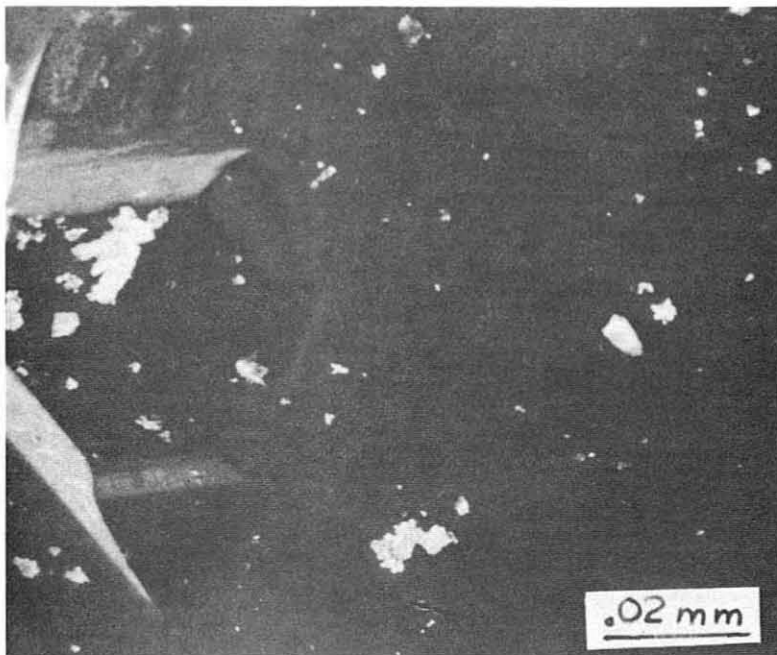of Fig. 68-a.

Figure 69-b.   SEM Detail of Fig. 69-a.
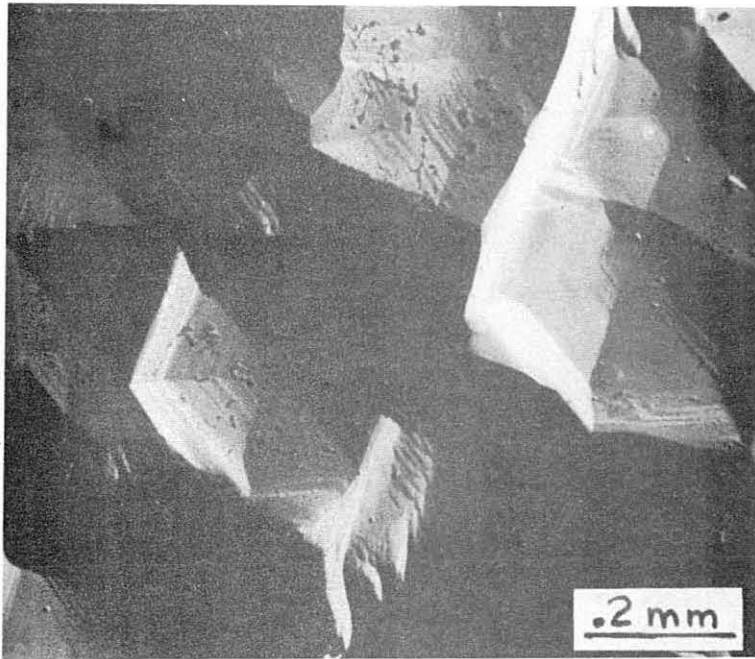
XBB703-1339

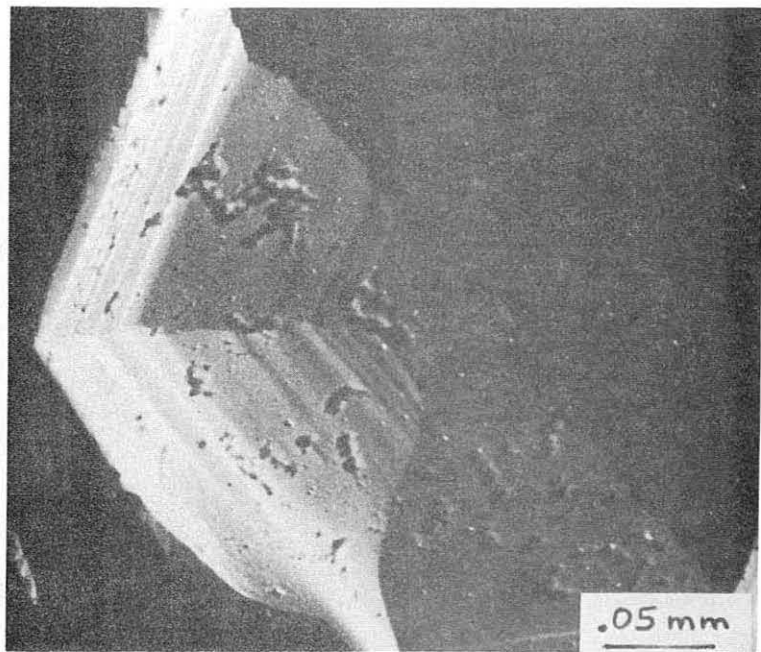Figure 70-a.   SEM of Cd(0001) Steady-State Surface

Figure 70-b.   Detail of Center Pit in Fig. 70-a.
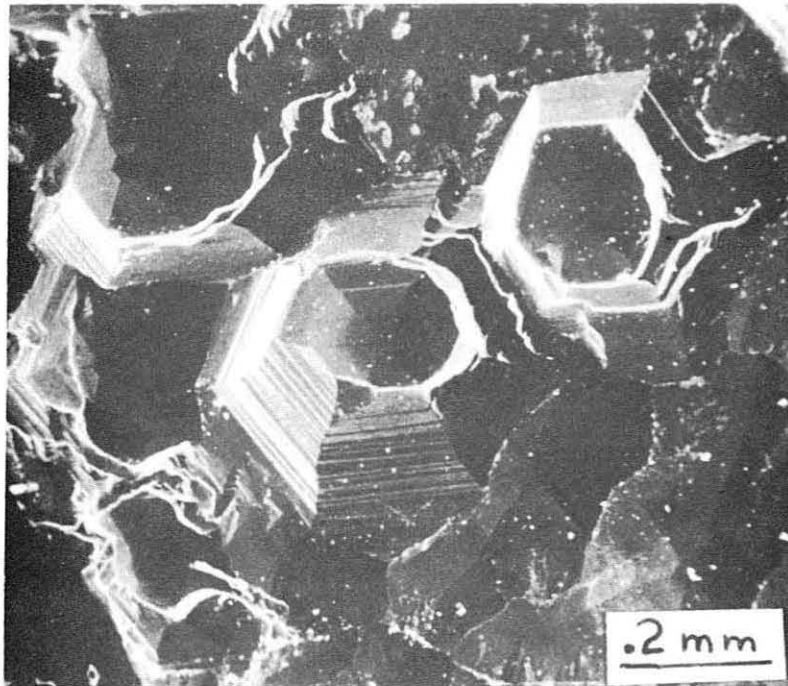
XBB703-1336
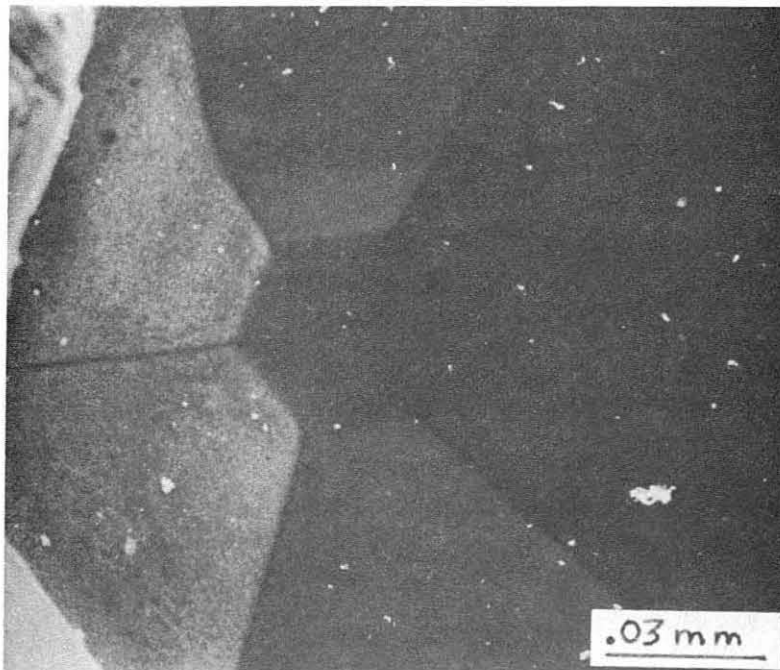
Figure 71-a.   SEM of Cd(0001) Steady-State Surface

Figure 71-b.   Detail of Pit in Upper Left Corner
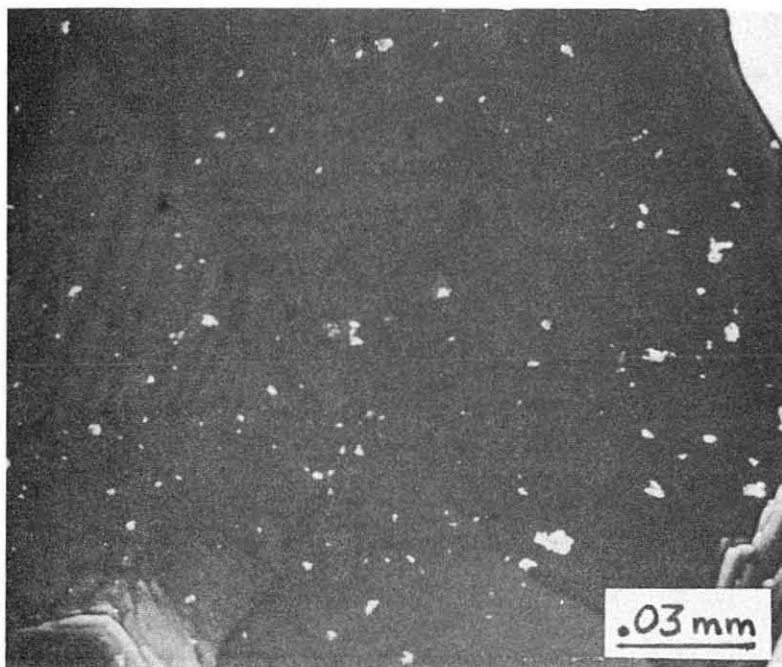of Fig. 71-a.

XBB703-1343

Figure 71-c. Detail of Pit in Upper Right Corner
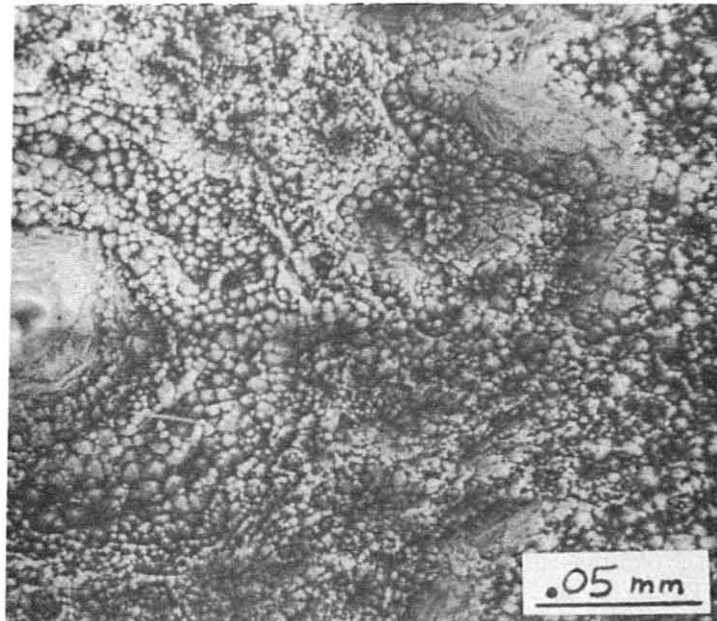of Fig. 71-a.

XBB703-1331

Figure 72-a.   SEM of S(000$\bar{1}$) Steady-State Surface (crystal number one)
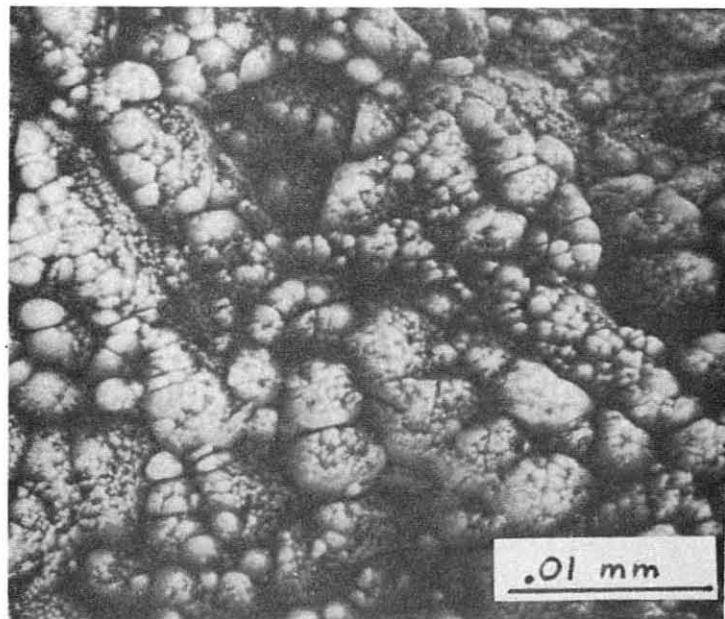

Figure 72-b.   Detail of Fig. 72-a.
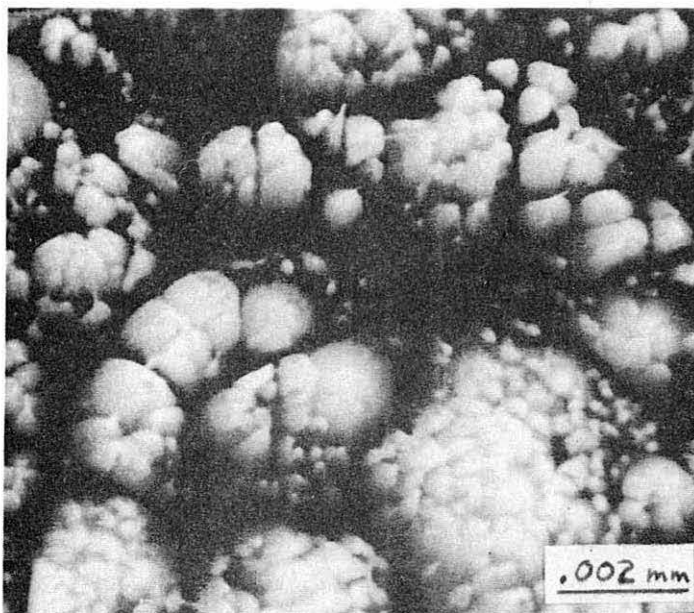
XBB703-1345

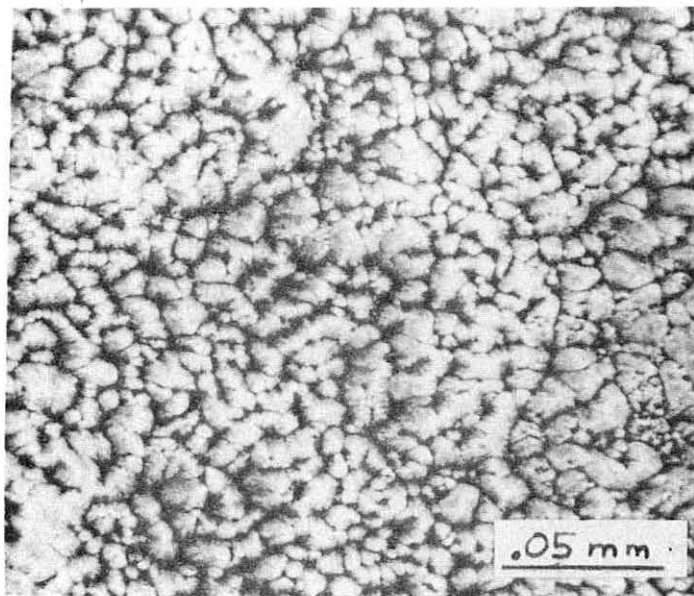Figure 72-c.   Detail of Fig. 72-b.

Figure 73-a.   SEM of S(000$\bar{1}$) Steady-State
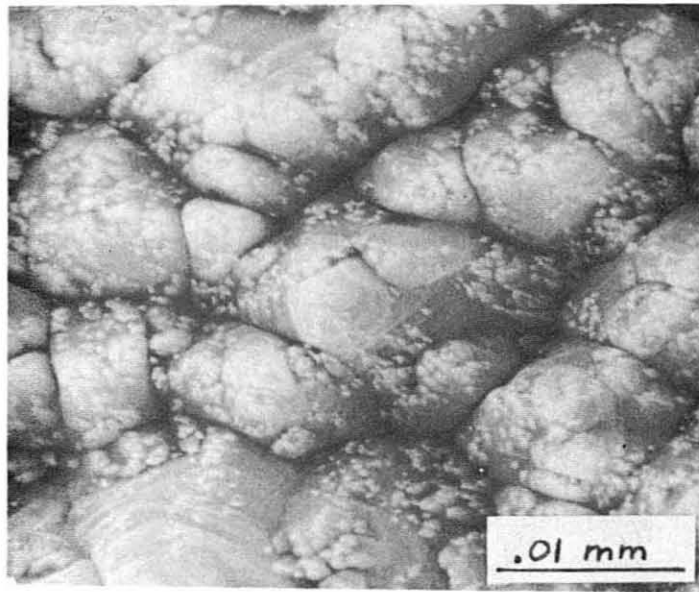Surface (crystal number two)

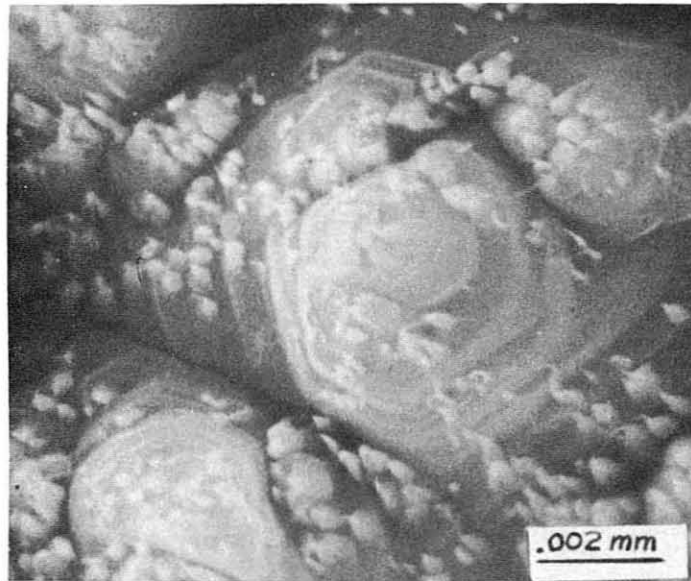XBB703-1346

Figure 73-b.   Detail of Fig. 73-a.

Figure 73-c.   Detail of Fig. 73-b.

XBB703-1348

VIII. DISCUSSION OF ZINC OXIDE AND CADMIUM SULFIDE RESULTS

Table 3 gives a brief summary of the morphologies and relative vaporization rates measured in this investigation.

TABLE 3

Crystal face	Chemical etch behavior	Steady-state vaporization morphology	Relative rate
Zn(0001)	hexagonal pits	sharp mountain peaks separated by narrow vallies	higher
O(000$\bar{1}$)	irregular/grainy	hexagonal pits	lower
Cd(0001)	hexagonal pits	hexagonal pits	higher
S(000$\bar{1}$)	irregular	rounded mountain peaks separated by narrow vallies	lower

The vaporization rate of opposite basal faces of zinc oxide differ by a factor of three at 1107°C and are constant with time. The prismatic faces exhibit a vaporization rate that is approximately equal to that of the O(000$\bar{1}$) face after 300 minutes, but the rate continues to increase as vaporization continues, and is apparently correlated with the slow development of "slit pits" which increases the effective surface area.

Hoenig[33] studied the vaporization behavior of the prismatic faces of two zinc oxide crystals over the temperature range of 1040° to 1240°C. The results for these two crystals differed by almost a factor of ten in addition to exhibiting a great deal of scatter. He measured the weight loss at a given temperature for periods of time ranging from 14 to 80 minutes, depending on the temperature. The results obtained in this study for the prismatic faces may explain Hoenig's

results. That is, the prismatic faces require a long time to develop a steady-state surface, during which time the vaporization rate increases. Hence, Hoenig's procedure of vaporizing the two crystals at various temperatures for short times in a random fashion might be expected to give erratic results since the respective morphologies would be in various stages of development.

A typical oxygen pressure from a Zn(0001) face in this study at 1107 $^\circ$C was 8.9×10^{-8} atm while Hoenig measured 9.2×10^{-8} atm from a prismatic face at 1104°C. These values are approximately two orders of magnitude lower than the equilibrium oxygen pressure over zinc oxide.

Excess zinc in zinc oxide must vaporize rapidly from the surface of the crystal, since the heavily zinc doped crystals were decolorized by loss of excess zinc within a few minutes.

An oxygen flux ten times the flux of vaporizing oxygen flux has no effect on the vaporization rate; although for cadmium sulfide, the vaporization rate is reduced in proportion to $P_{S_2}^{1/2}$.[39] However, the vaporization rate is reduced in oxygen flow experiments (P_{O_2} = 1 atm) as expected from the law of mass action.

Summary of Quenching Experiments on Zinc Oxide

(1) Cooling a crystal in oxygen, argon, or nitrogen and not exposing the crystal to laboratory air completely eliminated any induction period in the subsequent vaporization of $Zn(0001)$ faces.

(2) Exposing a crystal to laboratory air causes an induction period. Short exposures (1 hr or less) usually produce small induction periods, but occasionly produce none at all. Long exposures (greater than 1 hr) produce much more pronounced induction periods, with the extent of reduction for $Zn(0001)$ faces roughly related to the length of exposure.

(3) Room temperature storage of a crystal in water saturated air produces very large induction periods.

It seems certain that the induction periods are caused by adsorption of water on the surface at room temperature.

Dent andKokes[49] present evidence that water poisons the surface of zinc oxide and reduces the hydrogenation rate of ethylene at room temperature by a factor of four. They suggest that the water produces -OH groups which attach themselves to the zinc atoms on the surface. They did not investigate relative rates on opposite basal faces, which would be an extremely interesting project.

It seems likely that the water reacts with the surface to produce a "reaction layer" that, in turn, hinders the vaporization kinetics, even though the "reaction layer" may be only a monolayer. A high temperature anneal in water saturated argon, however, does not lead to an induction period. Apparently the protective layer cannot form by reaction with water when the surface is at high enough temperatures.

The temperature range in this work for the cadmium sulfide vaporization includes only the lower third of the temperature range of Munir.[46] The total pressure measured in this work for the Cd(0001) face is approximately 50% higher than that of Munir's while the total pressure from the S(000$\bar{1}$) face is coincident with that of Munir's average values. The total pressure measured by Somorjai is about a factor of three higher than those of this work and that of Munir's. The large amount of scatter observed in Munir's work is most likely due to the data points being collected with various combinations of Cd(0001) and S(000$\bar{1}$) faces. Munir[46] obtains $\Delta S^{\ddagger} = 41.30$ eu and $\Delta H^{\ddagger} = 87.20$ Kcal over the temperature range of 909° to 1083°K for apparent activation entropies and heats for the reaction

$$CdS_{(g)} \rightarrow Cd_{(g)} + \frac{1}{2} S_{2(g)}$$
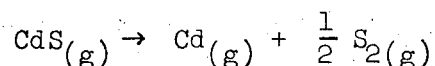
Average $\Delta H^{\ddagger}$ and $\Delta S^{\ddagger}$ values from the Cd(0001) face in this study were found to be $\Delta H^{\ddagger} = 85.41$ Kcal and $\Delta S^{\ddagger} = 47.60$ eu and from the S(000$\bar{1}$) face to be $\Delta H^{\ddagger} = 96.66$ Kcal and $\Delta S^{\ddagger} = 58.66$ eu for the same reaction.

No information is available as to the morphologies observed by other investigators for cadmium sulfide vaporizations. In this study the opposite faces are shown to be very different, but highly irregular.

The steady-state surface of the S(000$\bar{1}$) face can be approximated as an array of regular tetrahedrons, which leads to an estimate that the true area is three or four times the projected area. Since measured vaporization coefficients for the faces that were studied for cadmium sulfide and zinc oxide were about 0.1 and about 0.01, most molecules that collide with surface irregularities after vaporization would fail to condense and the total surface area rather than the projected area

should be used in calculations of the vaporization coefficient.

Inserting the corrected area into the previous calculation lowers $\Delta S^{\ddagger}$ by about 3 eu for the $S(000\bar{1})$ face. The true area of the $Cd(0001)$ face is about 2% higher than the projected area, and hence the corrected vaporization coefficient is almost the same as the measured value. However, the corrected vaporization coefficient for the $S(000\bar{1})$ face is about 0.03.

As mentioned previously, there are three possible reasons for the different vaporization behavior of opposite basal faces of zinc oxide and cadmium sulfide:

    (1)   direct influence of the asymmetry of the c-axis on

          vaporization

    (2)   c-axis asymmetry causing preferential impurity adsorption

    (3)   c-axis asymmetry causing preferential residual gas attack

The studies done in this work with methane, carbon monoxide, and oxygen seem to rule out the third possibility for zinc oxide. The pressure of the background gases introduced in this study provided a flux of incoming molecules that was approximately an order of magnitude. higher than the flux of vaporizing species. Vaporization of an $0(000\bar{1})$ face in the presence of water vapor gave no change in vaporization rate.

The asymmetry of the c-axis must be the basic cause of the difference in vaporization rates, whether it acts directly on the vaporizing crystal units or indirectly through selective impurity adsorption. To eliminate the possibility that differences in impurity adsorption on the different crystal faces is responsible for the observed differences in vaporization rates would require a far better vacuum than could be

obtained with this apparatus and very careful control of sample purity.

Some evidence about the effects of impurities, however, can be sum-

marized.

Impurities are known to affect vaporization. Young and Gwathmey[50]

found that single crystal spheres of 99.98% copper developed extensive

thermal pits while fewer pits were formed with 99.999% copper.

Mar[2] found that the vaporization coefficient was unity for the

(0001) face of high purity zinc (no detectable impurities with the

emission spectrograph) and 0.7 for 99.998% pure zinc. Furthermore, the

two types of zinc crystals developed different steady-state morphologies.

Budke[51] studied the vaporization of cleaved sodium chloride single

crystals and observed that the thermal pits developed could be correlated

with changes in surface contamination.

As mentioned previously, aluminum and silicon (presumably present

as oxides) on the surface of zinc oxide caused no difference in either

vaporization rates or steady-state morphologies.

On the other hand, the results of Wolff et al.,[52] may indicate an

impurity effect.

Wolff et al. have investigated the vaporization of zinc oxide and

have also found different behavior for opposite basal faces. Instead

of using a vaporization cell to expose a certain face for vaporization,

they used platinum or magnesium oxide to coat the faces which they

didn't want to vaporize. The measured activation enthalpy for the

crystal whose sides were coated with platinum was 45.8 Kcal/mole ZnO

while it was 103 Kcal/mole ZnO for the crystal whose sides were coated

with magnesium oxide.

This is a difference of more than 100% and probably was caused by surface diffusion of magnesium or platinum onto the vaporizing surface. Whether the surface was poisoned or catalyzed is unknown, but certainly this is an important question for further investigations.

It is only necessary to recognize that opposite crystal faces can have drastically different chemical and electrical environments to adapt the mechanism proposed by Somorjai and coworkers to the interpretation of data of the present study.

An effect of O_2 pressure in repressing zinc oxide vaporization similar to the repression found by Somorjai et al. for S_2 beams in cadmium sulfide vaporization was not found. But Somorjai et al. found that a cadmium vapor beam did not influence cadmium sulfide vaporization rates. It seems reasonable that zinc oxide vaporization rates may be limited by the concentration of self-adsorbed zinc, while cadmium sulfide vaporization rates are limited by the concentration of self-adsorbed sulfur. If this hypothesis is correct, zinc oxide vaporization rates might be reduced in a beam of zinc vapor.

An investigation of this question and of the effect of light in altering vaporization rates of zinc oxide would be valuable experimental undertakings, as would be the determination of the relative effect of light on opposite basal faces of cadmium sulfide.

The influence of the asymmetry of the c-axis on vaporization behavior had not been predicted from current vaporization theories and was entirely unexpected. This situation brings to mind the poem by Professor Emeritus Paul A. Weiss[53] of Rockefeller University:

"Something we find with intention

Commonly is called invention.

If the goal was practical,

Then, of course, it's tactical

To exploit its fruits for money,

Much as bees milk plants for honey.

But when I, of mind more humble

Just observing nature, stumble

Upon a discovery

What it holds as prize for me

Is the thrill to have detected

Something wholly unexpected."

ACKNOWLEDGEMENTS

REFERENCES

1. J. P. Hirth and G. M. Pound, J. Chem. Phys. 26, 1216 (1957).

2. R. W. Mar, Sublimation Kinetics of Zinc Single Crystals (Ph. D. Thesis), University of California, Berkeley, UCRL-18257, May 1968.

3. F. S. Taylor, The Alchemists (Collier Books, N. Y. 1962).

4. E. Scharowsky, Z. Physik 135, 318 (1953).

5. N. B. Hannay, Semiconductors (Reinhold Pub. Corp., New York 1959).

6. The 3M Co., Electrical Products Div., Minneapolis, Minn.

7. Y. S. Park and D. C. Reynolds, J. Appl. Phys. 38, 756 (1967).

8. See for example: S. R. Morrison and T. Freund, J. Chem. Phys. 47, 1543 (1967).

    H. C. Rowlinson and R. J. Cvetanovic, Adv. in Catalysis, Vol. IX (1956).

    G. Parravano and M. Boudart, ibid, Vol. VII (1954).

    H. Chon and C. Prater, Faraday Soc. Disc. No. 41, p. 320 (1966).

9. S. R. Morrison, Adv. in Catalysis, Vol. VII (1955).

10. G. Heiland and E. Mollwo, Solid State Physics, Vol. 8 (1959).

11. D. A. Melnick, J. Chem. Phys. 26, 1136 (1957).

12. D. B. Medved, J. Chem. Phys. 28, 879 (1958).

13. D. B. Medved, J. Phys. Chem. Solids 20, 255 (1961).

14. D. G. Thomas and J. J. Lander, J. Phys. Chem. Solids 2, 318 (1957).

15. R. J. Collins and D. G. Thomas, Phys. Rev. 112, 388 (1958).

16. A. R. Hutson, J. Phys. Chem. Solids 8, 467 (1959).

17. E. E. Hahn, J. Appl. Phys. 22, 855 (1951).

18. T. J. Gray, J. Am. Cer. Soc. 37, 534 (1954).

19. V. J. Lee and G. Parravano, J. Appl. Phys. 30, 1735 (1959).

20. D. G. Thomas and J. J. Lander, J. Chem. Phys. 25, 1136 (1956).

21. J. J. Lander, J. Phys. Chem. Solids 15, 324 (1960).

22. D. G. Thomas, J. Phys. Chem. Solids 9, 31 (1958).

23. C. B. G. Garrett, Adv. in Electronics and Electron Phys., Vol. XIV (1961).

24. E. A. Secco and W. J. Moore, J. Chem. Phys. 26, 942 (1957).

25. W. J. Moore and E. L. Williams, Faraday Soc. Disc. No. 28, p. 86 (1959).

26. D. G. Thomas, J. Phys. Chem. Solids 3, 229 (1957).

27. G. P. Mohanty and L. V. Azaroff, J. Chem. Phys. 35, 1268 (1961).

28. W. Ehret and A. Greenstone, J. Am. Chem. Soc. 65, 872 (1943).

29. S. Larach and J. Turkevich, J. Phys. Chem. Solids 29, 1519 (1968).

30. W. J. Moore, Department of Chemistry, Indiana University, private communication, August 1967.

31. D. F. Anthrop and A. W. Searcy, J. Phys. Chem. 68, 2335 (1964).

32. W. J. Moore and E. L. Williams, J. Phys. Chem. 63, 1516 (1959).

33. C. L. Hoenig, Vapor Pressure and Evaporation Coefficient Studies of Stannic Oxide, Zinc Oxide, and Beryllium Nitride (Ph. D. Thesis), University of California, Berkeley, UCRL-7521, April 1964.

34. E. P. Warekois, M. C. Lavine, A. N. Mariano, and H. C. Gatos, J. Appl. Phys. 33, 690 (1962).

    Errata, J. Appl. Phys. 37, 2203 (1966).

35. A. N. Mariano and R. E. Hanneman, J. Appl. Phys. 34, 384 (1963).

36. S. Kimoto and J. Russ, American Scientist 57, 112 (1969).

37. P. Goldfinger and M. Jeunehonne, Trans. Far. Soc., London 59, 2851 (1963).

38. G. A. Somorjai and N. R. Stemple, J. Appl. Phys. 35, 3398 (1964).

39. G. A. Somorjai and D. W. Jepsen, J. Chem. Phys. 41, 1389 (1964).

40. G. A. Somorjai and D. W. Jepsen, J. Chem. Phys. 41, 1394 (1964).

41. G. A. Somorjai and J. E. Lester, J. Chem. Phys. 43, 1450 (1965).

42. H. H. Woodbury, Phys. Rev. 134A, 492 (1964).

43. F. A. Kroger, H. J. Vink, and J. Van den Boomgard, Z. Phys. Chemie, 203, 1 (1954).

44. G. A. Somorjai and H. B. Lyon, J. Chem. Phys. 43, 1456 (1965).

45. G. A. Somorjai and J. E. Lester, Prog. Solid State Chem., 4, 1 (1967).

46. Z. A. Munir, High Temperature Sci., 2, 58 (1970).

47. D. P. Miller, J. G. Harper, and T. R. Perry, J. Electrochem. Soc. 108, 1123 (1961).

48. M. F. Millea and D. F. Kyser, J. Appl. Phys. 36, 308 (1965).

49. A. L. Dent and R. J. Kokes, J. Phys. Chem. 73, 3772 (1969) and 73, 3781 (1969).

50. F. E. Young, Jr. and A. T. Gwathmey, J. Appl. Phys. 31, 225 (1960).

51. J. Budke, J. Appl. Phys. 40, 641 (1969).

52. G. A. Wolff, et al., Tyco Labs., Inc., Waltham, Mass., Tech. Report AFML-TR-67-385 (1967) and Tech. Report AFML-TR-69-13 (1968).

53. Paul A. Weiss, Am. Scientist 57, 287 (1969).